A MIDBRAIN MECHANISM FOR COMPUTING ESCAPE DECISIONS IN THE MOUSE

DISSERTATION

submitted for the degree of
Doctor of Philosophy
in Biological Science

by

Dominic Evans
Darwin College
University of Cambridge

Neurobiology Division
MRC Laboratory of Molecular Biology
Francis Crick Avenue, Cambridge

Submitted in September, 2017

Preface

All the work described in this thesis was carried out in the Neurobiology Division of the Medical Research Council Laboratory of Molecular Biology, and the Sainsbury Wellcome Centre for Neural Circuits and Behaviour, under the supervision of Dr. Tiago Branco.

This dissertation is not substantially the same as any that I have submitted, or, is being concurrently submitted for a degree or diploma or other qualification at the University of Cambridge or any other University or similar institution except as declared in the Preface and specified in the text. It does not exceed 60,000 words, excluding figures, tables, appendices and bibliography, as specified by the Degree Committee. This dissertation is my own work and contains nothing which is the outcome of work done in collaboration with others except as specified in the text and summarised in the Statement of Contributions.

Statement of contributions

Due to the collaborative and interdisciplinary nature of this project, some of the data presented was acquired with the help of other people. These people are: **Dr. Tiago Branco**, and his lab members **Dr. Vanessa Stempel**, **Dr. Sabine Rühle** and **Dr. Ruben do Vale**. All experiments in this thesis were conceived and designed by my PhD supervisor, Dr. Tiago Branco and me, with additional input from the other investigators for the particular experiments they contributed to.

In the following I state the contribution of other people to the data presented by chapter:

Chapter 3
Dr. Tiago Branco contributed the behavioural modelling. Dr. Sabine Rühle assisted with preliminary behavioural experiments, the plasticity experiments, and final video annotation analysis.

Chapter 4
Some muscimol experiments were performed with the assistance Dr. Ruben do Vale and Dr. Sabine Rühle, and analysed with the help of Dr. Sabine Rühle. I performed all other inactivation experiments.

Chapter 5
I performed all calcium imaging experiments, and Dr. Tiago Branco contributed to the analysis.

Chapter 6
Dr. Sabine Rühle and Dr. Ruben do Vale assisted me with the preliminary optogenetic experiments. Dr. Vanessa Stempel performed the rabies tracing experiments, and the majority of the analysis, which I contributed to. Dr. Vanessa Stempel and Dr. Tiago Branco contributed the electrophysiological recordings and analysis, while I assisted with the injections.

Summary

Animals face frequent threats from predators and must generate appropriate behavioural responses to ensure their survival. To achieve this, they process sensory cues to correctly identify the presence and imminence of a predatory threat, and transform this information into defensive actions. However, despite much research in identifying the circuits that may be responsible for such transformations, little is known about how this occurs mechanistically.

We focus on how escape behaviour in the mouse is generated from visual predatory threats, and use a combination of behavioural, neurophysiological and anatomical methods to identify the relevant neurons and understand how they perform this computation.

In this work, we developed an innate decision making paradigm in which a mouse detects and assesses sensory stimuli of varying threat evidence during exploration, choosing whether to escape to a shelter, or not. The performance data in this task were best formalised with a drift-diffusion model of decision making, providing a framework to understand innate behavioural tasks in terms of evidence accumulation and boundaries.

Next, we performed calcium imaging in freely-moving mice to probe for neural correlates of decision elements and flight behaviour in brain areas that we show to be necessary for the flight responses: we found that VGluT2$^+$ neurons in the deeper medial superior colliculus (dmSC) increase their activity during a repeated threatening stimulus, while VGluT2$^+$ neurons of the dorsolateral periaqueductal gray (dPAG) are silent until just before the initiation of escape, and are maximally active during escape.

These results suggest that the dmSC accumulates evidence of threat which dPAG neurons threshold. This interpretation is supported by optogenetic activation of mSC-VGluT2$^+$ neurons *in vivo*, which recapitulates the statistics of escape probability evoked with a visual stimulus, while activation of VGluT2$^+$ neurons in the dPAG evokes an all-or-nothing escape response.

Finally, using channelrhodopsin-2-assisted circuit mapping and monosynaptic viral tracing, we reveal that over half of dPAG-VGluT2$^+$ neurons receive monosynaptic connections from mSC-VGluT2$^+$ neurons with a low probability of release, allowing this synapse to act as a high-pass filter and providing a mechanism for the computation of an escape decision. These findings advance our understanding of how defensive behaviours are generated at circuit and single-cell level, and of how neurons process information in a circuit critical for implementing basic behaviours.

Acknowledgments

First and foremost, I would like to thank *Tiago Branco* for his supervision, mentoring and encouragement throughout my PhD, and for taking me on to start with. Thank you for the opportunity to do this project and learn from you.

I would also like to thank the following people:

Sabine Rühle, Ruben do Vale and Vanessa Stempel, to whom I am greatly indebted for the work we've done together on a demanding project, and making it fun no matter how the experiments were going. It has been a great pleasure to be lucky enough to work with friends.

Past and present *Members of the Branco Lab*, for discussions (both scientific and less-so), coffee, fun, and an amazingly friendly and cooperative lab atmosphere.

Gregory Jefferis for his continued support throughout my PhD.

Ian Duguid, Adam Packer, Paavo Huoviala, Sina Tootoonian, Kevin Lloyd, Henry Dalgleish and Christoph Schmidt-Hieber for experimental advice and discussions.

Steve Scotcher and *Phil Heard* of the LMB Mechanical Workshop for building the arenas used in this study.

Kostas Betsios for programming the data acquisition software.

Florian Rau for imparting his typesetting prowess.

And last but not least; my parents, sister, and the rest of my family for their infallible support and encouragement, and in particular Vanessa for proofreading.

Contents

Illustrations

Figures

Tables

Abbreviations

A1	auditory cortex
AHN	anterior hypothalamic nucleus
AOB	accessory olfactory bulb
AOS	accessory olfactory system
aucROC	area under the receiver-operator characteristic curve
BLA	basolateral amygdala
BMA	basomedial amygdala
CEA	central amygdala
ChR2	channelrhodopsin-2
CuN	cuneiform nucleus
dlPAG	dorsolateral periaqueductal gray
dm/cVMH	dorsomedial and central VMH
dmPAG	dorsomedial periaqueductal gray
dmSC	deeper layers of the medial superior colliculus
dmVMH	dorsomedial VMH
dPAG	dorsal periaqueductal gray
DRN	dorsal raphe nucleus
dSC	deeper layers of the superior colliculus
EPSC	excitatory postsynaptic current
FID	flight initiation distance
GABA	gamma-aminobutyric acid
GRIN	gradient refractive index
IC	inferior colliculus
IR	infra-red
LA	lateral amygdala
LGN	lateral geniculate nucleus
lPAG	lateral periaqueductal gray
MEA	medial amygdala
MOB	main olfactory bulb
MOS	main olfactory system
mSC	medial superior colliculus
NMDA	N-Methyl-D-aspartic acid
PAG	periaqueductal gray
PBGN	parabigeminal nucleus
PBS	phosphate-buffered saline
PFA	para-formaldehyde
PFC	prefrontal cortex
PMD	dorsal premammillary nucleus
PPR	paired-pulse ratio
ROC	receiver-operator characteristic
ROI	region-of-interest
SC	superior colliculus
sSC	superficial layers of the superior colliculus
TMT	2,4,5-trimethylthiazoline
V1	primary visual cortex
VGluT2	vesicular glutamate transporter-2
vlPAG	ventrolateral periaqueductal gray
YFP	yellow fluorescent protein

1 Introduction

1.1 The neuroethology of instinctive defensive behaviours

The phenomenon of behaviour gives individual animals the ability to adapt to, and even control aspects of their changing environments on a vastly quicker timescale than evolution by natural selection (Anderson and Perona, 2014). Thus across animal phyla, brains have evolved to generate repertoires of instinctive behaviours that are specialised, yet flexible, conferring fitness to the host.

1.1.1 A historical account of instinct

In the case of humans, the evolution of our brains culminated in a degree of self-awareness that has led us to describe and record the behaviour of other animals.

In his *History of Animals*, Aristotle recorded not only anatomical characteristics, but species-specific behavioural observations ranging from the predatory strategies of different hawks to the reproductive patterns and parental behaviour of fish (Books V,VI,IX, trans. Thompson, 1910). His time at the lagoons of Lesbos led to brilliant observations of marine life; for example, in distinguishing anti-predator responses. He writes:

> "Of molluscs the sepia is the most cunning, and is the only species that employs its dark liquid for the sake of concealment as well as from fear: the octopus and calamari make the discharge solely from fear."

This aspect of Aristotle's work was pre-scientific, but used a detailed and investigative methodology that we could call 'proto-ethological'. However the influence of this way of studying behaviour was overshadowed by his non-religious taxonomy of plants and animals, which Christian scholars further bestowed with God and angelic entities to create the Great Chain of Being (*scala naturae*; ladder of beings). Under this strictly linear view of life, with God at the head of the chain, thinkers understandably attributed the generation of instinctive behaviour to the Creator, as expressed by Thomas Aquinas in the fourteenth century: "...this instinct is planted in them by the Divine Intellect that foresees the future" (Cziko, 2000). The notion of a divine puppet master continued over the following centuries: in the case of William Paley,

his application of the scientific method to making observations of instinctive behaviour, such as egg-laying behaviour of butterflies "which had no teacher in [their] caterpillar state", only strengthened the case for God's pervasion in the natural world (Paley, 1802; Cziko, 2000), and so instinct was simply intelligence by proxy (Browne, 2007). This concept hampered the revolution of evolutionary science and was not overcome until Darwin, and interestingly, progressionist expressions (e.g. 'more highly evolved') are still present even in leading journals of evolutionary biology (1.91% of articles published 2005-2010; Rigato and Minelli, 2013).

The existence of such once-in-a-lifetime reproductive behaviours as the butterfly, with outcomes of which the animal must be ignorant, were the bane of Lamarck's evolutionary theory that critically posited instinctive behaviours as being the learned behaviours of previous generations. Darwin dedicated the seventh chapter of his most famous work (On the Origin of Species, 1859) to instinct, where he was able to explain three particularly challenging examples of innate behaviours in terms of natural selection in order to corroborate his theory[1]; these being the egg-laying behaviour of cuckoos, the slave-making instinct of particular ants, and, the "most wonderful of all known instincts"; the ability of honey bees to create hexagonal combs. On this foundation of seeing instinctive behaviours as adaptations, the discipline of ethology was pioneered by Konrad Lorenz, Nicolaas Tinbergen and Karl Von Frisch towards the mid-twentieth century. Individual behaviours were viewed within the scope of natural selection as biological phenomena, and studied in the animal's natural environment, in contrast with the attention given to the learned components of behaviour in laboratory animals by the predominantly North American disciplines of comparative psychology and behaviourism (Bolhuis and Giraldeau, 2005). In one of the first ethological breakthroughs, published in 1935, Lorenz reported his theory of 'imprinting' to explain the surprising phenomenon that upon hatching many birds do not immediately recognise their own caregiver or even species, and will instinctively bond with the first animal or moving object that they see and eventually learn to treat them as conspecifics. Motivated by his mentor Oscar Heinroth and with the conviction that ethology could be as objective as comparative anatomy (Marler, 2004), he soon after published a monograph comparing twenty duck species bred in captivity, and found that all their species-specific behaviours, such as grunt-whistles in pair-forming or nod-swimming after mating, developed normally and thus appeared instinctive, or innate (Lorenz, 1937, 1941). Innateness became central to Lorenz's ethological concept, and Tinbergen espoused it in his book 'The Study of Instinct' (1951). So far I have been using the terms 'innate' and 'instinctive' to describe behaviour somewhat interchangeably, as these labels have become almost synonymous in modern science, but this was categorically not the case in the past. First, I will follow Tinbergen's definition of 'behaviour' as the "total of movements made by

[1] He did not totally abandon Lamarck's idea of acquired habits being inherited, acknowledging that this may happen, albeit rarely, in his introduction (see Boakes, 2010)

the intact animal" (Tinbergen, 1951). For a definition of 'instinctive', we can turn to Donald Hebb, who said a class of behaviour must be recognised "in which the motor pattern is variable but with an end result that is predictable from acknowledgment of the species, without knowing the history of the individual animal" (Hebb, 1949). This descriptive definition is intuitive and does not presume mechanisms. On the other hand, the definition of 'innate' is controversial, which is immediately apparent in its many different meanings, including "present at birth, a behavioural difference caused by a genetic difference, adapted over the course of evolution, unchanging throughout development, shared by all members of a species, present before the behaviour serves any function, [and] not learned" (Ewert, 2013). Using the term 'innate' to categorise a behaviour, or even a trait, is further problematic as a satisfactory definition cannot be arrived at based on one criterion, and each criterion that has been proposed has logical and scientific flaws (Cassidy, 1979; Marler, 2004; Griffiths, 2009; Mameli and Bateson, 2011). More specifically, a definition requires a binary answer to questions about the behaviour's (presumedly single) underlying cause, whereas in fact the answers likely lie on a continuum (Marler, 2004; Bateson, 2001). Such questions include: is the behaviour genetically determined? Is a process of learning absent? Is it robust in a range of developmental environments? Is it highly heritable? Our current understanding of epigenetics, flexible instinctive behaviours, and the observation that almost all behaviours can be split into component sub-behaviours makes giving stone-cast answers to these questions exceedingly difficult, and at worst, misleading. Clearly, there is neither a rigid question or set of questions across disciplines. For example, Tinbergen defines 'innate behaviour' as "behaviour that has not been changed by learning processes" (Tinbergen, 1951). In response to this accepted definition in ethology, the psychologist Daniel Lehrman made a cogent, direct and extreme criticism of the 'innate' vs 'learned' behaviour dichotomy, emphasising the importance of ignored environmental factors during development in shaping species-specific behavioural patterns, which led him to dismiss the concept of innateness as flawed by its 'preconceived and rigid ideas' (Lehrman, 1953). His critique was highly influential, and led to 'innate' becoming a taboo word even for Tinbergen[2]. For our purposes in neuroscience, it is still heuristically useful to identify highly stereotyped behavioural programs that are present at birth and appear to have a strong genetic basis as innate (for example, defensive behaviours or instinctive learning in songbirds), but we should do so as relativists, and not follow a strict dichotomy that could be counter-productive to finding the neural basis of the behaviour in question.

[2] Lehrman's position apparently led Tinbergen to add a fourth question to Huxley's famous questions for understanding a phenomenon *biologically*, these being the questions of causation or mechanism, of survival value, of evolution, and fourth; of ontogeny (development) (Tinbergen, 1963).

1.1.2 Scientific perspective

How, then, do we get from observing a behaviour to understanding it? I would like to briefly describe the thoughts of others towards tackling this question, which together have influenced the scientific approach of much research, including this thesis. Many people are interested in the link between brain and behaviour, but where should one begin? David Marr theorised that there are three levels of analysis that can be followed to deduce the mechanistic basis of complex systems; the computation (i.e. what is the goal, or computational problem, that is being performed by the system? e.g. a clock counting time), the algorithm (how is this performed in terms of input and output in the system? What are the rules? e.g. increment a counter at a fixed interval) and the implementation (how is the algorithm performed physically? e.g. a pendulum, springs, cogs and energy source; Marr, 1982[3]). Importantly, the strength of this approach is in the relationship between these levels, with each contributing to the interpretation of the others. This helps tease out the conundrum of there being many different possible algorithms for a given problem, while the low-level workings of a system do not easily reveal their function (Schall, 2004). There is a complementary argument for studying behaviours which are within the natural repertoire of the animal, and the importance of using naturalistic stimuli in experiments, which has recently been discussed by Krakauer et al. (2017). The authors argue that when relating recorded patterns of neural activity to behaviour (i.e. 'neural correlates'), behavioural tasks which are too far removed from species-typical behaviours will give correspondingly unnatural activity patterns, and perhaps one would be trying to understand the mapping of an unnatural algorithm to the circuit and cellular mechanisms of the brain. In this research, we have therefore tried to take a top-down, neuroethological approach in understanding the neural generation of an instinctive behaviour, within the constraints of a laboratory setting. We have aimed to understand the behavioural computation first, and bear in mind the perspectives discussed above.

1.1.3 The anti-predation strategies of prey

Predation is likely as old as cellular life itself, and has often been suggested as a driving force in the Cambrian explosion culminating 540 million years ago (Bengtson, 2002). As predation is a constant risk across all stages of life for the vast majority of animals, and successful predation by definition results in the death of the prey and the ultimate cost in not being able to reproduce, its selective importance to evolution is paramount (Nonacs and Blumstein, 2010). This strong

[3] In his book 'The Life of Vertebrates', J.Z. Young writes an earlier synthesis of the kinds of ideas formalised by Tinbergen and Marr, "A wide range of activities, therefore, goes to make up any one type of life, and we shall only appreciate these activities properly if we study that whole life as it is normally lived in its proper environment. The way to study animals or men is, first and foremost, to examine them whole, to see how their actions serve to meet the conditions of the environment and to allow preservation of the life of the individual and the race. Then, with this knowledge of how the animal 'uses' its parts we may be able to make more detailed studies, down to the molecular level, and show how together the activities form a single scheme of action." (Young, 1962)

selective pressure has led to a plethora of morphological, physiological and behavioural defences across prey species.

Even in vertebrates, some adaptive strategies have evolved to be morphological. The optimal defensive strategy for crucian carp is an inducible one, where the presence of pike in the environment causes an increase in body depth to prevent predation by the pike, which are gape-limited predators (Brönmark and Miner, 1992). Further research revealed part of the mechanism of this anti-predator response to be the chemical detection of 'alarm substance' (AS), a chemical stored in a set of epidermal cells which is released only upon physical damage, and is present in the odours of predators that consume AS-containing prey (Pettersson et al., 2000). Morphological changes are also not limited to body shape; for example, sticklebacks develop armour and lateral plates in habitats with high predator density (Abrahams, 2005; Gross, 1978). Fascinatingly, predators can induce transgenerational defences in the offspring of threatened parents. If the water flea *Daphnia cucullatta*, a small crustacean, is exposed to a kairomone of their predator *Chaoborus*, both the generation exposed and the unexposed neonate progeny invariably have larger protective helmets, lowering their capture success much like the carp (Agrawal et al., 1999). It is therefore possible that a run-away "arms race" between prey and predator adaptations and counter-adaptations (Dawkins and Krebs, 1979) could begin very rapidly[4].

Some of the most effective results of such an arms race are physiological, which can be conspicuous or subtle to human observers. To stop an ongoing biting attack or prevent it at close-quarters, many prey produce poisons, which can be internalised like tetrodotoxin in the majority of puffer fish, secreted onto the body, or used at range in a form of defensive attack. The bombardier beetle (of the Carabidae family) uses the latter form, ejecting an aimed 100 °C jet of irritating, even lethal, benzoquinones from a catalysed reaction of hydrogen peroxide and hydroquinones from their abdomen (Eisner and Aneshansley, 1999). As predators can produce their own venoms, physiological mechanisms have evolved to counter them. Californian ground squirrels (*Spermophilus beecheyi*) for example exhibit a surge in venom-binding proteins in their blood serum ten days before emerging from burrows for the first time, and before encountering rattlesnakes (*Crotalus oreganus*; Poran and Coss, 1990), making them highly resistant to rattlesnake venom (Owings and Coss, 2008). Upon encountering a snake, the adult squirrels display tail-flagging behaviour (consisting of side-to-side motion of the upright, piloerect tail) to the predator, and if it approaches, will engage in mobbing behaviour to protect its pups by kicking dirt into the face of the snake. The purpose of tail flagging has only recently been demonstrated:

[4] Predator-prey ecological relationships involve an asymmetric interaction leading to coevolution because the selective pressure of predators on prey species is stronger than vice versa, termed the "life-dinner principle": in a predatory encounter, failure by the predator is a lost meal, while failure on the part of the prey results in it *being* the meal (Dawkins and Krebs, 1979). Darwin seems to be referring to this asymmetry in writing: "Wonderful and admirable as most instincts are, yet they cannot be considered as absolutely perfect: there is a constant struggle going on throughout nature between the instinct of the one to escape its enemy and of the other to secure its prey" (from 'A posthumous essay on instinct' in Romanes and Darwin, 1883).

rather than a form of mobbing or stotting behaviour, it has only recently been revealed to be a vigilance signal to snakes in ambush, conveying that it knows the snakes location and is ready to take evasive action if it strikes (Barbour and Clark, 2012). Intriguingly, the tail flagging behaviour has evolved a physiological element utilising a unique communicative modality in mammals — infrared radiation. Experiments using infrared video and temperature-controlled biorobots have shown that the ground squirrels augment their tail-flagging signals with an infrared component from tail vasodilation only when confronting rattlesnakes which possess infrared-sensitive pit organs, but tail flag without boosting infrared emission when confronting infrared-insensitive gopher snakes (*Pituophis melanoleucus*; Rundus et al., 2007). This adaptation is particularly unexpected as ground squirrels do not use infrared signals for communication between themselves, and open an additional private communication channel only to one species of snake (Rundus et al., 2007; Barbour and Clark, 2012). It has thus has been cited as an pertinent example of how we should consider the animal-centred perceptual world, the *umwelt* (Uexküll, 1957), as paramount to understanding the mechanisms of animal behaviour (Blumstein, 2007).

For prey species, the best form of defence is to avoid an encounter with a predator in the first place. Many well known anti-predator adaptations involve camouflage (crypsis), or mimicry of noxious species, causing predators to fail at detecting or distinguishing potential prey (Barnard, 1983). While many mechanisms are morphological, crypsis and mimicry often depend on behaving appropriately. Appropriate behaviour can increase the effectiveness of morphological adaptations such as camouflage, but in rare cases, motion mimicry is used to imitate other animals entirely. For example, cephlapods are well known to use dynamic camouflage when stationary, but some octopus species such as *Thaumoctopus mimicus* also engage in motion mimicry of flounder fish, capturing both shape and movement pattern across the sea floor, as a primary defence to allow them to forage while avoiding predators (Hanlon, 2007; Hanlon et al., 2008). Amongst nocturnal mammals, locomotion strategies are the primary means of crypsis. Lorises and pottos, nocturnal primates in Asia and Africa respectively, move slowly, silently and without hopping (non-staltatory) in small groups to avoid arousing predators, showing increased olfactory communication and absent vocal communication compared to diurnal primates (Nekaris et al., 2007). Laboratory mice share defensive movement patterns with wild rodents, such as the stretch-attend posture, and avoiding illuminated open spaces much like wild spiny mice, who reduce activity and foraging in open spaces under moonlit nights (Jones et al., 2001). The stretch-attend posture is a risk-assessment behaviour where mice slowly stretch the body forward and orient the head toward perceived danger with the ears forward, and then slowly bob the head to facilitate olfactory and visual detection (Blanchard and Blanchard, 1989a). Although laboratory mice display this behaviour, it is with a reduced frequency compared to wild mice in the open field arenas and elevated plus mazes during exploration (Holmes et al.,

2000; Augustsson and Meyerson, 2004). Gerbils have been shown to display differential activity and foraging patterns following exposure to aerial versus ground predators (Kotler et al., 1992), indicating that defensive movement strategies are predator-specific in rodents.

Despite such strategies to avoid predatory encounters, once they occur the decision of whether to flee or not must be made.

1.2 Escaping from predators

1.2.1 Theory

In the late 1980s, two complementary theories of flight and defensive decisions emerged which have proven particularly influential. The first, published by Ydenberg and Dill (1986), posits an economic model of flight that predicts how balancing the costs of remaining and fleeing interact to produce an optimal distance between prey and predator at which the prey should flee. Their premise is that animals do not necessarily flee as soon as predators are detected, as assumed in much previous literature which equated detection with response, and that during this time period of predator approach after detection, the prey is continually choosing between staying put and fleeing (Ydenberg and Dill, 1986).

Fitness costs associated with flight might include the loss of food resources from decreased foraging (Sih, 1992), alerting further predators through movement, energetic cost[5], and halting other behaviours such as parental, courtship, social and territorial defence, while the cost of remaining is the level of risk of injury or predation, which is affected by factors such as the speed, species and size of the predator, and the preys detectability, fitness, activity level and habitat (Lima and Dill, 1990; Sih et al., 2000; Cooper, 2015). Providing the cost of fleeing outweighs the cost of remaining, the animal will stay put, but as the predator comes closer, the risk and thus cost of remaining increases, while the the cost of fleeing decreases, as the animal has had had more time to engage in survival behaviours and thus increase its fitness. Ydenberg and Dill therefore proposed that animals begin to flee only when these costs are equal, which is the intersection of the curves in Fig. 1.1 and termed the flight initiation distance (FID). The authors note that such decisions are not necessarily made cognitively, but that a computation is performed based on the perceived imminency of threat and the benefits of fleeing versus remaining. Although this graphical model seems deceptively simple, it represents the first successful model of flight behaviour and has amassed useful modifications to predict hiding behaviour (Martin and Lopez, 1999), to optimally predict FID based on fitness maximization rather than cost balancing (Cooper

[5] This energetic cost is composed of repaying oxygen debt potentially incurred from anaerobic respiration and metabolic stress through hormone release (Wootton, 1989; Ramasamy et al., 2015).

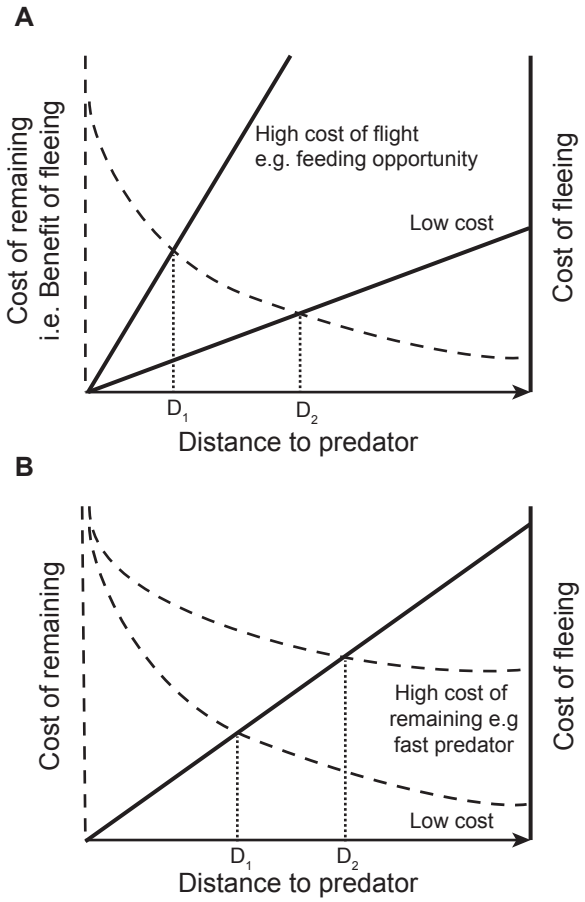

Figure 1.1 Summary of Ydenberg and Dill's (1986) model of flight initiation distance. The intersection of the curves predicts the optimal flight initiation distance (FID) to minimise net cost. **A:** If a predator approaches when there is a high cost of fleeing for the prey, e.g. the prey has a feeding opportunity, the optimal FID (D_1), will be shorter, as the animal will tolerate closer approaches, than if the cost of fleeing is low for the same predatory risk (D_2). **B:** If the cost of fleeing is the same in two cases, but the prey encounters a fast, dangerous approaching predator in one, and a slow predator in the other, the cost of remaining will be high even at long distances for the fast predator and thus the FID will be longer (D_2). Modified from Ydenberg and Dill (1986) and Nonacs and Blumstein (2010).

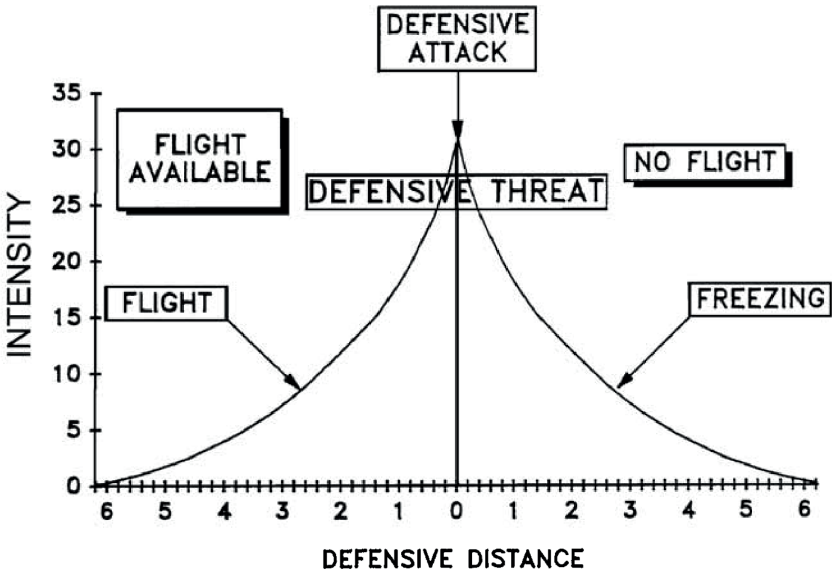

Figure 1.2 Summary of Blanchard and Blanchard's (1989) model of defensive behaviour as a function of defensive distance and the availability of an escape route. When flight is possible (left side) it is the dominant behaviour, and as a predator approaches it becomes more rapid. Shorter defensive distances lead to defensive threat behaviour such as vocalisations in rats, while jump attacks and biting are predominant as the predator approaches physical contact. When flight is not possible (right side), freezing responses become dominant. Modified from Blanchard and Blanchard (1989b) and McNaughton and Corr (2004).

and Frederick, 2007) and to account for behaviour at very short and long distances (Blumstein, 2003).

The second graphical model, by Blanchard and Blanchard (1989b), aims to explain the choice and intensity of multiple defensive behaviours as a joint function of threat level and the availability of escape. From their studies of wild rats in a laboratory setting (Blanchard et al., 1986), the authors provided a useful framework for understanding how a threatening stimulus and the environment drive different defensive behaviours, such as escape, freezing, defensive attack and threatening behaviour towards the predator (Fig. 1.2). Defensive distance is considered as the distance between predator and prey, but later came to be thought of as an internal, or cognitive, construct of perceived threat intensity (McNaughton and Corr, 2004). Depending on the ability to flee, for example whether an escape route or shelter is available, rats are biased towards displaying flight or freezing behaviour in the model, with an intensity (i.e. rapidity, or time spent) that is a function of the defensive distance.

1.2.2 Ethology of escape

Recently, laboratory experiments from our group have demonstrated that mice rapidly learn about the both the availability and location of a shelter in the environment, which enables first the selection of flight or freezing in response to a given threatening stimulus, and the subsequent computation of an escape vector to accurately reach an underground shelter in a maze (Vale et al., 2017). This suggests that flight in rodents is a flexible behaviour, and depends on dynamic knowledge of the spatial environment. In this section, I will discuss the characteristics of escape behaviour across species paying particular attention to rodents.

An escape response can mean diverse behaviours such as flight (e.g. in mammals), take-off (birds or flying insects), a C-start turn (fish), or a tail-flip (crayfish). Although escape reflexes exist, they have long been shown to be plastic (Krasne and Wine, 1975) rather than hard-wired and stereotypic, and in fact, complex escape responses also occur within the same animals. Each is composed of sequential, distinct behavioural events, such as the stages of take off in *Drosophila* (Card and Dickinson, 2008) or the movement components of flight in mice (see Chapter 3), which show plasticity in their selection and execution. For example, chaffinches display freezing behaviour before escape depending on whether the threat is a sparrowhawk or woodpigeon (Cresswell et al., 2009), while the turning speed and acceleration of escape in prey sharks is modulated by the speed, size and approach orientation of apex predators (Seamone et al., 2014).

In wild desert rodents, the locomotor mode and tactics of escape vary both across species and within species depending on habitat. While all being capable of different locomotor modes, the South American grass mouse (*Akodon molinae*) tends to use quadrupedal running during escape, but gerbil mice (*Eligmodontia typus*) and leaf-eared mice (*Graomys griseoflavu*) show equal frequencies of escapes using quadrupedal running, and bipedal hopping, which permits more rapid acceleration and direction changes. Interestingly, gerbil mice from different microhabitats show different proportions of hopping and running escapes depending on the afforded plant cover, and in open habitats sometimes display zig-zagging escape trajectories, while leaf-eared mice incorporate right-angle turns in theirs, neither of which was observed in the grass mouse (Taraborelli et al., 2003).

By definition, instinctive defensive behaviours do not require a learning process to assign a valence of danger to a threat, but despite this, prior experience can alter escape. One potential reason for this is that escape is energetically costly, so there may be selective pressure for prey to adjust their escape response to match the degree of threat posed by predators. By conditioning juvenile coral reef fish (spiny chromis; *Acanthochromis polyacanthus*) to the sight or odour of sound a predator (Dottyback fish; *Pseudochromis fuscus*), and providing a damage-released chemical alarm cue from conspecifics, the kinematics of fast-start escape (induced by a mechanical cue)

were potentiated, increasing the speed, acceleration and distance travelled while reducing the latency to escape (Ramasamy et al., 2015[6]).

Small body-sized prey like mice are particularly vulnerable to aerial predators, and recent work has focused on using simple, innately-threatening visual stimuli presented overhead to evoke escape in mice. It appears that the mouse has evolved a 'generalised' defensive response to overhead threats. This is similar to an innate avoidance response that mice and rats exhibit to 2-phenylethylamine, a carnivore-specific odour component, which does not require identification of the exact predator species (Ferrero et al., 2011; Fendt, 2006). For some overhead visual threats however, the elicitation of a defensive response is seemingly irrespective not only of the identification of a predatory species but does not require the identification of the threat as an animal. When a predator or object approaches an animal in its line of sight, it forms a distinct visual feature on the prey's retina of outward, expanding motion. This visual cue has been shown to evoke escape or defensive responses in animals across phyla, including insects (flies, praying mantids, locusts), crustaceans (crayfish), birds, frogs, fish and mammals (mice, primates including humans; Peek and Card, 2016). Yilmaz and Meister (2013) found that mice readily elicited escape responses (and less often, freezing) to such dark expanding disks against a grey background above an arena, whereas they rarely escaped to light expanding disks, and only displayed investigative rearing behaviour to white receding spots or static disks. Interestingly, these escape responses were low latency (<250ms), which limits the amount of time for processing in this sensory-motor loop, as noted by the authors. When they occurred, freezing events were unitary and prolonged (>9s), in contrast to short bouts of freezing with interspersed movement which mice perform in response to a ground predator like a rat (Griebel et al., 1996). This hints that the evoked behaviours are indeed defence mechanisms against predators, rather than simply against approaching objects (against which they argue that freezing would be of little value[7]), and that the responses are specifically against aerial predators based on the characteristics of freezing, which would serve to remove both visual motion for the predator seeking its target and any movement-induced noise. In the next section, I will introduce the candidate circuits which may underly this escape behaviour, with emphasis on the midbrain which is identified as critical in this thesis.

[6] This example is somewhat problematic, as the innate response was altered with experimenter-directed associative learning, and thus the behaviour may be notionally generated through independent neural mechanisms for learned fear.

[7] Although one could argue that freezing could make an object miss the animal if it was on a perfect collision course.

1.3 Circuits for defensive behaviour

Neural defensive systems have evolved across species to generate this plethora of escape behaviours, such as the Mauthner system in fish (Abrahams, 2005), and the giant and non-giant fibre systems of invertebrates (Herberholz and Marquart, 2012; Peek and Card, 2016; De Vries and Clandinin, 2012), but they are beyond the scope of this thesis. In this section, I will describe the mammalian defensive system with a focus on instinctive defence, and introduce its circuit elements. This includes a more detailed account of the midbrain, which is thought of as a critical region in generating defence and is the subject of much current research aimed at elucidating its precise role in escape.

1.3.1 The amygdala and hypothalamic systems

The mammalian brain appears to have parallel, mostly separate pathways for processing defensive responses to different types of threats; these being against predators, against aggressive individuals of the same species (conspecifics), and of learned fear involving pain (Gross and Canteras, 2012, Silva et al. 2013). We do not know whether non-human animals experience states of consciousness like the human feeling of being afraid, and instead by convention, the term 'fear' is also applied in neuroscience to the brain systems involved in threat detection and responding to danger defensively (LeDoux, 2014). 'Innate fear' describes defensive responses which occur to stimuli that the animal has not associated with harm through experience or a learning process, which might, but not necessarily, be predators, pain, conspecifics, heights or other dangers in the environment (Silva et al., 2016a; Blanchard and Blanchard, 1989b). In rodents, these parallel pathways can exist in distinct nuclei of common brain regions, for example; different elements of the medial hypothalamic zone are activated during different types of fear response (Dielenberg et al., 2001, Canteras et al., 1994), and the interactions between these pathways are under intense investigation (Isosaka et al., 2015). The sensory modality of the perceived threat, however, appears to further define the pathways which are activated to drive a defensive response, and this thesis presents evidence of a 'shortcut' pathway for imminent visual and auditory threats which is influenced by, but does not require, some of these circuit elements.

A large body of literature has implicated the amygdala as a key brain region in learned and innate fear behaviour, so much so that this highly differentiated region is often considered the brain's 'emotion centre' (LeDoux, 2000, 2003; Mcgaugh, 2004; Fox et al., 2015). Anatomically, it is partitioned into a cortical region comprised of the cortical, lateral (LA), basolateral (BLA), and basomedial amygdala (BMA) nuclei, and a striatal region, including the medial (MEA) and central (CEA) amygdala, and there are thought to be specific roles for these different nuclei in fear and olfactory processing (Swanson and Petrovich, 1998; Gross and Canteras, 2012).Rodents use

olfactory signals to identify threats and guide their behaviour, with the amygdala constituting the second major node in this process after olfactory detection. Interestingly, partial divergence in the responsible defensive circuits already begins at the sensory level, with the main olfactory system (MOS) detecting a wide-range of innate and learned volatile odours via the main olfactory bulb (MOB; Kobayakawa et al., 2007), while the accessory olfactory system (AOS) is more specialised for the detection of non-volatile kairomones and pheromones (from predators and conspecifics respectively) via the vomeronasal organ (VNO) and accessory olfactory bulb (AOB; Takahashi, 2014; Papes et al., 2010; Isogai et al., 2011; Silva et al., 2016a; Stowers and Kuo, 2015). A volatile molecule derived from fox faeces, 2,4,5-trimethylthiazoline (TMT), has been identified as a potential predator signal (Rosen et al., 2015[8]) and widely exploited in laboratory studies. This has revealed that, while TMT induces activity in the MEA and CEA (Day et al., 2004), it is primarily the cortical amygdala that is activated by TMT via a connection from the MOB, and that this projection is necessary and sufficient for TMT-induced aversive defensive behaviours (Root et al., 2014). The MEA, meanwhile, receives input from the AOB and has been shown as critical region for defensive behaviours in response to threatening odours from both conspecifics and predators, as well as live predators (Martinez et al., 2011[9]), in lesion studies and activity mapping studies using the immediate-early gene *c-Fos* (Motta et al., 2009; Li et al., 2004; Blanchard et al., 2005; Silva et al., 2016a). Consistent with the idea that there are parallel defensive circuits, rats exposed to a natural predator or its odour show preferentially high activation in the posteroventral part (pvMEA; Dielenberg et al., 2001), while the posterodorsal part (pdMEA) is more active in response to aggressive conspecifics in hamsters (Kollack-Walker et al., 1999). Exposure to a live predator also activates the LA and posterior BMA in rats, while lesioning these areas reduces defensive responses (Martinez et al., 2011). As these nuclei receive projections from higher-order (but not primary) visual and auditory cortical areas consistently across mammals (Mcdonald, 1998), it has been suggested that they may play a role in integrating sensory cues across modalities (Gross and Canteras, 2012). Decades of research has shown that amygdala is vitally important for learned fear, and the nuclei involved in associative learning between conditioned and unconditioned stimuli, as well as the expression of related defensive behaviours, seem largely distinct from those mediating innate fear (Tovote et al., 2015). The LA is a necessary site for this associative learning, as demonstrated by lesions or pharmacological inactivation which prevent both the acquisition and the expression of conditioned fear to footshocks, using olfactory, visual or auditory cues (LeDoux, 2000; Johansen et al., 2011; Tovote et al., 2015). It also appears to be involved in the conditioned fear related to predators (Gross and Canteras, 2012), and projects to BLA and CEA.

[8] See Buron et al., 2007; McGregor et al., 2002 and Apfelbach et al., 2005 for discussion of whether it is a generally aversive, or even noxious, signal.

[9] MEA lesions reduced displays of freezing, crouch sniffing and stretch-attend postures in response to cat exposure but escape behaviour was not assessed.

Disruption of the CEA selectively blocks the expression of conditioned fear to footshocks, while it is thought to leave conditioned fear to predators intact (Martinez et al., 2011) as this is thought to be mediated by the MEA (Gross and Canteras, 2012). In a recent study investigating the interaction between innate and learned olfactory threat processing, it has been shown that a population of CEA neurons expressing the serotonin-2A receptor (Htr2a gene) show selective activity suppression in response to innately aversive odours, and that inhibition of these neurons upregulates innate defensive responses over learned ones (Isosaka et al., 2015). This suggests that a subpopulation of the CEA may play a role in generating a hierarchy of innate and learned fear when faced with conflicting threats, as well as generating innate freezing responses via the vlPAG (Haubensak et al., 2010; Tovote et al., 2016).

This parallel structure of threat processing is continued in a downstream group of highly interconnected hypothalamic nuclei, termed the 'medial hypothalamic defensive system'. This system comprises the anterior hypothalamic nucleus (AHN), the dorsomedial part of the ventromedial hypothalamus (dmVMH), and the dorsal premammillary nucleus (PMD) for responding to predatory threats (Silva et al., 2016a; Canteras et al., 1997; Wang et al., 2015; Kunwar et al., 2015), while anatomically distinct parts of the same nuclei control defensive and aggressive responses to conspecifics (Silva et al., 2013; Lee et al., 2014; Motta et al., 2009; Yang et al., 2013). These nuclei are proposed to integrate threat information and orchestrate defensive behaviour at a more direct level than the amygdala (Canteras, 2002; Sternson, 2013), but they have alternatively been proposed to function as a relay between the amygdala and brain areas controlling autonomic, behavioural and endocrine responses (LeDoux, 2000) and the VMH in particular has been described as a motivation centre (Kunwar et al., 2015) and has been shown to be required for the acquisition and recall of memories related to predatory fear (Silva et al., 2016b). The medial hypothalamic defensive system is well placed to orchestrate defence: the VMH receives strong innervation from the MEA, further input from the BMA which may constitute processed sensory information (Canteras, 2002; Silva et al., 2016a) and there are topographic projections from subregions of the VMH to areas in the PAG (Dielenberg et al., 2001, Canteras et al., 1994) which is considered as a final output for defensive behaviours and is discussed in detail in the following section. Accordingly, artificial activation of the dmVMH in rodents and cats can promote motor and autonomic responses which resemble behaviour when apposed to natural threats (Hunsperger, 1956; Canteras et al., 1997; Canteras, 2002; Blanchard et al., 2005). Furthermore, the observations that electrical stimulation of the dmVMH in humans elicits panic attacks (Wilent et al., 2010), and attack and flight responses in non-human primates (Lipp and Hunsperger, 1978), suggests that a role for the VMH in fear and defence is conserved in mammals.

Recently, a number of groups have aimed to deconstruct the role of the VMH in defensive behaviours using refined manipulations on a population of neurons restricted to the dorsomedial

and central VMH (dm/cVMH), which express the transcription factor steroidogenic factor 1 (SF-1; also known by its encoding gene, Nr5a1) and constitute about two-thirds of all cells in this region (Dhillon et al., 2006; Kunwar et al., 2015). After optogenetic activation of this dm/cVMH population (Lin et al., 2011) was shown to elicit immobility or flight in mice (in line with past region-wide electrical and chemical activation studies; Hess and Brügger, 1943; Brown et al., 1969; Lipp and Hunsperger, 1978), Silva et al. (2013) reported that silencing of the same neurons with the pharmacogenetic tool hM4D caused a reduction in certain defensive behaviours to a rat, namely immobility and stretch postures, but not to other types of threats, such as an aggressive conspecific or footshocks, thus confirming that the dm/cVMH is preferentially involved in predatory threat-related behaviours. In addition to immobility, further optogenetic activation experiments in SF-1 neurons showed that they can drive avoidance behaviour, autonomic responses, and increase the frequency of running and escape-jumping events, albeit with a long latency from stimulation onset (mean latency >20s at 20Hz stimulation frequency; Wang et al., 2015). To see if particular pathways mediated these different responses, the authors then selectively stimulated SF-1 axons terminating in the PAG and the AHN, which are the two principal output centres of the VMH (at least two-thirds of all dm/cVMH cells project to them), while blocking voltage-gated sodium channels in the VMH to prevent antidromic spiking. In the PAG, dm/cVMH axons are concentrated in the dorsal half rostrally, and both dorsal and ventral halves more caudally. Surprisingly, they found that the VMH-AHN projections induced avoidance, running and escape jumping, but never immobility, while the VMH-PAG collateral projections only induced immobility (Wang et al., 2015). As the AHN projects to all PAG subdivisions (Vianna and Brandão, 2003), and also projects to the PMD (Comoli et al., 2000) (lesions of which have been shown to reduce escape responses in rats to cats; Canteras et al., 1997), it is thus plausible that artificially activated SF-1^{+} neurons could evoke escape via a multisynaptic pathway to the PAG, or SF-1^{-} neurons via a connection to the PAG. However, the very long latencies between stimulation and evoking these behaviours suggest that these pathways are unlikely to be critical during short duration predator-prey interactions where escape must be initiated quickly, and instead the VMH appears to drive a general defensive state which is necessary for some but not all predator interactions. This is supported by experiments by Kunwar et al. (2015), that show persistent defensive responses to SF-1^{+} neuronal activation, including escape responses only after prolonged stimulation or at stimulation offset, and demonstrate their necessity to live predator avoidance behaviour and conditioned fear. Strikingly, genetic ablation of these neurons did not affect escape responses to innately aversive overhead visual stimuli (Kunwar et al., 2015).

1.4 The midbrain defensive system

Two key areas in defensive behaviour are the PAG, which is considered a final integrator of defensive behaviour as it receives input from the amygdala and VMH directly, and the SC, a multi-sensory region which plays a prominent role in visually guided behaviours. These brain regions are the focus of this thesis, and will be described in general before discussing their role in defensive behaviour.

1.4.1 Overview of the periaqueductal gray

The periaqueductal gray (PAG; also known as the central gray or substantia grisea centralis) is an elongated structure extended along the rostrocaudal axis of the midbrain, which is highly conserved across vertebrate species (Linnman et al., 2012), even in jawless fish (Olsson et al., 2017). Although it is considered a key neural circuit involved in defensive behaviours (Bandler and Carrive, 1988; Brandao et al., 1999; Dean et al., 1989), it is also critically involved in a variety of basic functions including pain processing and modulation, lordosis, micturition, vocalisation and autonomic functions such as cardiovascular regulation (Depaulis and Bandler, 1991; Behbehani, 1995). The precise roles and mechanisms of action of the PAG in relation to some of these behaviours is now beginning to be understood at a physiological level (Han et al., 2017; Tovote et al., 2016; Franklin et al., 2017; Ozawa et al., 2017).

The PAG is not a homogeneous structure. In fact, it is divided into four parallel columns named according to their location in respect to the aqueduct (dorsomedial, dmPAG; dorsolateral, dlPAG; lateral, lPAG and ventrolateral, vlPAG) (Fig. 1.3; Benarroch, 2012; Mantyh, 1982). Its different functional modules can be broadly mapped onto the columnar structure of the PAG and along its longitudinal axis, with defensive behaviours being controlled by the rostral part of the dorsal PAG (dPAG, comprising dmPAG and dlPAG, which appear to be strongly inter-connected; Schenberg et al., 2005), and the vlPAG. Cytoarchitecturally, the PAG is similar across mammals and contains mostly small- to medium-sized neurons (5-40 µm in diameter), with soma size increasing with distance from the aqueduct, which are of fusiform, triangular, and stellate-shapes and possess 2 to 7 dendrites that are generally oriented in the coronal plane (Mantyh, 1982; Beitz, 1985; Keay and Bandler, 2004). Furthermore, the existence of dendritic spines has been demonstrated in the rat and cat (Gioia et al., 1998), although these are thought to be scarce (Buma et al., 1992). All the major glutamate receptor types are present in the PAG, including AMPA/kainate, NMDA and metabotropic receptors (Albin et al., 1990), while $GABA_A$ receptors are also present in a high density. The principal excitatory transmitter is glutamate, with roughly equal numbers of glutamatergic and GABA-ergic neurons, and it appears that many GABA-ergic neurons are tonically active interneurons (Chiou and Chou, 2000).

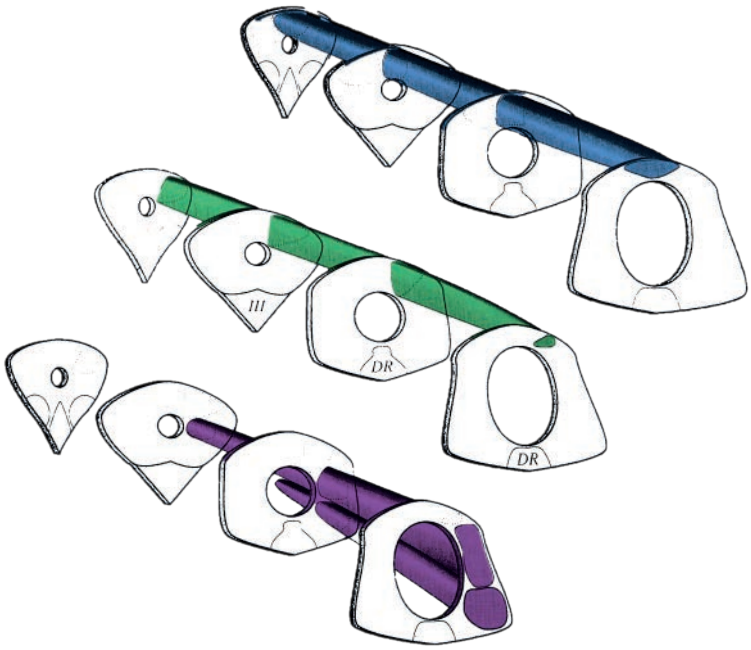

Figure 1.3 Columnar structure of the periaqueductal gray. The shaded area represents the extent of the dorsomedial PAG (top), dorsolateral PAG (middle), which together form the dPAG, and lateral/ventrolateral PAG columns (bottom), within the (from left to right) rostral PAG, the rostral intermediate PAG, the caudal intermediate PAG and the caudal PAG. Modified from Depaulis and Bandler (1991).

The PAG receives inputs from several brain areas which are differentially distributed to its subdivisions. The most prominent inputs to the dPAG are the PMD, inferior colliculus (IC), VMH, prefrontal cortex (PFC), cuneiform nucleus, nucleus prepositus hypoglossi, dorsal raphe nucleus (DRN), while the ventral PAG (vlPAG and lPAG) receives spinal afferents (including trigeminal, consistent with its role in pain processing), central and medial amygdalae, the medial hypothalamic system (An et al., 1998; Floyd et al., 2000; Beitz, 1982, 1989; Schenberg et al., 2005; Franklin et al., 2017). Anatomical tracing experiments suggest that the SC connects to the PAG, although this connection and its properties have yet to be demonstrated functionally using electrophysiology (An et al., 1998; Floyd et al., 2000; Mantyh, 1983; Canteras, 1992). Recently, cell-type specific rabies tracing in the dPAG has revealed that glutamatergic cells alone, and not inhibitory neurons, receive cortical input (Franklin et al., 2017). In turn, the PAG has ascending projections to the hypothalamus and thalamus, and descending projections to the medulla, while there are prominent dPAG projections to the cuneiform nucleus, parabrachial nucleus and locus coeruleus, and a lack of direct medulla efferents (Cameron et al., 1995; Redgrave et al., 1988; Keay and Bandler, 2004; Schenberg et al., 2005). To elicit motor responses, the PAG must ultimately engage with spinal motor circuits, but it is not yet known how this occurs to generate defensive responses. Spinal motor circuits could be activated by direct innervation of the spinal ventral horn, or indirectly, perhaps via its projections to the pre-motor lateral reticular nucleus

and inferior olive (the sole source of cerebellar climbing fibres), thus engaging the cerebellum (Koutsikou et al., 2014, 2017; Tovote et al., 2016).

1.4.2 The periaqueductal gray and defensive behaviour

There is mounting evidence that the PAG acts as the final common pathway for initiating defensive behaviours in response to fearful stimuli (Mongeau et al., 2003, Bittencourt et al., 2004). This was first suggested by Hunsperger (1956), who showed that electrical stimulation of the hypothalamus or amygdala that caused hissing and flight in cats could be suppressed by lesioning the PAG, while stimulation of the intact PAG elicited these responses even after extensive amygdala or hypothalamic lesions (Hunsperger, 1956; De Molina and Hunsperger, 1962). Lesions of the PAG in laboratory and wild rats were subsequently shown to decrease and even abolish defensive behaviours, including flight, freezing and defensive attack, in response to unconditioned threats from conspecifics, humans, and predators (Halpern, 1968; Blanchard et al., 1981). In rats, c-Fos mapping studies revealed that the PAG, and the dorsolateral subregion (dlPAG) in particular, shows high activation when the animal is exposed to a live cat or predator odour (Cezario et al., 2008; Sukikara et al., 2010; Canteras and Goto, 1999; Comoli et al., 2003). In keeping with its asserted role as a final integrator for different modes of threat, the PAG also shows high levels of c-Fos in response to innately aversive sounds (Mongeau et al., 2003), aggressive conspecifics (Motta et al., 2009) and footshock stimuli (Silva et al., 2016a). Electrical and neurochemical stimulation studies of the dlPAG and dmPAG elicits strong flight responses in cats and rats (Bittencourt et al., 2004; Vargas et al., 2000) whereas stimulation of the vlPAG produces immobility and freezing (Behbehani, 1995; Tovote et al., 2016). Similarly, in human patients, electrical stimulation of the dPAG produces a sensation of fear, panic and impending death(Nashold et al., 1969; Amano et al., 1978, 1982; De Oca et al., 1998) indicating that defensive and fear-like functions of the PAG are highly conserved. However, there is debate over the extent to which the PAG can be considered part of the fear processing circuit, versus an independent executor of defensive action. For example, in rats, dPAG activation can act as an unconditioned stimulus in Pavlovian fear learning (Di Scala et al., 1987; Johansen et al., 2010; Kincheski et al., 2012; Kim et al., 2013; Motta et al., 2017) and neural correlates of fear conditioning in the dPAG have been observed (Watson et al., 2016). The putative circuit underlying this possible role for the dPAG in fear learning consists of ascending projections from dPAG to the PMD (via the AHN and lateral hypothalamic area), which targets the ventral part of the anteromedial thalamic nucleus (AMv; Motta et al., 2017). Interestingly, pharmacological inactivation of AMv reduces contextual fear responses to both predator-associated, and social defeat-associated environments (Carvalho-Netto et al., 2010; Rangel et al., 2018), perhaps by virtue of its amygdalar and hippocampal connections (Motta et al., 2017). While this suggests a potential role for the dPAG in fear memory, in mice

however dPAG inhibition only affects the expression of defensive behaviours to acute predatory encounters and not learned foot-shock or predatory contexts (Silva et al., 2013, 2016b), arguing against its inclusion as part of the fear memory circuit of the brain[10]. It is therefore not currently known whether such differences reflect variation in the PAG function across species, or is a result of experimental design factors (Silva et al., 2016b); this question which could be resolved by further activity monitoring experiments during behaviour, or activity manipulations aiming to recapitulate endogenous activity levels to complement previous activation studies, as another explanation for this discrepancy could be that activation experiments may over-estimate the role of the dPAG in fear learning, for example by artificially recruiting higher fear circuits in a different manner to physiological activation during natural behaviour[11].

Over the past decades, activation studies have given rise to the idea that the dmPAG, dlPAG and lPAG are involved in the 'active' defensive responses of escape, defensive attack, tachycardia, hypertension and freezing[12], while the vlPAG initiates 'passive' responses such as quiescent behaviours (freezing or immobility), analgesia, bradycardia and hypotension (Depaulis and Bandler, 1991). While the vlPAG has been shown to mediate freezing behaviour in response to conditioned stimuli (De Oca et al., 1998; Fanselow, 1994; Fanselow and DeCola, 1995), attributing the generation of freezing behaviour in response to innately threatening stimuli to a particular PAG column has been contentious. Lesions of the vlPAG which disrupt conditioned freezing do not affect freezing or flight elicited by dlPAG stimulation in the rat (Vianna et al., 2001)[13], suggesting that the vlPAG is only involved in conditioned freezing, while unconditioned freezing may be controlled by the dPAG. Recently, Silva et al. (2013) targeted neurons in dPAG using the inhibitory pharamacogenetic tool hM4D (under the Synapsin-1 promoter), and found that this decreased immobility and stretch posture behaviours in response to a live rat or aggressive conspecific, but not in response to footshocks, demonstrating not only that the dPAG is important for the expression of defensive behaviours against predatory and social threats, but also suggesting that innate freezing may be mediated by the dPAG. It seems that freezing evoked by dmVMH stimulation is mediated by a dmVMH-dlPAG projection (Wang et al., 2015), further supporting this idea. Experiments by Tovote et al. (2016), however, have shown that optogenetic inhibition of vlPAG VGluT2^{+} cells strongly reduced freezing behaviour to both conditioned stimuli and an innately aversive robotic snake. Alternatively we can speculate that there could be several modes of freezing-like behaviour which appear qualitatively similar but which have different circuit mechanisms and behavioural roles. For example, freezing as an initial defensive response when

[10] Although Deng et al. (2016) report that dPAG optogenetic activation in mice causes avoidance of a stimulation area that is persistent after 24hours, it appears that overlying SC could also have been activated, confounding the interpretation.
[11] But see Kincheski et al. (2012) for evidence that low levels of dPAG activation favour the formation of a US-CS association more successfully than high levels of stimulation that result in vigourous defensive behaviours.
[12] Freezing has not been commonly observed across research groups as the initial behaviour evoked by stimulation, but freezing frequently follows evoked escape.
[13] However, it can be argued that the lesions presented in this study are not extensive enough to entirely discount the idea.

shelter is unavailable may not invoke the same circuits as immobility during risk-assessment in the presence of a predator, which could be different again to 'post-escape' freezing which occurs when an animal reaches a safe location. Interestingly, pharamacogenetic inhibition of excitatory and inhibitory neurons in the dPAG (expressing VGluT2 and Gad2 respectively) has shown that only VGluT2$^+$ neurons are involved in social avoidance of conspecifics, quantified as the time spent investigating an aggressor (Franklin et al., 2017), which demonstrates that a cell type-specific dissection of behavioural function in the PAG may be achievable.

Defensives responses have also been reported using optogenetic activation of excitatory dPAG cells in mice, which seem qualitatively similar to responses evoked by electrical and neurochemical stimulation[14]. Optogenetic activation of VGluT2$^+$ cells in the dl/lPAG of mice causes flight and an intermediate level of freezing in comparison to the vlPAG (Tovote et al., 2016; Assareh et al., 2016). Stimulus-locked flight, and post-stimulation freezing and avoidance behaviours have also been reported using CaMKIIa$^+$ cell activation in the dPAG, with the speed of evoked running and length of freezing increasing with increasing frequency or intensity of stimulation (Deng et al., 2016). Recordings in freely-moving animals have begun to reveal the how these behaviours may be generated by endogenous neural activity in the PAG. In a fear conditioning assay, rat dlPAG cells have been shown to fire selectively during periods of increased movement speed and flight behaviour in response to conditioned stimuli, but not when immobility was induced by the same stimulus (Halladay and Blair, 2015). dPAG cells have also been shown to be responsive to cat odour, and considerably more so than vPAG cells (Watson et al., 2016). Similarly, when mice are exposed to a segregated rat, dPAG cells spike when the mouse investigates the rat while demonstrating stretch-attend postures, and a largely separate population is active when the animal flees (Deng et al., 2016). As risk assessment has not previously been reported in any dPAG activation experiments, and the recorded flight/risk-assessment populations were largely non-overlapping, it seems likely that there are sub-populations of cells which are specifically involved in different defensive behaviours in the PAG which are not possible to dissociate in current manipulation experiments, and that higher levels of cell-type specificity in future experiments, perhaps based on afferent or efferent targets or novel genetic markers, may further our understanding of how the PAG performs diverse behavioural functions.

1.4.3 Overview of the superior colliculus

The mammalian superior colliculus is a laminated midbrain structure that acts as a major centre for visual and multisensory processing, and further integrates cognitive and motor

[14] Electrical stimulation is indiscriminate in terms of cell identity and can activate fibres of passage, while neurochemical stimulation has poor time resolution, and only provides specificity in regards to the receptor composition in a brain region, thus optogenetic tools provide a valuable manipulation to further deconstruct the behaviours in terms of cell types in a given region.

information to drive behaviours including orienting movements towards or away from objects (Gandhi and Katnani, 2011), but exactly how this occurs at a neuronal and network level is a mystery. Together with its non-mammalian homologue, the optic tectum, it is conserved in vertebrates, but the weighting of its sensory inputs and the exact repertoire of its functions varies in relation to the importance of a particular modality to a species: for example, the rat SC receives more trigeminotectal connections than in monkeys (May, 2006), and SC stimulation can evoke whisker and pinnae movements (Hemelt and Keller, 2008), reflecting the greater dependence on whisker-based somatosensation in rodents, such as in aiding prey capture (Favaro et al., 2011).

Structure and anatomical connections of mammalian SC The SC is composed of seven layers with distinct cyto- and myeoarchitectures, which can be grouped by their functions and connections into the superficial (sSC, comprising zonal, SZ; superficial grey, SGS, and optic layers, SO) and deep compartments (dSC, comprising intermediate grey, SGI; intermediate white, SAI; deep grey, SGP, and deep white layers, SAP; Sparks and Hartwich-Young, 1989). The superficial layers are primarily visual sensory (Dräger and Hubel, 1976), and receive direct retinal innervation via the SO layer which is species-dependent in density: from between 70-90% of retinal ganglion cells in the mouse, to 50% and 10% in cats and primates respectively (May, 2006; Ellis et al., 2016). Further visual input is provided by the LGN and visual cortex (Edwards et al., 1979). The constituent cell types of the SC are not well understood except perhaps morphologically, while an appreciation of how electrophysiology, morphology and in particular, genetic markers, are related to processing has only been attempted by one study to the best of my knowledge (Gale and Murphy, 2014). In the sSC, five classes of cells have been generally agreed based on somatodendritic morphology (May, 2006), which is reduced to four classes when electrophysiological characteristics are considered (Gale and Murphy, 2014), while screening of possible genetic markers has identified ten putative classes (Byun et al., 2016). The four principal sSC classes appear to be wide-field (WF), narrow-field (NF), horizontal and stellate neurons (May, 2006). Interestingly, only NF cells send their axons into the dSC, while other classes send projecting axons to the lateral geniculate nucleus (LGN), the lateral posterior nucleus of the thalamus (LP; also called the pulvinar) and the parabigeminal nucleus[15] (Gale and Murphy, 2014) as well as presumably synapsing within SGS. dSC cell types on the other hand appear more heterogeneous, with many multipolar cells, including some which send their dendrites up into SO and even SGS thus providing a further means for sSC and dSC to connect other than the NF cells, or perhaps synapse with retinal axons directly (Mooney et al., 1992). In further contrast to the primarily visual sSC, the dSC

[15] The midbrain parabigeminal nucleus (PBGN) is a visual area that has been described as a satellite nucleus of the SC, as it receives little input from sources other than the sSC and none from other visual structures (Graybiel, 1978), and projects back to the SC (Usunoff et al., 2007; Baleydier and Magnin, 1979; Jiang et al., 1996). Interestingly, its function in visual processing is not yet clear. PBGN cells have similar visual response characteristics to the SC in the cat, although it can fire at faster frequencies and appears less velocity and direction selective than the SC (Sherk, 1979).

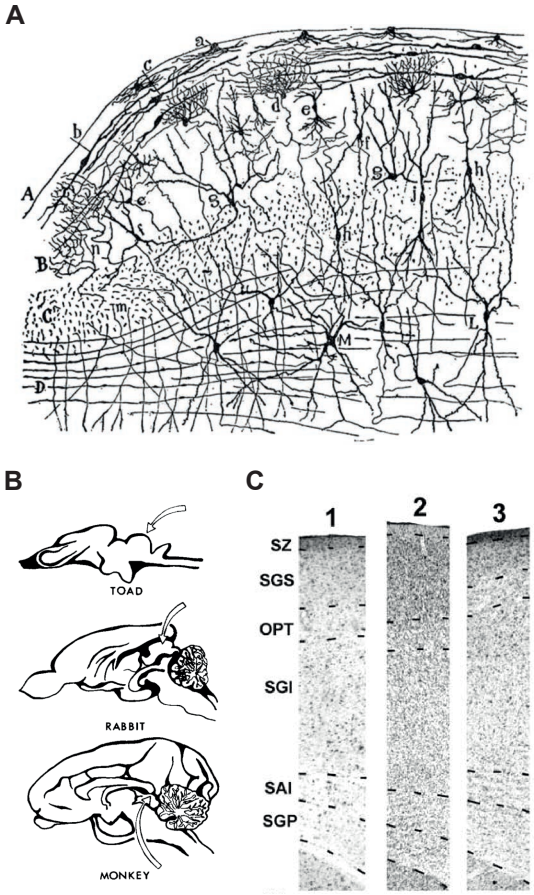

Figure 1.4 Structure of the superior colliculus. **A:** Drawing by Santiago Ramón y Cajal of neurons in a coronal section of rabbit superior colliculus, stained using the Golgi method, showing a diversity of cell types and dendritic branching in one hemipshere. Taken from Ramón y Cajal (1909) reprinted in Isa and Hall (2009). **B:** Sagittal sections of toad, rabbit, and monkey brain, with arrows showing the location of superior colliculus and its non-mammalian homologue, the optic tectum. This structure is conserved across species, but with a significant difference among these species in the relative amount of brain tissue devoted to the colliculus and telencephalon. Modified from Schiller (1984). **C:** Vertical slices showing cytoarchitecture of the superior colliculus in the SC of cat (1), squirrel (2), and the macaque *M. fascicularis* (3), stained with cresyl violet. Although the relative size of laminae varies across species, all laminae appear to be conserved in mammals. See text for details. Modified from May (2006).

receives descending and ascending afferents from cortical and subcortical regions concerned with auditory, somatosensory and motor function, often reciprocally (Sparks and Hartwich-Young, 1989). The efferent connections of the dSC can be grouped into two categories, those comprising an ascending thalamic pathway which can recruit the basal ganglia and cortical regions, and descending pathways which target midbrain and brainstem regions. The latter includes regions such as medullary and pontine nuclei, the cuneiform nucleus, the PBGN, the mesencephalic reticular formation and the PAG (Sparks and Hartwich-Young, 1989).

Maps, neural encoding, and movements Retinal innervation of the sSC is organised so that sSC neurons inherit and encode a retinotopic map representing the contralateral visual field (Dräger

and Hubel, 1976), where the azimuthal (horizontal) plane is represented along the rostrocaudal axis, with the temporal extent being the most caudal, whereas elevation (vertical) is represented mediolaterally, with the upper visual field being medial. In keeping with its multisensory and movement role, the receptive fields of neurons in the dSC form superimposed eye or body-centred topographic maps of visual, auditory and somatosensory space (Dräger and Hubel, 1976; Sparks, 1988), while their movement fields form maps of oculomotor and motor space (i.e vector maps of movements caused by microstimulation) which are increasingly being recognised as dynamic, both during development and in the adult. In development, sSC retinotopy is established before eye opening coarsely through guidance molecules then precisely by retinal waves (Brown et al., 2000; Mrsic-Flogel et al., 2005). Subsequently, the other maps are broadly aligned to it by experience-dependent mechanisms, which occurs successfully even during manipulations of sensory input such as through ear plugging (King, 1993) or placing prisms in front of the eye (Rees, 1996). The result of this alignment is such that in one column perpendicular to the collicular surface, cells will respond to different modalities providing sensory input from approximately the same parts of space. This dynamism is not just to align maps in during development, but exists in real-time in behaving adults. dSC motor maps must be dynamic so that movement kinetics match the myriad of starting positions for the head and eyes in a freely moving animal (Knudsen, 1991), and similarly, the auditory map must be dynamic to account for relative eye, ear and head positions which would take the auditory and visual maps out of alignment except for when eyes and ears are pointing straight ahead (Rees, 1996). In the monkey SC, this dynamism has been extended to the sSC where it appears a visual saliency map is present while complex visual features have not found to be encoded as in cortical areas (White et al., 2017).

The SC is considered to have multiple patterns of organisation, such as patches of afferents from the same region distributed across laminae, which is hypothesised to help form processing modules in the SC (Sparks and Hartwich-Young, 1989). Intriguingly, recent two-photon imaging of the mouse sSC has revealed that cells of similar orientation tuning are arranged in columns, unlike mouse V1 and in fact unlike the sSC of any known species, although the behavioural consequences of this are unknown (Feinberg and Meister, 2015; Ahmadlou and Heimel, 2015). Direction-selective neurons have also been described in the mouse sSC (Wang et al., 2010; Inayat et al., 2015), which inherit their direction selectivity from the retina (Shi et al., 2017), but they are not similarly arranged in columns.

The SC produces a repertoire of movements in response to its sensory input and experimental activation. How then does one network process numerous streams of disparate information continuously while instigating both small and large-scale movements? The most intensely studied SC-related output is the generation of eye movements in head-fixed primates. dSC neurons fire in bursts prior to contraversive saccades, but this response profile exists only for a

range of vectors for each cell, termed its movement field. Cells are arranged topographically by movement field, with the largest amplitude movements represented caudally, small movements represented rostrally, while upward and downward movements are represented medially and laterally, respectively. Prior to a single saccade, around 28% of dSC neurons fire bursts (Gandhi and Katnani, 2011), and it has been demonstrated that the central locus of this population response across the SC matches to the locus for the given saccade vector which is produced. In foveated mammals, gaze shifts occur when the head is free to move, which are combinations of eye, head and even body movements to change the visual axis to a new point in space (Gandhi and Katnani, 2011). To stress the point that although saccades are the best known function of the SC, the SC is not simply the saccade generator of the brain, and it is worth noting that the SC alone (nor the frontal eye fields nor visual cortex) is not necessary for visually-triggered saccadic eye movements (Sparks and Hartwich-Young, 1989). In rodents, the SC is large relative to the visual cortex in comparison other mammals, and is suspected to perform some functions that are carried out cortically in mammals with proportionally larger neocortices. Conversely, it may be that the role of the SC in other behaviours in other mammals could have been underestimated due to the traditional research focus on saccade generation (Huberman and Niell, 2011).

1.4.4 The role of the superior colliculus in defensive behaviour

Despite many decades of research into the functions of the SC, perhaps its least well understood role is under conditions where a sensory stimulus is deemed threatening, and how it contributes to defensive behaviour (May, 2006). Defensive responses to SC stimulation in rats were first reported by Olds and colleagues in the early 60s (Olds and Olds, 1962)[16], while the first attempts to systematically map defensive responses came 20 years later, using electrical stimulation (Sahibzada et al., 1986), and then glutamate to avoid axons of passage (Dean et al., 1988). These studies corroborated previous observations using electrical stimulation and GABA receptor antagonists (Stein, 1965; Cools et al., 1983, 1984) showing that while stimulation of the medial deeper layers can evoke defensive behaviour and lateral stimulation causes orienting but not defence, they did not find evidence for a fine scale map for defensive behaviour as there is for movements. In these pioneering studies, observed defensive behaviours include freezing, flinching, jumping and running resembling flight from a predator (Dean et al., 1989, Sudre et al., 1993; Vargas et al., 2000) Whether the SC actually produces these behaviours in the intact animal, as suggested by Dean, Redgrave and colleagues, or rather processes threatening information and relays it to other centres to generate defensive responses, is still an unresolved question (Bittencourt et al., 2005; Shang et al., 2015). An influential lesion study by Blanchard

[16] Although Hunsperger (1956) notes that the PAG and posterior hypothalamus are each "surrounded by a larger common field from which flight responses were obtained", which implicates the SC.

and colleagues in wild rats demonstrated that the superior colliculus was indeed involved in the detection of threatening visual stimuli (Blanchard et al., 1981). When an experimenter approached the rats (with total sSC lesion, and 75-100% dSC lesion), they no longer oriented towards them, and the distance at which they elicited flights was decreased. However, the flights were similar to the pre-lesion test once elicited by touching, and they were less responsive to tactile and vibrissal stimulation. It is still difficult to disentangle the effects of lesioning on the sensory, motor, attention and modulatory functions of the SC: for example, the SC could still be responsible for driving visually-evoked escape, but a separate pathway responsible for tactile-evoked escape.

Since visually-guided escape has been demonstrated in mice using expanding spot stimuli (Yilmaz and Meister, 2013), a number of studies have been sought to investigate and propose circuits which might underlie this behaviour, each identifying the SC as critical. Approach-sensitive cells have been reported in the lower superficial layers of the cat SC (Liu et al. 2011), and the superficial layers of mouse SC (Zhao et al., 2014; Shang et al., 2015), as well as in the rat superior colliculus, where 10% of cells were found only to respond to looming-type stimuli but not light flashes or moving disks (Westby et al., 1990). It is not currently known whether these response properties are computed *de novo* in the SC, or inherited from the retina where there are candidate retinal ganglion cells that are sensitive to threatening stimuli. These include the PV-5 cell, one of seven morphologically distinct parvalbumin-expressing (PV^+) ganglion cells, which selectively responses to approaching motion while being suppressed by lateral motion (Münch et al., 2009) and the W3 cell, which only responds to small moving objects against uniform backgrounds, such as an aerial predator in the sky, as shown by stimulating the *ex vivo* retina with naturalistic video recorded from the head of a freely moving rat and video of an an approaching owl (Zhang et al., 2012). Recently, several pathways have been proposed that seek to explain the SC's role in driving mouse defensive behaviours in response to innately threatening visual stimuli. Using optogenetic activation and head-fixed optrode recordings, Shang et al. (2015) found that PV^+ neurons in the SC can drive escape behaviour and subsequent freezing. They found that this population of neurons is excitatory, and are located throughout the SC, with an extensive distribution in the superficial layers, and roughly half as many PV^+ neurons in the deeper layers, with a small number of neurons labelled in the dPAG. Anaesthetised optrode recordings showed that the sSC PV^+ cells respond to approaching motion, with their firing rate increasing with angular speed (Peek and Card, 2016), although it is unclear whether this is a population-specific response, as the response properties of PV^- neurons and the relative proportions of responsivity are not given. Optogenetic activation showed that these neurons drive escape when stimulated in the SC, and as there is a high density of their axons projecting to the parabigeminal nucleus (PBGN), the authors stimulated axons

in the PBGN directly, also driving escape responses. As a control for pathway specificity and antidromic spiking, that could allow the axonal stimulation to cause cell body spiking in the SC and thus the escape be mediated by alternate SC pathways, the authors also stimulated the low-density projections to the pontine nucleus (PN), which did not cause defensive behaviour. In anterograde and retrograde tracing experiments, they show that the PBGN projects to the CEA, and as they could use ChR2 stimulation of SC PV^+ cells as an unconditioned stimulus in a fear conditioning assay, they suggest that visually evoked defensive responses are evoked by a SC-PBGN-amygdala-hypothalamus pathway. However, this conclusion is contentious, and alternative interpretations are evident in the data. The authors show that retrograde tracers injected into the PN only label a subset of neurons in the deeper layers of the SC, while in separate experiments, PBGN injections show stronger retrograde labelling in the deeper layers, and very extensive labelling superficial layer. This suggests that PBGN- and PN-projecting SC cells only partially overlap in their locations, and they do not show collaterals with dual-retrograde experiments. Thus PN-axonal stimulation does not control for antidromic stimulation in the PBGN and PBGN-axonal stimulation could therefore be evoking escape by an alternate SC pathway, such as via the dPAG. [17] The precise role of this proposed pathway in escape behaviour is therefore unclear, and loss-of-function experiments in a region or pathway specific manner are not reported. An alternate pathway for processing innately aversive visual cues was proposed by Wei et al. (2015). The authors found that optogenetic activation of $CaMKIIa^+$ cells in the medial region of the SC intermediate layers, which highly overlap with VGluT2 $^+$ glutamatergic neurons (Wei et al., 2015; also observed by group of T. Branco), causes either immediate freezing responses or escape followed by freezing, while optogenetic inactivation of these neurons could reduce the level of freezing evoked by an expanding visual stimulus. The authors found that injections of muscimol into the amygdala could strongly reduce the level of freezing evoked by optogenetic activation of the intermediate mSC, suggesting that these neurons are important for evoking innate defensive responses. Interestingly, the authors identified a projection from these neurons to the lateral posterior nucleus of the thalamus (LP) which is required for freezing responses evoked by optogenetic activation of the intermediate SC population, which they suggest is a relay to the lateral amygdala. The authors therefore proposed that visually-evoked freezing behaviour is mediated by a circuit constituting intermediate mSC-LP-lateral amygdala (Wei et al., 2015). The output for this circuit to initiate freezing would likely be a CEA-vlPAG pathway as described earlier (Haubensak et al., 2010). The role of cortical sensory regions in innate defensive behaviours evoked by the SC are also under intense investigation. While recording from sSC cells in the awake mouse, Zhao et al. (2014) found that inhibition of the visual cortex (V1 and

[17] Furthermore, the PBGN has reciprocal projections with the SC and projects strongly to the dPAG (Usunoff et al., 2007; Baleydier and Magnin, 1979; Jiang et al., 1996), which is clear in their histological data but not investigated.

surrounding higher areas) roughly halved the firing frequency of loom-evoked responses, while leaving the speed tuning and time course of responses intact. This suggests that the visual cortex has the ability to modulate the gain of visual threat detection in the SC, a finding supported by a second study looking at temporary arrest behaviour in head-fixed mice in response to flashes of light (Liang et al., 2015). Optogenetic activation of corticotectal projections from the auditory cortex (A1) to the dSC, or V1 to the sSC, are able to drive escape and freezing respectively (Zingg et al., 2016), suggesting that the cortex can exert control over the expression of defensive behaviour. However, these are unlikely to be necessary physiological paths of SC activation in the behaving animal, as extensive inactivation of visual cortex does not prevent looming responses in the SC (Zhao et al., 2014), and likewise, inactivation of the auditory cortex roughly halves the speed of escape evoked by innately aversive sounds (Xiong et al., 2015). The inferior colliculus (IC), the principal midbrain nucleus in the auditory pathway, is adjacent to the SC (Rees, 1996). Recently, it has been shown that the IC is necessary for flight responses to an innately aversive broadband noise (1-64 kHz; 5s duration; Xiong et al., 2015). The external cortical shell of the IC (ICx) projects to both the deeper layers of the SC and directly to the dPAG, a projection which the authors show to be sufficient to drive escape using optogenetics (Xiong et al., 2015). Taken together, these recent studies suggest that there are redundant pathways for evoking innate visual and auditory defensive responses which involve the SC (Silva et al., 2016a), and the possibility of direct connections from the SC to the dPAG have been largely unexplored (except by Xiong et al., 2015). It is also possible that these pathways are not redundant but contribute different aspects to a coordinated defensive response, including associated fear processing in higher brain areas, and that further behavioural dissection is necessary to understand how the midbrain defensive system interacts with cortical, hypothalamic, amygdala circuits in naturalistic assays.

1.5 Aims of this study

Over the last decades, studies in multiple mammalian species have elucidated key brain regions, namely the amygdala, medial hypothalamic zone, SC, and PAG, which are involved in a range of defensive behaviours. However, a precise understanding of how circuit and cellular mechanisms give rise to individual instinctive defensive behaviours is lacking. For example, despite strong evidence for the involvement of the midbrain in escape behaviour, very little is known about how its neurons compute instinctive defensive behaviours in response to threatening stimuli at the network and cellular level.

The aims of this thesis are to develop an ethologically-relevant assay for studying how mice decide to initiate or withhold innate escape responses, to further describe the murine circuit

which is necessary for escape behaviour, and to understand, mechanistically, the computations that these circuit elements perform to produce escape responses.

2 Methods

2.1 Animals

Male and female C57BL/6J wild-type, VGluT2-ires-Cre (Jackson Laboratory, stock #016963) and VGluT2::EYFP (from an in-house cross of VGluT2-ires-Cre with R26 EYFP; Jackson Laboratory #006148) mice were used for experiments at 6–12 weeks old unless otherwise stated. Animals were housed with ad libitum access to chow and water on a 12h light cycle and tested during the light phase. All experiments were performed under the UK Animals (Scientific Procedures) Act of 1986 (PPL 70/7652) following local ethical approval.

2.2 Behavioural assay

2.2.1 Experimental set-up

Preliminary experiments using arenas of different sizes, shapes and complexity led us to design a modular perspex arena that consists of an open corridor, with the length adjusted by using slotted wall inserts at 10cm intervals (W 20cm x L max.100cm x H 40cm): the standard size was 20cm by 60cm. The arena floor was made of opaque white perspex, the sides of clear transparent, and the end walls of red transparent, housed within a sound-deadening, light-proofed cabinet. A movable red tinted shelter (19cm x 10cm x 13.5cm) was placed at one end. A screen (90cm x 70cm; '100 micron drafting film', Elmstock, UK)) was suspended 64cm above the arena floor, and a DLP projector (IN3126, InFocus) back-projected a grey uniform background onto it via a mirror, providing ~7-8lx at the arena floor. Six infra-red (IR) LED illuminators (TV6700, Abus) directed at the screen provided diffuse lighting for the arena that is not visible to the mouse. Experiments were recorded at 50 frames per second with a near-IR GigE camera (acA1300-60gmNIR, Basler) positioned centrally above the screen, with the lens (H2Z0414C-MP, Computar) directed through a small hole in the screen. A longpass filter (700nm; FGL695, Thorlabs) was mounted in front of the camera sensor to preclude the effects of projector flicker. Video recording, sensory and optogenetic stimulation was controlled by software we developed in LabVIEW (2015 64-bit, National Instruments), programmed by Kostas Betsios, which allowed the centre-of-mass

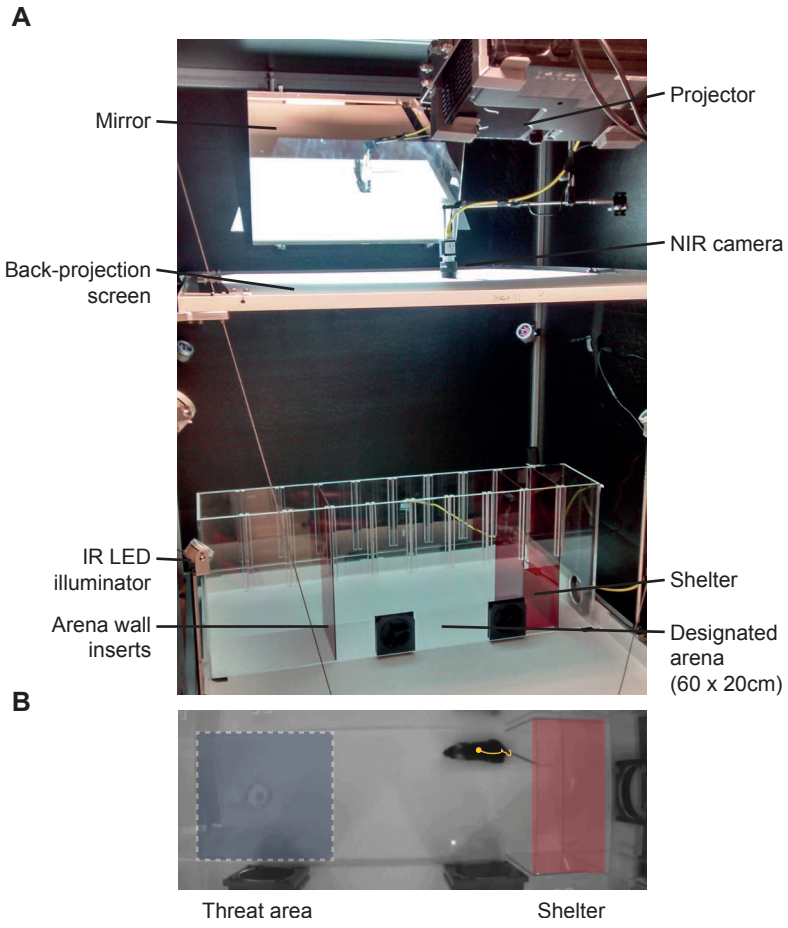

Figure 2.1 Experimental set-up for escape behaviour assay **A:** Annotated image of the custom-built setup. **B:** Still frame of an experimental video of the arena through top-mounted NIR camera, showing the shelter and software-defined threat area for stimulation. The yellow spot depicts the tracking coordinate of the animal (centre-of-mass of background-subtracted image, with erosion and dilation steps), while the yellow line shows the evolution of the position over the preceding 5 video frames.

coordinate of the animal to be tracked in real-time, including erosion and dilation steps to remove patch cords, and was thus used to trigger stimuli when the animal entered a predefined 'threat area' (21cm x 20cm area at opposite end to shelter). In the centre of the threat area, an empty plastic Petri dish (replaced fresh for each animal; 35mm) was affixed to the arena floor to enrich the environment and encourage foraging. The camera was triggered on each frame using hardware-timed signals from an I/O board (PCIe-6351, National Instruments) via a BNC connector block (2090A, National Instruments). This board was also used to acquire timing signals for video, stimuli and physiological recordings for synchronisation of data. For each experiment, this system produced an MP4 video file (1050 x 400 pixel resolution) and a data file containing the tracking data, stimulus log and analog synchronisation signals.

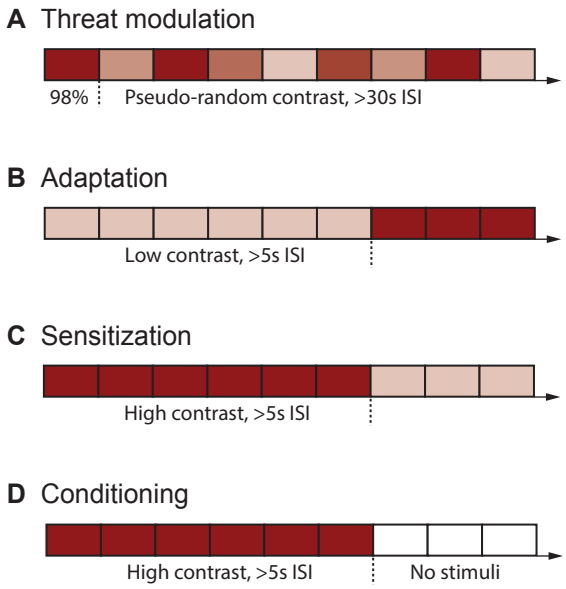

Figure 2.2 Behavioural protocols for visually-evoked escape. Schematic showing the stimulus sequence of expanding spot trials at different contrasts, where each coloured box is a trial at a particular contrast, for **A** threat modulation,**B** adaptation, **C** sensitization and **D** conditioning experiments.

2.2.2 Protocols

Male and female C57BL/6J mice were placed in the arena and given 8min to explore the new environment, after which sensory stimuli were delivered when the animal entered the threat area longer than 100ms. A typical experiment lasted 30min-1hr. In the standard visual stimulation protocol, the first stimulus was at 98% contrast, followed by stimuli at different contrasts ordered arbitrarily with at least 30s inter-stimulus interval (Fig. 2.2*A*). For the adaption protocol, after a 10min acclimatisation period, spot presentations were repeated (range, 4-13 trials; mean, 6.5 trials) at low contrast (30-40%) with a short inter-stimulus interval (stimulus was delivered upon the next threat area entry once a 5s refractory period elapsed), followed by presentations of 98% contrast (Fig. 2.2*B*). For the sensitisation and conditioning protocols, repeated presentations (range, 3-6 trials; mean, 3.5 trials) at 98% contrast were delivered with with a short inter-stimulus interval (same as for adaptation protocol) after a 10min acclimatisation period, followed by 40% contrast trials, or free exploration, respectively (Fig. 2.2*C-D*).

2.2.3 Sensory stimuli

The standard visual stimulus was a sequence of five dark expanding circles, and unless otherwise stated, each subtended a visual angle of 2.6° at onset and expanded linearly at 118 °/s to 47° over 380ms, after which it maintained the same size for 250ms and began an inter-stimulus interval of 500ms (Fig. 2.3). The contrast of the spot was varied in a number of experiments, and for clarity is reported as a positive percentage (low to high; e.g 20% to 98%), converted from the negative

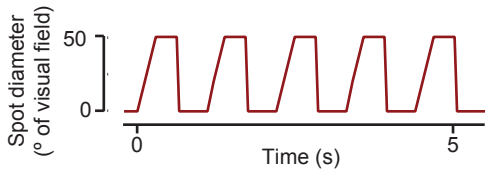

Figure 2.3 Expansion profile of threatening visual stimulus.

Weber fraction (low to high; -0.2 to -0.98). The contrast was varied by altering the intensity of the spot against a grey screen maintained at constant luminance (standard luminance, 7.95 cd/m^2). The spot was located on the screen directly above the centre of the threat area, ~15° from the animals' zenith.

The auditory stimulus consisted of a train of a frequency modulated upsweep from 17 to 20kHz over 3s (Mongeau et al., 2003). Waveform files were created in MATLAB (Mathworks), and the sound was generated in LabVIEW, amplified and delivered via an ultrasound speaker (L60, Pettersson) positioned 50-56cm above the arena, centred over the threat area.

2.2.4 Analysis

Behavioural video and tracking data was sorted into peri-stimulus trials and manually annotated frame-by-frame. Detection of the threat stimulus was assumed if the animal showed a startle-like response, in which the ears of the animal move posteriorly and ventrally, which precedes interruption or commencement of body movement. The first video frame depicting this startle-like movement was annotated as the detection time and trials with no startle response were excluded from the analysis. The onset of escape was measured as the first video frame marking the onset of a continuous movement consisting of a head turn followed by a full-body turn towards the shelter. Successful escape was annotated automatically and defined as the animal moving to enter the shelter in a single movement without stopping, within 0.9s after stimulus termination (or 6s after approaching a 15cm boundary from threat area for spontaneous escapes after conditioning). Entry to the nest was annotated when the body of the animal, excluding the tail, was inside the nest entrance. The escape probability for a given stimulus was calculated by pooling all trials from all animals, and is reported as the fraction of trials which led to an escape to the shelter. This was done to maximize the sample size from which we estimated the probabilities, and thus avoided calculating misleading probabilities from relatively small numbers of trials at a particular contrast for a given mouse (e.g. for a given contrast, if only 3 trials were acquired for a particular animal which escaped twice, then calculating the escape probability as the fraction of trials with escape would be a poor estimate). Fisher's exact test was used to test significance of pooled escape probability data, as it is appropriate for nominal

variables (in our case, 'escape' vs 'no escape'), and is more accurate than the chi-square test for sample sizes <1000 (McDonald, 2014). For consistency we therefore also pooled speed, detection time and reaction time measurements of escape. We quantified the escape vigour as maximum speed of the escape, calculated as the peak value of the speed trace between the onset of escape and entry to the nest.

2.2.5 Behavioural Model

To model the behavioural statistics of the escape task, we modified a decision making model (Shea-Brown et al., 2008), which is itself a variant of the drift-diffusion model (Gold and Shadlen, 2007). The threat level (T) evolves over time according to

$$\tau_T \frac{dT}{dt} = -T + C\alpha(t) + \sigma_N dW$$

where α(t) is the diameter of the expanding visual spot scaled by the spot contrast C. The variable τ_T sets the time constant for changing the threat level and dW is a white-noise Wiener process parametrised by σN. At each time point, T is compared against a threshold B, and escape initiated if $T > B$. The reaction time is the time at threshold crossing measured relative to stimulus onset. In this model we allow the threat level to continue evolving after the threshold has been crossed, similar to previous work on changes of mind during decision making (Resulaj et al., 2009), and escape vigour V is computed from the peak of the threat level as a logistic function:

$$V = \frac{1}{1 + e^{(-k(T-B_s))}}$$

The model was first fitted with three free parameters (B, σ_N) to the reaction time and escape probability data simultaneously by simulating 10,000 trials for each parameter set and using the brute force method in LMFIT Python 2.7 package. Escape vigour was then fitted to the average peak threat levels across all trials with free parameters k and s using least-squares minimisation in LMFIT.

2.3 General surgical procedures

Animals were anaesthetised with an intraperitoneal injection of ketamine (95 mg/kg) and xylazine (15.2 mg/kg), and carpofen (5 mg/kg) was administered subcutaneously. After shaving the scalp, the animal was placed on a heat pad and secured in a stereotaxic frame (Model 1900 and 963, Kopf Instruments), with eye gel (Lubrithal) applied to prevent dehydration. Oxygen (1 l/min) was provided throughout surgery, and the pedal withdrawal reflex and respiratory rate was used

to monitor the plane of anaesthesia: isoflurane (0.5-2.5%) was provided to keep a surgical plane rather than re-administer ketamine. The scalp was incised, and resected by 2-4 mm if implants were to be affixed, and the fascia scraped from the skull. A drop of saline was applied to increase visibility of the sutures and the skull was levelled. Craniotomies were made using a 0.5mm burr and a dental drill, and viral vectors were delivered using pulled glass pipettes (10 µl Wiretrol II with a Sutter P-97): these were backfilled with mineral oil and frontfilled with vector using an injection system coupled to a hydraulic micromanipulator (MO-10, Narishige). Once inserted into the brain at the target depth, the needle was retracted by 50 µm and the virus delivered at ~30 nl/min; the pipette was withdrawn 5-10min after injection. Implants were affixed using light-cured dental cement (RelyX Unicem 2, 3M) and the wound closed either by absorable sutures (6-0, Vicryl Rapide) or cyanoacrylate glue (Vetbond). Upon completion of the procedure, a low-dose of atipamezole (0.03 mg/kg) was administered subcutaneously if the animal had been anaesthetised for between 45min-1.5hrs and the animal was placed in a 28 °C recovery chamber.

Notes on refinement of procedures Over the course of the project, we refined surgical procedures in order to do more intricate surgeries and enhance the recovery of animals. Such refinements include: use of fast action light-curable cement instead of acrylic to increase speed of surgery and long-term reliability of implant, refinement of durotomy procedure to increase success rate of GRIN lens experiments, use of magnetic fibre-optic cannulae to attach patchcords without restraint or anaesthesia, use of mixed injectable and inhalation anaesthetics to better control anaesthesia during long procedures, use of dissolvable sutures to prevent wound re-opening.

2.4 Viruses

The following viruses were used in this study and are referred to by contractions in the text. For optogenetic activation, AAV2-EF1a-DIO-hChR2(H134R)-EYFP-WPRE (3.9×10^{12} GC/ml), AAV2-EF1a-DIO-hChR2(H134R)-mCherry-WPRE (6.6×10^{12} GC/ml; Deisseroth) were acquired from the UNC Vector Core (USA). For control and calcium imaging experiments respectively, AAV2-EF1a-DIO-eYFP-WPRE (4.0×10^{12} GC/ml) and AAV9-CAG-Flex-GCaMP6s-WPRE (6.25×10^{12} GC/ml) were acquired from Penn Vector Core (USA). For retrograde rabies tracing, EnvA pseudotyped SADB19 rabies virus (EnvA-dG-RV-mCherry) was used in combination with AAV8 coding for TVA and rabies virus glycoprotein (RG) that were prepared from pAAV-EF1a-FLEX-GT (Addgene plasmid #26198, Callaway) and pAAV-Syn-Flex-RG-Cerulean (Addgene plasmid #98221, Margrie). All viruses used for rabies tracing were a gift from Troy Margrie (Vélez-Fort et al., 2014). Additionally, a recombinant AAV with retrograde functionality (rAAV2-retro-mCherry, Addgene plasmid #81070) was used (Tervo et al., 2016).

2.5 Neural activity manipulations in behaving animals

2.5.1 Optogenetic activation

Animals and experimental set-up VGlut2-Cre and VGlut2::eYFP mice were injected with AAV-FLEX-ChR2-EYFP or -mCherry, (see Viruses) into the dmSC (80-120 nl, ML; ±0.2, AP; -0.25-0.45 from lambda, DV; -1.4-1.55) or dPAG (40-80 nl per side ML; ±0.0-0.2l, AP; -0.4-0.6 from lambda, DV; -1.95-2.2). Control animals were injected with 120 nl AAV2-DIO-eYFP into the dPAG. One optic fibre (200 µm diameter, MFC-SMR; Doric Lenses Inc.) was implanted per animal, medially, 250-300 µm dorsal to the injection site. For optical stimulation, light was delivered by a 473 nm solid-state laser (CNI Ltd.) in conjunction with a continuous ND filter wheel for varying light intensity (NDC-50C-4M, Thorlabs) and a shutter (LS6, Uniblitz), via a thorlabs patch cord (200 µm diameter, 0.39NA; Thorlabs), driven by trains of pulses generated in LabVIEW. In some experiments, this system was substituted by a laser diode module (Stradus, Vortran) with direct analogue modulation of laser intensity. Magnetic patchcords (Doric Lenses Inc.) were combined with a rotary joint (FRJ 1x1, Doric Lenses Inc.) to allow the cannula to be connected without restraint and allow unhindered movement.

Protocols In all experiments, animals were placed in the standard arena and given 8min to acclimatise. For the intensity modulation assay, the laser intensity was set initially to give a low irradiance (0.1-0.2 mW/mm^2) that did not evoke an observable behavioural response. Mice were photostimulated (473 nm, train of 10 light pulses of 10ms at 10Hz) upon entering the threat area with an inter-stimulus interval of at least 30s. After at least three trials of this intensity, the irradiance was increased by 0.1-0.3 mW/mm^2 until a behavioural response was observed, after which 8-15 trials were obtained at a given intensity, before further increasing the light intensity. This process was iterated until an intensity was reached which always evoked a flight response (P_{escape}=1). For one animal, the standard stimulus was not sufficient to reach P_{escape}=1 and the curve was acquired with a higher frequency stimulus (10 light pulses of 10ms at 20Hz). If the animal stopped exploring the arena, precluding P_{escape}=1 from being obtained, the experiment was terminated after 4hrs and not analysed. In the frequency modulation assay, high laser power was used (range, 12.0-13.5 mW/mm^2) and the stimulus consisted of 10 light pulses of 10ms at either 2, 5, 10, 20 and 40Hz, delivered in a random order.

Histology For histological confirmation of the injection site, animals were anaesthetised with Euthatal (0.15-0.2ml) and transcardially perfused with 10ml of ice-cold phosphate-buffered saline (PBS) with heparin (0.02mg/ml) followed by 4% para-formaldehyde (PFA) in PBS solution. Brains were post-fixed overnight at 4° then transferred to 30% sucrose solution for 48h. A brain

matrix was used to make coronal cut at bregma, and brains were placed rostrally in a mould, covered in embedding medium (VWR) and frozen on dry ice, after which they were kept at –20 °C or –80 °C for short or long-term storage. 30 µm sections were cut with a cryostat (Leica CM3050S) and a standard free-floating immunohistochemical protocol was used to increase the signal of the tagged channelrhodopsins and counter-stain neurons. The primary antibodies used were anti-GFP (1:1000, chicken; A10262, or rabbit; A11122, Life Technologies), anti-RFP (1:1000, rabbit; 600-401-379, Rockland) and anti-NeuN (1:1000, mouse; MAB-377, Millipore) and the secondary antibodies were Alexa-488 Donkey anti-rabbit and Goat anti-chicken, Alexa-568 Donkey anti-rabbit and Donkey anti-mouse, and Alexa-647 Donkey anti-mouse (1:1000, Life Technologies). Brain sections, typically a sample of one section every 180 µm covering the brain region of interest or throughout the brain in order to see projection targets, were mounted on charged slides using the mounting medium SlowFade Gold (containing DAPI; S36938, Life Technologies), and imaged using a wide-field microscope (Nikon TE2000). Tile scans of the entire section were acquired with a 10x or 20x air objective (NA 0.3, 0.5; CFI Plan Fluor, Nikon) at 16bit depth.

Data analysis Stimulation intensity was normalised in order to compare stimulus-response curves across animals and as a precaution against variability in infection or light transmission between preparations. To achieve this, trials were first automatically classified as escape if the animal reached the shelter within 5s of stimulation onset and the fraction of successful escape trials at each intensity was calculated. The escape probability curve of each animal was then fitted with a logistic function (1/(1+e-k(x-x0)), and light intensities were normalised to x0, (i.e. the intensity at which the fit gives P_{escape}=0.5). The data for each group were then binned and averaged across the normalised intensity range, and fitted with the same logistic function. In order to quantify escape latency and speed, trials were manually annotated to get the onset times of escape and the animal reaching the shelter, plotted against the normalised intensity range, and fitted linearly.

2.5.2 Genetic ablation

VGluT2::YFP animals were injected with AAV2-flex-taCasp3-TEVp (Nirao Shah; UNC Vector Core) or a control virus of the same serotype (AAV2-DIO-ChR2-mCherry; without optic fibre implant) into the mSC or dPAG with 80-200 nl per hemisphere (for coordinates, see Optogenetic Activation above). Before surgery, all animals were exposed to a single visual stimulus trial to confirm robust escape responses. In initial tests, we found that co-injection of AAV-Casp3 with a control fluorophore virus was not sufficient to visualise the extent of ablation, while crossing VGluT2-Cre to a reporter line allows precise assessment and demonstrates the presence

of abrupt borders around the ablated population, in agreement with the idea that exploiting cell-autonomous apoptosis for ablation limits toxicity (Yang et al., 2013). After 16-21 days, animals were placed in the arena for 8mins and then exposed to visual stimuli. Behavioural data was analysed as described and statistical tests were carried out against the control group.

2.5.3 Optogenetic inhibition

VGluT2-Cre animals were injected with AAV2-EF1a-DIO-eArch3.0-EYFP (80-120 nl; Deisseroth; UNC Vector Core) into the dPAG and implanted with an optic fibre 300 µm dorsal to the injection site. At least 2 weeks after surgery, animals were placed in the arena and, after a 8min acclimatisation period, several trials were used to assess a mid-contrast visual stimulus of five expanding spots that would evoke long latency escape responses, and the contrast was adjusted by 10-20% if necessary. Animals were then subjected to alternating trials of (1) this visual stimulus alone (2) visual stimulation during a 5s continuous stimulation of green laser light, the onset of which preceded the visual stimulus by 900ms. Trials for each stimulation type were sorted and pooled across animals to calculate escape probability.

2.5.4 Pharmacological inactivation

Experimental procedures Animals were bilaterally implanted with guide cannulae (Plastics One, Bilaney Consultants) over the target region (Table 2.1) and given at least 48h for recovery. On test day, mice were placed in the standard arena for 10min and escape responses were assessed with a single visual stimulus (one 98% contrast expanding spot) or auditory stimulus, after which they were allowed to explore the threat area once more to minimise aversion of the area. Additionally, in PBG-cannulated SCm- VGlut2::ChR2 animals, optogenetic responses were also evoked. The animals were then lightly anaesthetised in an induction chamber and placed on an insulating pad where anaesthesia was maintained with a nose-cone (2% isoflurane, 1l/min). Internal cannulae were inserted and sealed with Kwik-Sil, which we found to be essential in ensuring consistent infusion volumes. Muscimol-BODIPY-TMR-X (0.5 mg/ml) or Alexa-555 (100 µM; Life Technologies), dissolved in 1:1 PBS: 0.9% saline with 1% DMSO, was then infused at a rate of 70-100 nl/min using a microinjection unit (10 µl Model 1701 syringe; Hamilton, in unit Model 5000; Kopf Instruments) followed by a 5min wait period per hemisphere. Animals spent no longer than 30mins under anaesthesia and were given 30min to recover in the homecage, after which they were placed back in the cleaned arena and subjected to visual or auditory stimulation. PBGN-cannulated SCm-VGlut2::ChR2 animals were also subjected to optogenetic activation.

Table 2.1 Experimental parameters for pharmacological inactivation of circuit elements. Cannula implant coordinates are specified from bregma (b) or lambda (λ). The final target depth is the sum of the DV and Internal lengths. When dual implants were used, the width between the cannulae is given. All regions were targeted bilaterally.

	Coordinates (mm)			Cannula (mm)		
Target region	ML	AP	DV	Dual	Internal	Volume (µL)
Amygdala	±2.80	−1.60b	−4.75	—	−0.75	1.2-1.5
Periaqueductal gray, dorsal	±0.60	−0.45λ	−2.20	1.2	−0.50	0.6-0.8
Superior colliculus, medial	±0.50-0.60	−0.20λ	−1.50	1.0-1.2	−0.50	1.0
V1	±2.50	+0.50λ	−0.30	—	−0.75	1.0
Parabigeminal nucleus [1]	±2.40	−0.35λ	−2.75	—	−0.75	0.8
Ventromedial hypothalamus	±0.60	−1.65b	−5.0-5.25	1.2	−0.50	1.1

[1] mSC VGLUT2::ChR2 and optic fibre implant performed in same surgery. Cannulae angled 15º lateral from zenith.

Histology Immediately upon termination of the behavioural assay, animals were anaesthetised with isoflurane (5%, 2L/min) and decapitated with sharp scissors. Before dissection, the Kwik-Sil seal formed around the cannula was removed, and the internal cannula extracted, in order to minimise a suction effect drawing in more drug and damage to tissue by the internals. Acute slices (150 µm) were cut using a microtome (Campden 7000 or Leica VT1200S) in ice-cold phosphate-buffered saline (PBS) (0.1M), directly transferred to 4% para-formaldehyde (PFA) solution, and kept for 20min at 4 °C. The slices were then rinsed in PBS, counter-stained with DAPI (3 µM) in PBS), and mounted in SlowFade Gold (Life Technologies) with the coverslip supported by coverslips (22x22mm, No.1) at each end of the slide to prevent crushing of the tissue. Slices were imaged (wide-field, Nikon TE2000) on the same day to confirm the site of infusion.

Data analysis Behavioural data was annotated as described. For the calculation of the maximum foraging speed, the peak speed of the 8min acclimatisation period before stimulation was used.

2.6 Calcium imaging during escape behaviour

2.6.1 Data acquisition

A miniaturised head-mounted fluorescence microscope (Model L, Doric Lenses Inc.; (Fig. 2.4*A*)) was used to image GCaMP6s in neurons of male VGlut2-Cre mice. A large craniotomy (~2 x 3mm) was made, centred on lambda and AAV9-CAG-Flex-GCaMP6s (300-550nl; Penn Vector

Core) was injected into the mSC (AP: 0.2 to 0.5 from lambda, ML: +0.25, DV: 1.6) or dPAG (AP: 0.4 to 0.6 from lambda, ML:+0.25, DV: 2.2). At the level of the inferior colliculus, the dura was incised using a 30G needle, and gently pulled forward to partially reveal the SC. A GRIN lens-equipped cannula (SICL_V_500_80; Doric Lenses Inc.) was inserted to the same depth as the injection coordinates, the craniotomy covered with Kwik-Cast and the cannula affixed with dental cement. For SC-targeted animals, the cannula placed just above the brain surface and used to push forward transverse sinus to allow insertion at a rostral position without damaging the sinus. At least 21days after surgery, the microscope was attached to the mouse without anaesthesia, and the animal was placed back in the homecage for 5-10min, for acclimatisation to the microscope. During this period, the optimal imaging parameters for the preparation were determined: the acquisition rate was 14.2Hz in most experiments (median; range, 10-20 Hz) with an excitation power of 450 µW (median; range 0.2-1.1 mW) at maximum gain[1]. After a baseline period of 7min, animals were exposed to visual and/or auditory stimulation. For the visual stimulation, the inter-stimulus interval was 750ms, and post expansion period was 20ms, with the total epoch length and expansion rate unchanged. A typical session lasted 1.5hr (1-3 sessions per animal), with imaging data acquired during stimulation and control trials in ~5min epochs, with at least 2 days between sessions. If prolonged bouts of animal inactivity occurred, imaging was halted to minimize photobleaching. Fluorescence and behavioural frame trigger signals were acquired at 10kHz for offline synchronisation. Images were acquired as 10bit TIFF files.

2.6.2 Image analysis

Behavioural video and tracking data were sorted into peri-stimulus trials and manually annotated to mark behavioural events as described above. Fluorescence stacks were aligned using a non-rigid algorithm (Guizar-Sicairos et al., 2008; Fig. 2.4*A*) and background-subtracted (50px rolling ball radius; Fiji). Regions-of-interest were manually drawn in Fiji, based on maximum intensity z-projections of the raw and background-subtracted movies in parallel: we tested auto-segmentation algorithms designed for two-photon datasets (including SIMA; Kaifosh et al., 2014, and routines based on independent component analysis; Mukamel et al., 2009) but this required extensive manual correction so this approach was abandoned due to the relatively small number of ROIs per experiment (typically 10-30). Neuropil signals (presumably from out of focus cells and processes) were avoided when drawing ROIs (Fig. 2.4*C*) and were distinguishable by comparing raw and background-subtracted movies. Mean intensity traces were extracted for each ROI and further analysed in custom routines written in Python 2.7. The traces were first linearly interpolated with the behavioural video frames and tracking data, and the z-score

[1] In contrast to confocal and multiphoton imaging, the lack of optical sectioning in epifluorescent functional measurements requires the use of low power excitation and high gain in order to get the best signal-to-noise ratio, where there is a contribution to noise by the background emission of photons from other planes.

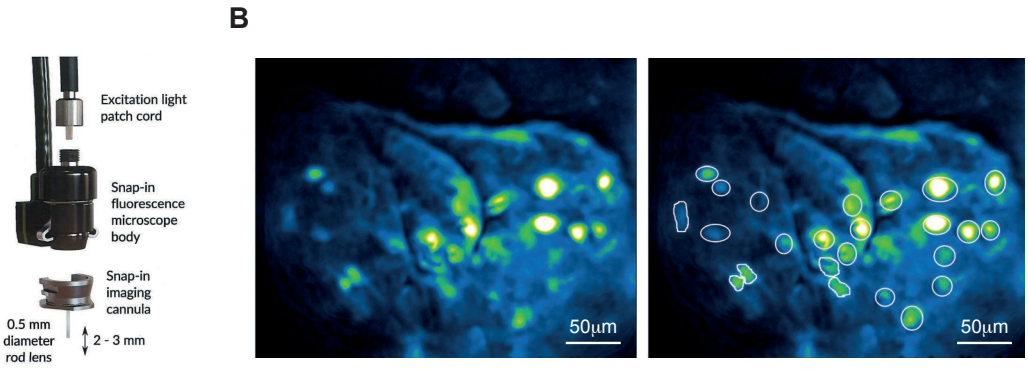

Figure 2.4 In vivo calcium imaging using head-mounted one-photon microscopes and data analysis. **A:** Schematic of proprietary microscope and GRIN lens cannula (Doric Lenses. Inc) **B:** Time-series SD projection image of an 8053 frame recording from VGluT2$^+$ cells in the deep medial superior colliculus after registration and deconvolution (left) and with ROI mask (right) showing cells against neuropil and blood vessels, and indicating successful alignment.

and $\Delta F/F$ calculated on a trial-by-trial basis with a baseline of 5s before stimulus onset. ROIs were classified as active if the peak z-score was greater than 2 at any time during a trial. For the receiver-operator characteristic (ROC) analysis, the annotated behavioural outcomes were used to sort data into 'Escape' and 'No Escape' classes, and the ROC curves and aucROC statistics were calculated using the open-source package Scikit-learn. The onset of calcium signals was measured by finding the time of the peak and iteratively moving backwards along the signal to determine the time point at which the signal reaches the baseline. The standard deviation for the AUC was estimated using bootstrapping. 'Peri' and 'Pre-escape' time periods were defined as escape onset ±1s and <1s, respectively. For the plot in Fig, 5.3*B*, which shows the correlation between the rise slope of population calcium activity versus escape latency, escape latencies were first binned and average calcium signal waveforms calculated for each bin, and the signal rise slope was then obtained by fitting a linear function (y = mx+b).

2.7 In vitro electrophysiology and circuit mapping

2.7.1 Data acquisition

Coronal slices were prepared from VGlut2::EYFP mice aged 6-12 weeks. Brains were quickly removed and transferred to ice-cold slicing solution containing (in mM): 87 NaCl, 26 $NaHCO_3$, 50 sucrose, 10 glucose, 2.5 KCl, 1.25 NaH_2PO_4, 3 $MgCl_2$, 0.5 $CaCl_2$. Acute coronal slices of 250 µm thickness were prepared at the level of the SC and PAG (-4.8 to -4.1mm from bregma) using a vibratome (VT1200, Leica or 7000smz-2, Campden). Slices were then stored under submerged conditions, at near-physiological temperature (35°) for 30min before being cooled down to room temperature (19-23°). For recordings, slices were transferred to a submerged

chamber and perfused with ACSF containing (in mM): NaCl, 119; $NaHCO_3$, 26; glucose, 10; KCl, 2.5; $CaCl_2$, 2; $MgCl_2$, 1; NaH_2PO_4, 1 (heated to 33 ° °C at a rate of 2-3 ml/min). ACSF was equilibrated with carbogen (95% O2, 5% CO2, final pH 7.3). Whole-cell patch-clamp recordings were performed with an EPC 800 amplifier (HEKA). Data was digitised at 25kHz (PCI 6035E, National Instruments), filtered at 5kHz and recorded in LabVIEW using custom software. Pipettes were pulled from borosilicate glass capillaries (Harvard Apparatus, 1.5mm OD, 0.85mm ID) with a micropipette puller (P-1000, Sutter, USA or P-10, Narishige, Japan) to a final resistance of 4-6MΩ. Pipettes were backfilled with internal solution containing (in mM): 130 KGluconate or $KMeSO_3$, 10 KCl, 10 HEPES, 5 phosphocreatine, 2 Mg-ATP, 2 Na-ATP, 1 EGTA, 0.5 Na_3-GTP, 285-290mOsm, pH 7.3, adjusted with KOH. $VGluT2^+$ dPAG and dmSC cells were visualised on an upright Slicescope (Scientifica) using a 60x objective (N.A. 1.0, water immersion; Olympus) and identified based on location and EYFP expression. The resting membrane potential (RMP) was determined immediately after establishing the whole-cell configuration and experiments were only continued if cells had a RMP more hyperpolarised than -50mV. Input resistance (R_{in}) and series resistance (R_s) were monitored continuously throughout the experiment, and R_s was compensated in current-clamp recordings. Only cells with a stable R_s <30MΩ were analysed. No drugs were added to the ACSF, except for miniature EPSCs (mEPSCs) which were recorded 5-10min after bath application of 1 µM Tetrodotoxin (TTX, Sigma Aldrich). For ChR2-assisted circuit mapping, recordings were made 10-14 days after injection of AAV2-FLEX-ChR2-mCherry into the mSC or dPAG of VGlut2::EYFP mice. ChR2 was stimulated with wide-field 490nm LED illumination (pe-100, CoolLED, 1ms or 10ms pulse length).

2.7.2 Data analysis

Analysis was performed using custom-written procedures in Python 2.7, except for the analysis of sEPSCs and mEPSCs which was done in IGOR Pro 6 (WaveMetrics) using TaroTools (by Taro Ishikawa). The R_{in} was calculated from the steady-state voltage measured in response to a hyperpolarising test pulse of 500ms duration at a holding potential of -60mV. The membrane time constant was calculated by fitting the decay of the test pulse with a single exponential ($y = y0+Ae^{-(x-x0)/\tau}$). The membrane potential values stated in the text are not corrected for liquid junction potentials. The sEPSC frequency before and after ChR2 stimulation was calculated from 6-8 repetitions per cell. Failures of light-evoked synaptic transmission were defined as a peak amplitude of less than the mean current baseline +2SD in a time window defined by the onset of the mean evoked synaptic current ±5ms. Quantal content calculated by the direct method (Isaacson and Walmsley, 1995; Del Castillo and Katz, 1954) was obtained by dividing the peak amplitude of the evoked current by the peak amplitude of the sEPSCs in the same cell (which is

not significantly different from the mEPSC amplitude, see Fig.6.7). Quantal content calculated by the method of failures was obtained using the following equation:

$$m = \ln\left(\frac{N_{failures}}{N_{stimuli}}\right)^{-1}$$

The paired-pulse ratio was calculated as the ratio of peak amplitudes between the second and first EPSCs in a train.

2.8 Retrograde circuit tracing

For monosynaptic rabies tracing from the dPAG, TVA and RG were injected unilaterally into the dPAG with an angled approach from the contralateral hemisphere to avoid infection of the SC in the target hemisphere (20°, AP: -0.45 to -0.5, ML: -0.6, DV: -2.2, from lambda). EnvA-dG-RV-mCherry was injected into the dPAG vertically (AP: -0.4, ML: +0.5, DV: -2.1, from lambda) 10-14days later. Animals were perfused seven days post-rabies virus injection. Brains were cut at 100 µm thickness on a microtome (HM650V, Microm). All sections containing the PAG and SC were mounted in SlowFade Gold, and imaged using a confocal microscope (SP8, Leica). Tile scans of the entire section were acquired with a 25x water objective (Olympus) at five depths (10 µm intervals) and maximum projections of these stacks were used for subsequent analysis. Cell counting was done manually (Cell counter plug-in, Fiji) in reference to the Paxinos and Franklin atlas (Paxinos and Franklin, 2012). To quantify the position of presynaptic SC cells along the mediolateral axis, the coordinates of the counted cells were normalised to the medial and lateral extents of the SC for each brain slice, and a kernel density estimation was performed (Scikit-learn, Python).

For retrograde tracing from the dmSC, rAAV2-retro-mCherry was injected unilaterally. AAV2-CamkII-GFP was co-injected to label the injection site in 2 out of 3 brains. Animals were sacrificed 14-18 days afterwards and their brains processed as described above. Every third section along the rostrocaudal axis of the SC was imaged with on an Axio Imager 2 (Zeiss) and presynaptic cells in the dPAG and auditory cortex were counted manually.

2.9 General data analysis

Data analysis was performed using custom-written routines in Python 2.7. Data are reported as mean ±SEM unless otherwise indicated. Statistical comparisons using were made in SciPy Stats and GraphPad Prism, and statistical significance was considered when $P<0.05$. The distribution of data was assessed with the D'Agostino and Pearson omnibus normality test, and normally

distributed data sets were compared with a two-tailed Student's t-test, unless otherwise indicated. The Mann-Whitney U-test was used as indicated for nonparametric datasets.

3 A behavioural assay for controlling escape behaviour in mice suggests an underlying decision process

We sought to develop a behavioural paradigm in which a particular defensive response in adult mice could be not only evoked but the statistics of the response controlled robustly — a prerequisite for understanding an innate behaviour within a theoretical and physiological framework. Recent behavioural work found that innate defensive behaviour can be readily elicited in mice using simple visual stimuli (Yilmaz and Meister, 2013), and specifically, overhead fast expanding spots were found to evoke escape responses. This stimulus-response relationship is intriguing for its specificity and experimental tractability. Previously, escape behaviour in laboratory mice had been successfully studied using live predators (Blanchard et al., 2003) or innately aversive sounds (Mongeau et al., 2003), while predator odours do not appear to be used for processing imminent threats and preferentially promote avoidance and risk assessment behaviour (Papes et al., 2010). Not only does using the visual modality allow precise spatiotemporal control and reproducibility of stimulation, but approach-sensitive neurons have been described in the mouse retina (Münch et al., 2009; Zhang et al., 2012), the superior colliculus of the cat (Liu et al., 2011), and more recently, the mouse (Shang et al., 2015), implicating the superior colliculus as a candidate region in the circuit responsible for this behaviour, and thus providing a potential starting point to understand visually-evoked escape behaviour neurophysiologically. We therefore extended the paradigm of Yilmaz and Meister (2013) to exert control over the process of initiating escape and the statistics of the behavioural characteristics.

3.1 Escape behaviour is controlled by threat intensity

To investigate instinctive escape behaviour in mice, we used overhead expanding spots, which are innately aversive as they mimic an approaching predator or object (Yilmaz and Meister 2013; Peek and Card 2016; Herberholz and Marquart 2012; Fotowat and Gabbiani 2011), and an ultrasound stimulus which has similar characteristics to vocalisations of rats, which predate mice (Mongeau et al., 2003; Blanchard et al., 1993). In our assay, animals were placed in an open corridor arena with a shelter at one end, and a grey back projection screen above, providing a low-level of illuminance at the arena surface. In an acclimatisation period lasting 8min, mice

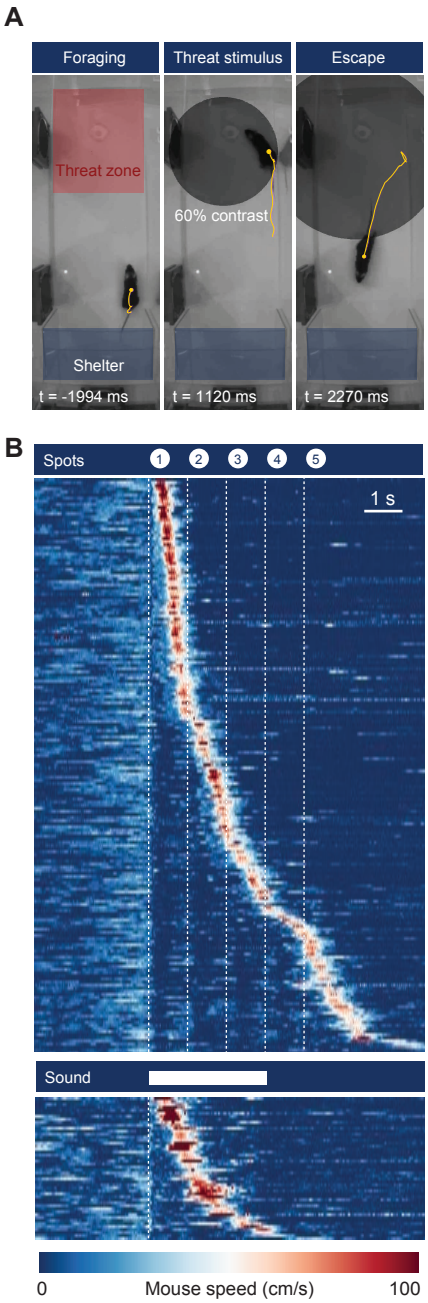

Figure 3.1 Escape behaviour is evoked and modulated by threats of varying intensity. **A:** Video frames from one trial showing a foraging trip from the shelter (left), stimulation with an expanding spot projected from above (middle), and an evoked escape response back to the shelter (right). Yellow lines indicate the mouse trajectory during the preceding 2s and frame times are relative to stimulus onset. **B:** Raster plot of mouse speed for all successful escape trials for visual (top) and sound (bottom) stimulation, from 13 animals, sorted by reaction time. Note interruption of foraging movement with a short delay from stimulus onset, and a variable delay until escape.

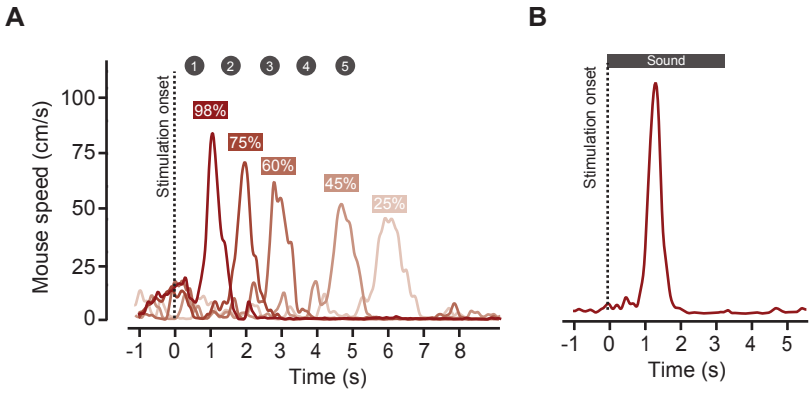

Figure 3.2 Escape speed and reaction time is determined by threat intensity within single animals. **A:** Example speed traces from one mouse in response to a train of spots at different contrasts and **B** to sound stimulation. Traces are from single trials.

spontaneously explored the whole arena and treated the shelter as a home-base, from which they would make foraging trips around the arena (Benjamini et al., 2011). The movement of animals was tracked online using video from overhead camera. At the far end of the arena, a threat area was predefined (21x20cm), and stimuli were presented 100ms after an animal entered this threat area spontaneously with its head-direction opposite to the shelter, resulting in escape towards the shelter (Fig. 3.1*A*). From frame-by-frame annotation of the behavioural video, we observed a sequence of behavioural actions which constitutes a successful escape to an overhead threat. The animals showed a startle-like response, in which the ears move posteriorly and ventrally, and the current movement is interrupted. A head turn was then initiated towards the shelter, evolving into a full-body turn and continuous movement in a straight line towards the shelter. We never observed zig-zag escape paths nor jumping, although in preliminary experiments using the same stimulus in the animals home cage, jumping could be elicited, presumably as there was no shelter to escape to or the animal recognised that it was already in its shelter. The onsets of the startle-like response and head turns were used to classify the onset of detection and escape, respectively, and the reaction time was defined as the difference between the escape and detection times. Upon reaching the shelter, animals usually displayed freezing behaviour for a variable period of time (3s to minutes), and infrequently displayed tail rattling, before resuming movement first within the shelter, and then engaged in foraging trips outside.

Preliminary experiments showed that varying the angular velocity of spot expansion could change the latency to escape (see Appendix), as demonstrated in Yilmaz and Meister (2013). However, we found that by varying the stimulus contrast to manipulate threat intensity, the latency and speed of escape responses could be modulated over a larger dynamic range (Fig. 3.1*B*) and within single animals (Fig. 3.2). Escape responses evoked with high contrast expanding spots were robust and stereotyped, with a high probability of escape being initiated (P_{escape}=94.4%,

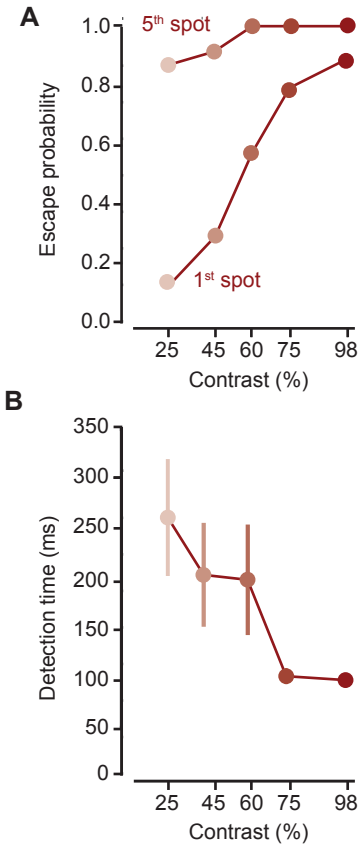

Figure 3.3 Probability of escape over consecutive spot presentations, and detection time over contrast. **A:** Escape probability after the first (shown in Figure 3.4*B*) and fifth spot, during the presentation of 5 consecutive expanding spots. **B:** The latency between stimulus onset and the time of detection is low across all contrasts, and decreases with increasing contrast.

N=13 mice, 36 trials) and the onset of escape usually occurring during the expansion of the first spot in the sequence of five (Fig. 3.3*A*). Decreasing the contrast resulted in escape responses which were more variable and probabilistic: we observed a progressive increase in reaction time, a reduction in escape probability and a reduction in the vigour of escape, quantified as the peak speed of the escape movement.

We also observed a small but consistent increase in the detection time of the stimulus as contrast decreased (Fig. 3.3*B*). However, across contrasts, the detection time was during the first spot presentation on average (t=99±2ms mean detection time for 98% contrast, t=261%±58ms, mean detection time for 30% contrast v.s. t=1140ms for onset of second spot presentation; N=13 animals, 177 trials, Fig. 3.3*B*), suggesting that irrespective of contrast, the detection time of the stimulus was usually on the first spot: this suggests that the variability in the time taken to escape reflects a decision process, which can be modulated by contrast. The reaction time is measurable between the initial detection of the stimulus and the onset of escape, and the existence of this relatively invariant detection time and variable decision time argues strongly

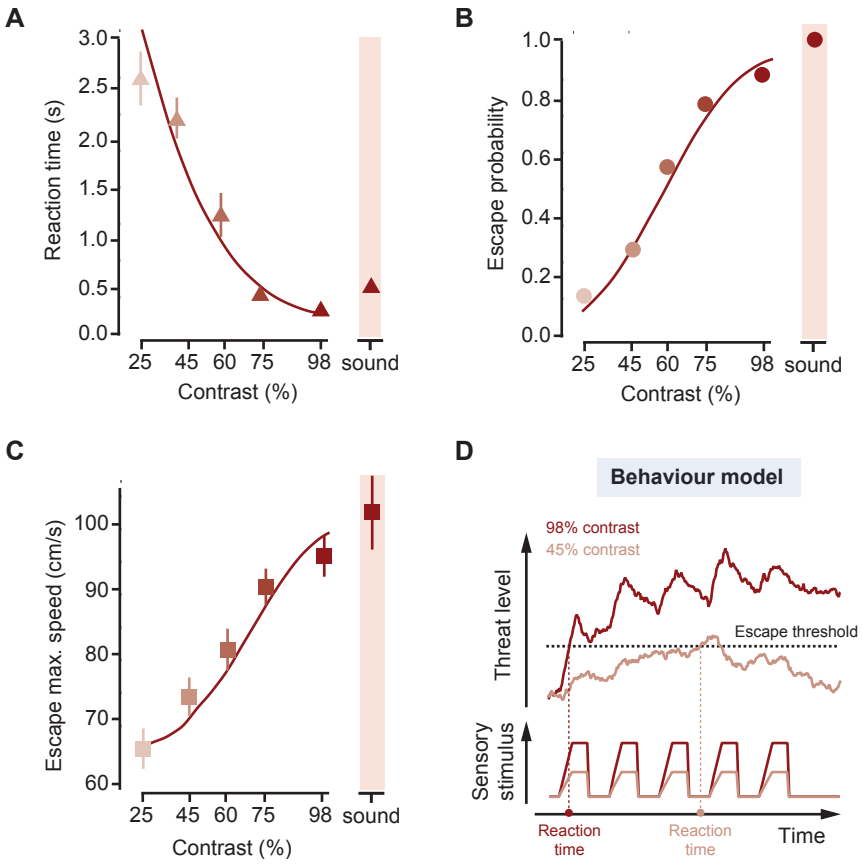

Figure 3.4 Stimulus-response curves for escape parameters, and a theoretical model for computing escape. **A:** Chronometric and **B** psychometric curve for stimulus intensity and escape behaviour, obtained by pooling data from all animals. Escape probability in **B** is for the first spot presentation (0-1140ms). **C:** Summary plot from all animals showing that escape vigour increases as a function of stimulus intensity. In **A-C**, the red lines are the model fitted to the data with the fit parameters: B=0.165, τ_T=1200ms, σ_N=0.6, k=90, s=1.5. Datapoint error bars in A and C are s.e.m. **D:** Schematic illustrating a model for computing escape behaviour threats of varying intensity. A sensory stimulus is integrated into threat level over time, and escape is initiated if the level goes above the threshold for escape. The process is noisy, and as the threat level decreases the probability of crossing the threshold decreases. The sensory stimulus trace shows the expansion of the spot over time scaled by the contrast. The threat level traces are example trials from simulations using the model parameters fit to the data.

against the alternative which is that the contrast solely affects the saliency of the stimulus, and that variability in the reaction time is dictated from variability in the initial detection time of the stimulus.

We found that contrast modulation of threat level produced chronometric and psychometric curves qualitatively similar to those obtained in learned perceptual categorisation tasks (Brunton et al., 2013) (N=13 mice, 209 trials; Fig. 3.4*A-B*; $P=1.6x10^{-9}$ for reaction time, repeated measures ANOVA). In addition, the vigour of the response, quantified as the maximal escape speed, also increased gradually as a function of contrast ($P=1.1x10^{-7}$, repeated measures ANOVA, Fig. 3.4*C*), showing that the probability, reaction time and vigour of instinctive escape are innately matched to the intensity of the threat stimulus. This demonstrates that escape responses of mice are not a reflexive action, but a flexible, probabilistic behaviour, and that the selection and strength of behavioural output is linked to features of a threatening stimulus.

3.2 A theoretical model for computing escape

We next modelled this relationship by modifying a single-layer network model previously applied to learned decision-making tasks (Shea-Brown, Gilzenrat, and Cohen 2008). This is a variant of drift-diffusion models (Gold and Shadlen, 2007; Ratcliff and Rouder, 1998) that integrates a variable over time and implements the decision to escape as a threshold-crossing process. The key variable in the model is the threat level, which increases with sensory evidence of threat and decays over time (Fig. 3.4*D*, see *Methods*). The threat level is treated as a noisy decision variable, and escape is initiated when the variable crosses the escape threshold. In this model, the probability of escape and reaction time depend on the strength of sensory evidence and on the accumulated noise, and escape vigour is computed as a function of the peak threat level. This model produced a very good fit to the behavioural data obtained from visual stimulation (lines in Fig. 3.4*A-C*). As a further test, we used innately aversive ultrasonic sweeps (Mongeau et al. 2003), which generated escape with high probability, short reaction times and high vigour (Fig. 3.4*A-C*), thus supporting a generic relationship between these variables.

3.3 Plasticity of defensive behaviour against visual threats

Escape in mice is a flexible behaviour (Vale et al., 2017), and accordingly, we observed that the escape responses elicited in this assay mice exhibit adaptation and sensitization to threatening visual stimuli. It has previously been shown that the state of an animal and its prior experience influence both predator avoidance and escape behaviour in a number of species (Filosa et al., 2016; Ramasamy et al., 2015), suggesting that mice might modulate their escape response over a

longer timescale than that afforded by early sensory system plasticity, which serves to prevent saturation when encoding the moment-to-moment changes of the visual scene. The question arose as to whether we could reliably induce adaptation and sensitisation to innately aversive visual cues, and if so, what parameters of the escape response might be modulated.

To induce adaptation to threat stimuli, animals were repeatedly presented with low contrast spots in quick succession (30-40% contrast; minimum ISI=5s, stimulation time determined by next entry into threat area), which elicited flight at low probability or were subthreshold, after which, high contrast (98%) stimuli were then presented to probe escape responses (Fig. 3.5*A*). We found that the probability of escape to strong visual threats was significantly reduced compared to naive animals (P_{escape}=35.7% by 5th spot; N=8 animals, 42 trials, vs control, P_{escape}=100%; N=6 animals, 20 trials, P=<0.0001 Fisher test; Fig. 3.5*B-left*) while the vigour of these post-adaptation escape responses was also significantly reduced (Fig. 3.5*B-right*)). We noted that animals hardly ever escaped on the first spot of the trial sequence (P_{escape}=2.3%; Fig. 3.5*B-left*). Accordingly, the reaction time between stimulus detection and escape initiation was found to be significantly longer on average, and more variable, that control animals, consistent with a right-ward shift in the the reaction time of escape (Fig. 3.5*C*). Intriguingly, we did not measure a significant change in the time taken for animals to detect the stimulus, suggesting that adaptation is not occurring in early visual system sensory processing but is instead influencing the decision period, thus supporting the idea that escape behaviour might be modelled as a decision process. In conclusion, adaptation causes a coherent right-ward shift in the chronometric, psychometric and vigour stimulus-response curves of escape, as presented in Fig. 3.4*A-C*, and is consistent with a model in which these variables are highly correlated.

We found that sensitisation could be induced by the inverse protocol (Fig. 3.5*D*). Repeated presentations of high contrast stimuli caused subsequent low contrast stimuli to evoke escape at a significantly higher probability than low contrast stimuli in naive animals (P_{escape}=100%; N=6 animals, 15 trials, vs control, P_{escape}=14%; N=8 animals, 50 trials, P=<0.0001 Fisher test), and at increased vigour (Fig. 3.5*E*). Detection times were again unaffected but strikingly, the reaction times were significantly reduced (Fig. 3.5*F*), consistent with a left-ward shift in the stimulus response curves.

As a dark expanding visual stimulus can trigger immediate innate defensive reactions in a range of animals, we asked whether this stimulus is also sufficient to induce innate aversion of the stimulation area. We therefore exposed animals to repeated high intensity threats, and quantified their movements during free exploration immediately afterwards. We found that animals developed strong place aversion, quantified as a decrease in both the time spent in the threat area, and the frequency of visits to it (time spent in threat area=35.1±3.5% for naive animals vs 5.1±2.0% after conditioning, N=7 mice, P=2.2×10^{-5}, two-tailed t-test, Fig. 3.6*A-C*). In

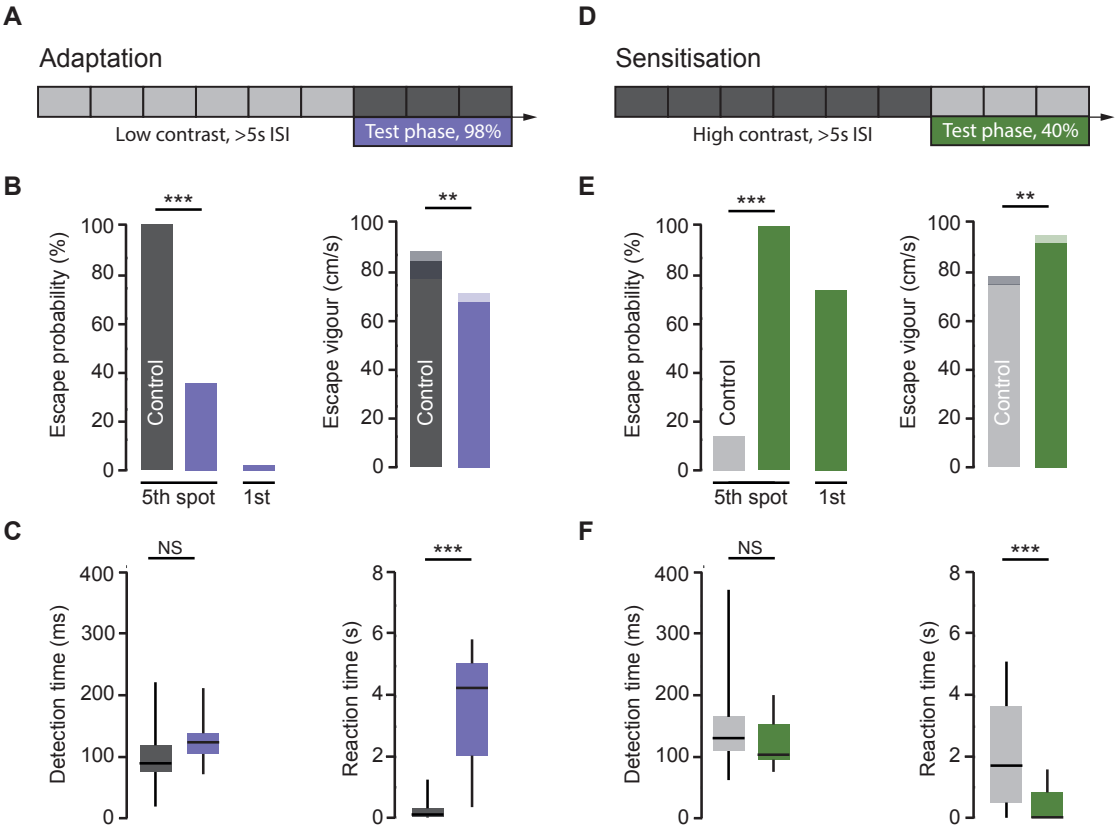

Figure 3.5 Escape behaviour is modifiable by past experience, exhibiting adaptation and sensitisation to threats. **A:** Strategy to assess adaptation to visual threats. **B:** Repeated exposure to weakly threatening stimuli causes a significant reduction in escape probability (left) and vigour (right) when presented with stimuli which usually are usually highly threatening (control). P_{escape} on the first spot in the stimulus sequence of five is also shown. Maximum speed of escape=68±3cm/s; N=5 animals, 18 trials, vs control 84±4cm/s; N=10 animals, 20 trials, P=0.0048 two-tailed t-test. **C:** The time between stimulus onset and detection was not significantly altered by adaptation (left), while the reaction time to escape was greatly increased (right). Mean detection time=128±8ms after adaptation; N=6 animals, 37 trials, vs control 101±12ms; N=10 animals, 20 trials; P=0.0528, two-tailed t-test. Mean reaction time=3.78±0.41s after adaptation; N=5 animals, 16 trials, vs 0.23±0.07s for control; N=10 animals, 18 trials; P=<0.0001, two-tailed t-test. **D:** Strategy to assess sensitisation to visual threats. **E:** Repeated exposure to highly threatening stimuli causes a significant increase in escape probability (left) and vigour (right) when presented with stimuli which usually are usually weakly threatening (control). Maximum speed of escape=91±3cm/s after sensitisation; N=6 animals, 15 trials, vs control 74±3cm/s; N=11 animals, 31 trials, P=0.0028, two-tailed t-test. **F:** Sensitisation does not change stimulus detection time (left), but greatly reduces the reaction time when escaping from low contrast stimuli (right). Mean detection time=122±9ms; N=6 animals, 15 trials, vs control 101±12ms; N=11 animals, 33 trials; P=0.148, two-tailed t-test. Mean reaction time=0.36±0.14s; N=6 animals, 15 trials, vs control 1.95±0.29s; N=11 animals, 31 trials; P=0.0007, two-tailed t-test. Box–and–whisker plots indicate median, interquartile range and the 5th–95th percentiles of the distribution. Bars indicate mean with shaded s.e.m.

control experiments with no stimulation, we observed that when naive animals explored the arena, they occasionally initiated spontaneous escapes back to the shelter upon approaching the threat area ($P_{spontaneous\ escape}$=3.1% of excursions approaching the threat area), which could be due to a difference between the perceived environmental threat of the open part of the arena and the shelter, or could constitute a behavioural module of exploratory behaviour movement patterns where fast trips are made to the home base (in this instance, the shelter of the arena). Interestingly, after conditioning we observed that the frequency of spontaneous flight initiation upon approaching the threat presentation area increased 5-fold, with a speed profile highly comparable to low vigour stimulus-evoked escapes ($P_{spontaneous\ escape}$ 3.1% for naive animals versus 16.0% after conditioning, N=13 mice; P=$3.3x10^{-10}$, Fisher test; Fig. 3.6*D*).

3.4 Summary

In conclusion, escape behaviour in mice is not a reflex-like reaction, but a reactive behaviour that demonstrates flexibility in its initiation and vigour within single animals, and can be modified by recent experience. In this chapter, stimulus-response curves were presented from our behaviour assay that strongly suggest that escape can be thought of as an innate decision-making task. We reported behavioural paradigms and a theoretical framework to dissect these phenomena and understand escape in terms of a decision process which integrates threat information over time.

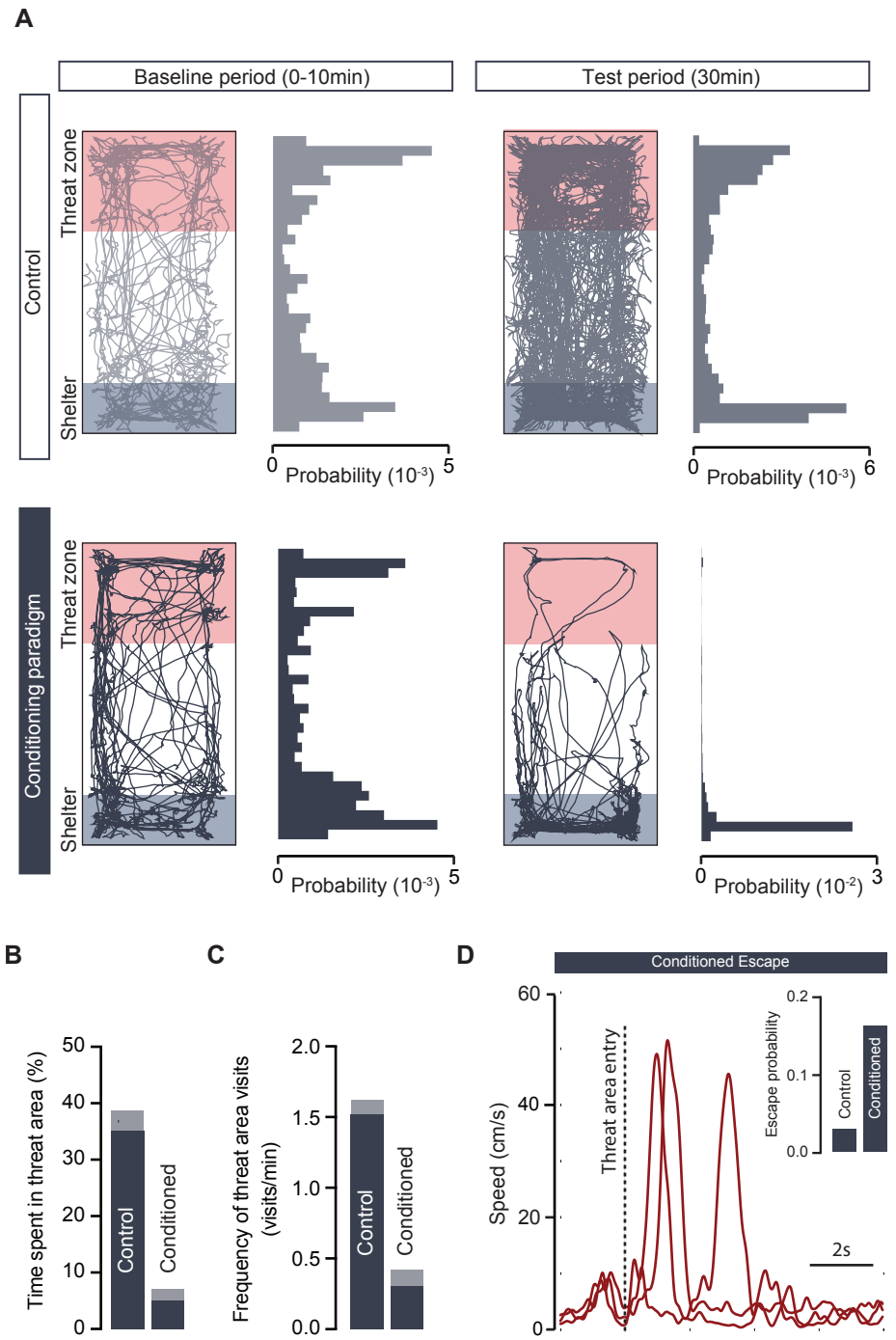

Figure 3.6 Exposure to repeated high contrast visual stimulation causes short-term aversion of the threat area and spontaneous escapes. **A:** Traces and probability distributions for the location of two example animals during free exploration (top), and before and after a high contrast visual stimulation conditioning paradigm (bottom), showing avoidance of the threat area (bottom right). **B:** Time spent in the threat area by the animal decreases with the conditioning paradigm (35.1±3.5% for naive animals vs 5.1±2.0% after conditioning, N=7 mice, $P=2.2x10^{-5}$, two-tailed t-test). **C:** The frequency of visits to the threat area by the animals also decreases (1.51±0.10 visits/min for naive animals vs 0.30±0.12 after conditioning, N=7 mice, $P=<1x10^{-4}$, two-tailed t-test). **D:** Example speed traces from three animals showing spontaneous escape after conditioning, initiated shortly after entering the threat area. Animals also exhibit spontaneous escapes in the vicinity of the threat area boundary. Inset, conditioning increases the frequency of spontaneous escapes.

4 Two midbrain circuit elements are necessary for escape behaviour

4.1 Glutamatergic neurons in the medial superior colliculus are required for escape from visual threats

Previous work has suggested a role for multiple brain regions in processing visually-evoked instinctive defensive behaviours (Zhao et al., 2014; Shang et al., 2015; Wei et al., 2015; Dean et al., 1989), so we next aimed to define circuit nodes and cell-types that are critical for computing escape. Currently, researchers do not have reliable genetic access to the superior colliculus and periaqueductal gray in a layer- or column-specific manner respectively, nor does there exist a broad array of cell-type specific driver lines in these regions such as in the cortex, retina or parts of the hypothalamus (see Introduction). We hypothesised that excitatory neurons in the superior colliculus may be involved, or even necessary, in the computation of sensory-evoked escape behaviour based on the following premises: (1) the superior colliculus receives direct retinal input (Apter, 1945; Sperry, 1963; Schiller, 1984), (2) the latency from stimulus onset to escape onset can be as low as 40ms in our behavioural assay, suggesting a short pathway from sensory input to motor output in terms of number of synapses, (3) microinjections of glutamate[1] targeted to it have been shown to elicit defensive behaviours (Dean et al., 1988)[2], (4) in cats and mice, neurons in the SC have been to shown to respond to looming stimuli in vivo (Liu et al., 2011; Zhao et al., 2014) . Furthermore, the superior colliculus is retinotopically organised, with the upper visual field (and therefore presumably the overhead visual stimulus) being represented in the medial part of the superior colliculus (Dräger and Hubel, 1976), which in rodents is suggested to have a preferential role in defence, versus a preferential role in approach behaviours suggested for the lateral region (Westby et al., 1990; Comoli, 2012).

In order to test the role of excitatory neurons in the medial superior colliculus, we first chose to genetically ablate glutamatergic neurons in the mSC of VGluT2:YFP mice by using Cre-dependent viral expression of a genetically engineered caspase, which triggers cell-autonomous apoptosis

[1] By directly activating dendrites and somata, this avoids the en passant axonal activation that can occur with electrical stimulation.

[2] Recently published optogenetic experiments (Shang et al., 2015) had not been reported at the time of our experiments.

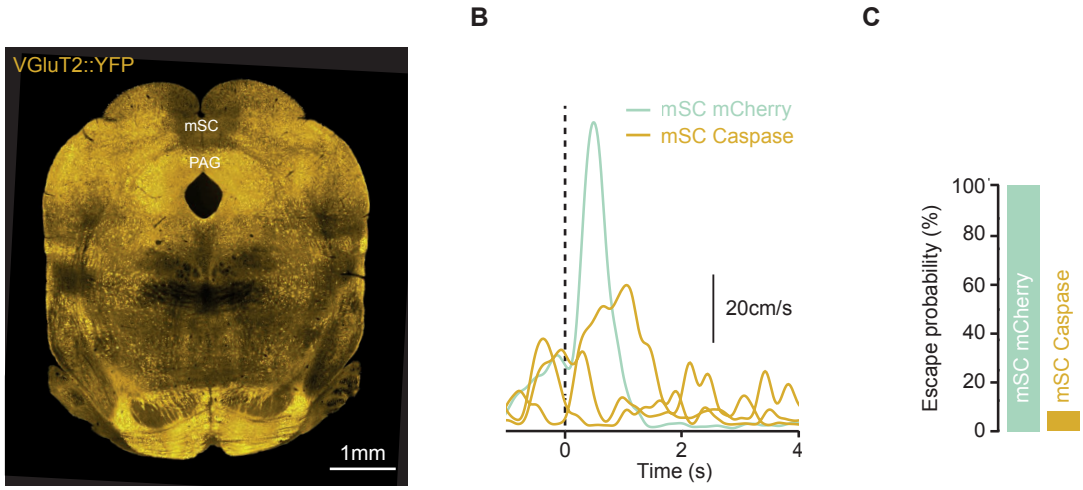

Figure 4.1 Glutamatergic medial superior colliculus neurons are necessary for escape **A:** Genetic ablation of VGluT2$^+$ neurons expressing YFP specifically in the medial superior colliculus. **B:** Example speed traces from three mSC VGluT2::Casp animals (yellow) showing that foraging movement is unaffected by visual stimulation, and one control animal (VGluT2::mCherry; green) showing escape to the same stimulus. Dotted line shows the onset of visual stimulus. **C:** Visually-evoked scape is effectively abolished in caspase treated animals (see text for details).

(Yang et al., 2013) (See Methods). First, VGlut2::YFP animals were placed in the arena and exposed to one high contrast visual stimulus to confirm their escape responses were intact before surgery. The mSC was then injected with AAV2-flex-taCasp3 (VGluT2::Casp; Fig. 4.1*A*) or a control virus (VGluT2::mCherry), and escape responses were assessed after 14-16days using visual stimuli. Strikingly, VGluT2::Casp animals did not display startle-like reactions to the stimuli ($P_{startle}$=0%; N=4 animals, 25 trials, vs control, $P_{startle}$ =100%; N=3 animals, 13 trials, P=<0.0001 Fisher test), and had severely impaired escape responses (P_{escape}=8%; N=4 animals, 25 trials, vs control P_{escape} =100%; N=3 animals, 13 trials, P=<0.0001 Fisher test; Fig. 4.1*B-C*). Furthermore, in the 2/25 trials with escape responses, animals engaged in slow escapes >2s after the onset of the stimulus without displaying a behavioural reaction to the expanding spot (such as a brief startle or pause correlated with stimulus onset), suggesting that these are spontaneous escapes or trips back to the nest, rather than stimulus-evoked escapes. These results demonstrate that glutamatergic neurons in the mSC are necessary for visually-evoked escape behaviour.

The dorsal periaqueductal gray is considered to be a key area in the expression of defensive behaviours, including flight reactions (Gross and Canteras, 2012), so we next targeted the dPAG of VGluT2:YFP mice with caspase to investigate the role of its excitatory neurons in escape. Despite ablating VGluT2$^+$ neurons bilaterally in the dPAG, escape behaviour was not significantly impaired (P_{escape}=81%; N=6 animals, 27 trials, vs control P_{escape} =100%; N=3 animals, 13 trials, P=0.154 Fisher test; Fig. 4.2*B-C*). As genetic ablation is a chronic manipulation, and other projection targets of the mSC such as the PBGN and cuneiform nucleus (CuN) are also sufficient to induce escape upon stimulation (Shang et al., 2015; Mitchell et al., 1988), we speculated

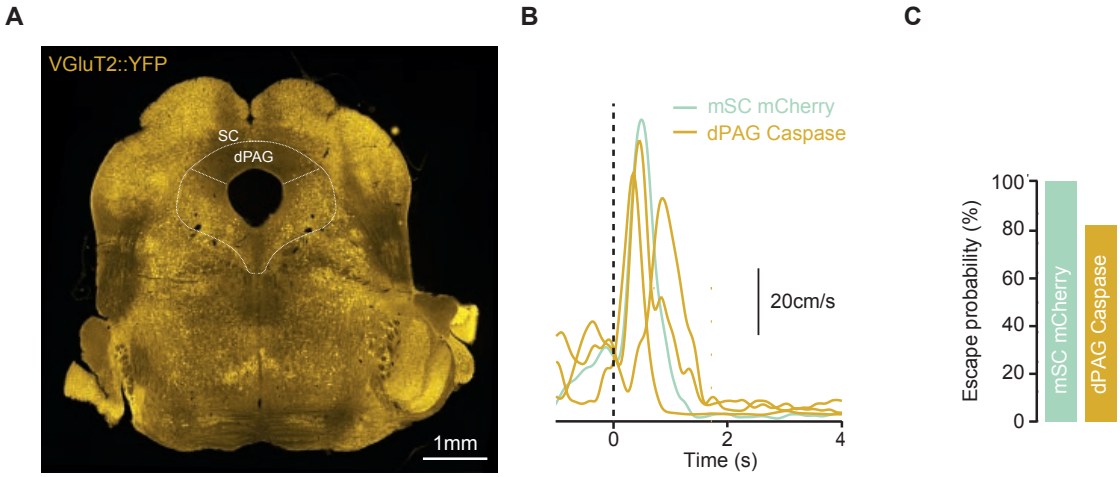

Figure 4.2 Ablation of glutamatergic dorsal PAG neurons does not affect escape **A:** Genetic ablation of VGluT2$^+$ neurons expressing YFP specifically in the dorsal PAG. **B:** Example speed traces from three dPAG VGluT2::Casp animals (yellow) and one control animal (VGluT2::mCherry; green), showing that escape responses are intact. Dotted line shows the onset of visual stimulus. **C:** Visually-evoked scape is not significantly reduced in caspase treated animals (see text for details).

that either the remaining non-ablated cells of the dPAG were still sufficient to evoke escape, or other circuit elements may compensate for the dPAG and provide an alternate pathway for escape. Therefore, we next decided to use optogenetic inhibition to target glutamatergic dPAG neurons acutely, using the light-activated outward proton pump eArch3.0. The viral vector AAV-DIO-eArch3.0-eYFP was injected into the dPAG of VGluT2-Cre animals (N=6, single injection into dPAG; N=2, injection into the dPAG at multiple anteroposterior sites) and an optic fibre implanted dorsal to the injection site. Animals were subjected to alternating trials of visual stimulation alone, and visual stimulation during green light stimulation. However, optogenetic inhibition did not significantly affect flight probability, although we observed a trend towards reduction (P_{escape}=50% for visual stimulation, vs P_{escape}=36% for visual and laser stimulation; P=0.0645 Fisher test; N=8 animals, 100 trials visual stimulation only, 102 trials visual stimulation during laser). As lesion and inactivation studies have previously linked the PAG to flight behaviour (Blanchard et al., 1981), the *in vivo* efficacy of eArch3.0 to silence neurons in our preparation was unknown[3], and we not observe any overt behavioural phenotypes from light stimulation alone which would help us assess the function of the manipulation, we resolved to inactivate the dPAG with an acute method that would provide the maximum effect size, and did not investigate the role of other brain areas in escape behaviour using Arch.

[3] See Tovote et al. (2016) for successful application of Arch to VGluT2$^+$ neurons in the vlPAG, demonstrating their necessity to conditioned freezing.

4.2 The dorsal PAG is necessary for initiating escape

To inactivate circuit elements both acutely and robustly, we next performed targeted infusions of muscimol, an agonist of $GABA_A$ receptors, conjugated to a fluorescent label. First, we confirmed the finding that the mSC is necessary for visually-evoked escape behaviour. After implanting guide cannulae in the mSC, animals were tested by using sensory stimulation to evoke flight responses (pre-drug), then infused with muscimol or vehicle through internal cannulae (see *Methods*), and again tested using sensory stimulation after 30min. Visual stimulation after inactivation of the mSC severely affected escape behaviour in an identical manner to genetic ablation, producing no detectable behavioural response (P_{escape}=0%, N=6 mice, P=4.3x10^{-8} Fisher test comparison between pre- and post-drug; Fig. 4.3*A*), again suggesting that the link between sensory stimulus and initiation of a response to threat was critically compromised.

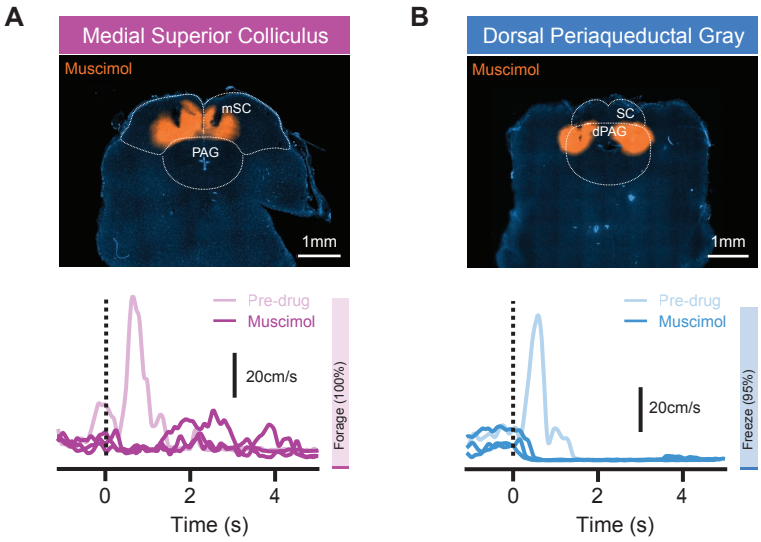

Figure 4.3 Inactivation of medial superior colliculus and dorsal periaqueductal gray affect escape behaviour in distinct manners. **A:** Example image of muscimol infusion in the mSC with internal cannulae tracks visible in each hemisphere (top). Below, example speed traces are shown in response to threat before ('pre-drug') and 30min after infusion ('muscimol') for one animal, showing that mSC-inactivated animals do not interrupt foraging and do not initiate a defensive response when faced with threat, with bar (bottom right) showing the pooled foraging rate for all animals after infusion. Onset of visual stimulus is t=0s. **B:** Example image of muscimol infusion in the dPAG. Below, example speed traces are shown as in **A**. Threat presentation after muscimol infusion into the dPAG causes a switch from escape to freezing. Bar (bottom right) shows the pooled freezing rate for all animals.

We next performed the inactivation assay using muscimol targeted to the dPAG. Remarkably, inactivation of the dPAG led to a complete switch from escape to freezing in response to threats (P_{escape}=0%, P_{freeze}=95%, mean freezing duration=18.5±3s; N=6 mice, P=1.2x10^{-7} Fisher test for comparison between pre- and post-drug; Fig. 4.3*B*), indicating that the threat was still detected and a defensive action initiated, and that the dPAG is specifically required to initiate escape. For both mSC and dPAG inactivation, escape responses to sound stimuli were also impaired (Fig.

4.4*A*), suggesting that the mSC and dPAG process both visual and auditory threat information to initiate escape. Interestingly, dPAG muscimol inactivation did not significantly affect the time taken for the stimulus to be detected (mean latency to startle response = 92±7% of pre-drug, N=6, vs 91±13% for dPAG vehicle, N=3, P=0.92 U-Test; Fig. 4.4*B*), further supporting the idea that threat detection was intact, and only escape initiation was inhibited. In a set of control experiments, we found that vehicle infusion into either the mSC or dPAG did not affect escape probability (mSC, P_{escape}=96% N=3 animals, 25 trials; dPAG, P_{escape}=95.7%, N=3 animals, 23 trials, for each group P=1 for Fisher test comparison between post-drug and 100%; Fig. 4.4*C*), which strongly suggests that the distinct effects on escape that we observed using muscimol were indeed specific to neuronal silencing within the target regions, rather than adverse effects of cannula insertion or liquid infusion. Importantly, neither did we observe a difference in the foraging speed of the animal between muscimol and vehicle infusion in the 10min acclimatisation periods pre- and post-drug, indicating that the effects on escape behaviour were not due to a non-specific disruption of general motor function (Fig. 4.4*D*).

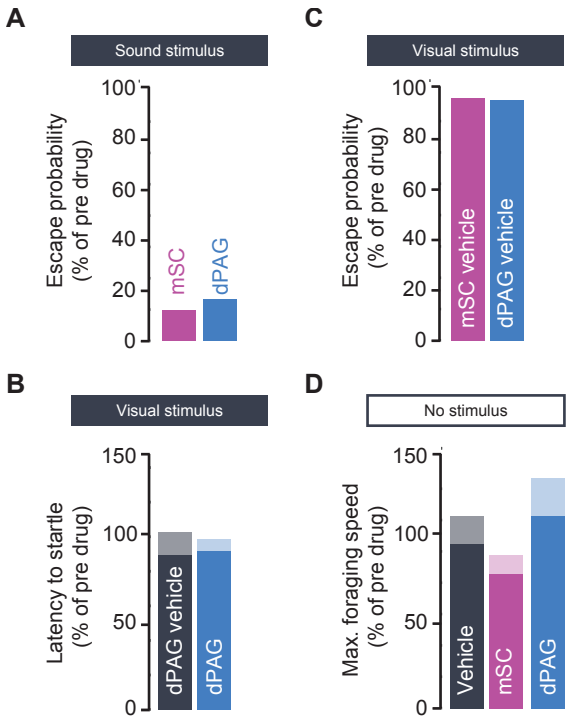

Figure 4.4 Inactivation selectively abolishes escape behaviour. **A:** Muscimol infusion in the mSC and dPAG causes a strong reduction in escape probability in response to threatening sound stimuli (SC: N=5, P=4.6x10^{-6} for probability, Fisher test; PAG: N=2, P=0.04 for probability, Fisher test). **B:** Muscimol infusion in the dPAG does not change the latency to stimulus detection, as quantified by the onset time of a startle-like response. **C:** Vehicle infusion in the mSC or dPAG does not change threat-evoked escape probability (mSC; N=3, P=1 Fisher test; dPAG; N=3, P=1 Fisher test). **D:** Inactivation of mSC and dPAG does not affect running speed during foraging behaviour. Animals with vehicle infusion into mSC and dPAG are pooled. (N=6 each, vehicle vs mSC; P=0.36, vehicle vs dPAG; P=0.56, two-tailed t-test). In all bar plots shaded area shows s.e.m.

4.3 Inactivation of additional brain regions implicated in visually-evoked and defensive behaviour

4.3.1 Visual cortex and amygdala are not vital circuit elements

Having demonstrated that mSC and dPAG have necessary and distinct roles in escape behaviour, we next targeted other brain regions that are part of defensive circuits. Recently, visual cortex (V1) has been shown to modulate the gain of looming responses in the SC (Zhao et al., 2014) and a corticotectal projection from layer 5 of V1 to SC was sufficient to drive defensive behaviours when stimulated optogenetically (Liang et al., 2015). However, as the SC is heavily innervated by retinal ganglion cells and LGN directly, we predicted that V1 would not be necessary for visually-evoked escape behaviour. We found that bilateral inactivation of V1 did not have an effect on escape probability, while showing a non-significant trend towards decreased response vigour (N=2, P=1 for probability, Fisher test; P=0.09 for vigour, Mann-Whitney U-test; Fig. 4.5). This is consistent with the reported modulatory role for V1, and suggests that it is not a critical relay in the computation of escape behaviour.

Subregions of the amygdala are thought to have distinct roles in the expression of learned and innate defensive behaviours(LeDoux, 2003): for example, the central nucleus can drive conditioned flight (Fadok et al., 2017), and freezing behaviour via the vlPAG (Tovote et al., 2016), while lesions of the medial amygdala decrease the innate fear responses to live predators (Gross and Canteras, 2012). It has also been proposed that the amygdala receives visual threat information from the superior colliculus via the lateral posterior nucleus of the thalamus (Wei et al., 2015). We therefore broadly targeted the amygdala, using long internal cannulae and a large volume of muscimol (see *Methods*) to inactivate central, basal and medial amygdala bilaterally in the same animal. We found that escape probability was not significantly affected, but observed a significant reduction in vigour (N=4, P=0.39 for probability, Fisher test; P=0.027 for vigour, two-tailed t-test; Fig. 4.6). This suggests that the amygdala plays a modulatory role in escape, but it does not appear to be a necessary circuit element.

4.3.2 Evidence that the parabigeminal nucleus is dispensable in flight behaviour

One recent study has suggested that the superior colliculus activates escape responses to expanding spot stimuli through a projection to the parabigeminal nucleus (PBGN; Shang et al., 2015). To test whether the PBGN is a necessary relay in the generation of escape, we bilaterally targeted the PBGN of VGluT2-Cre mice with muscimol infusions, which also partially spread to the surrounding cuneiform nucleus. As the study by (Shang et al., 2015) stimulated the terminals of SC neurons expressing channelrhodopsin-2 (ChR2) in the PBGN to conclude that this pathway

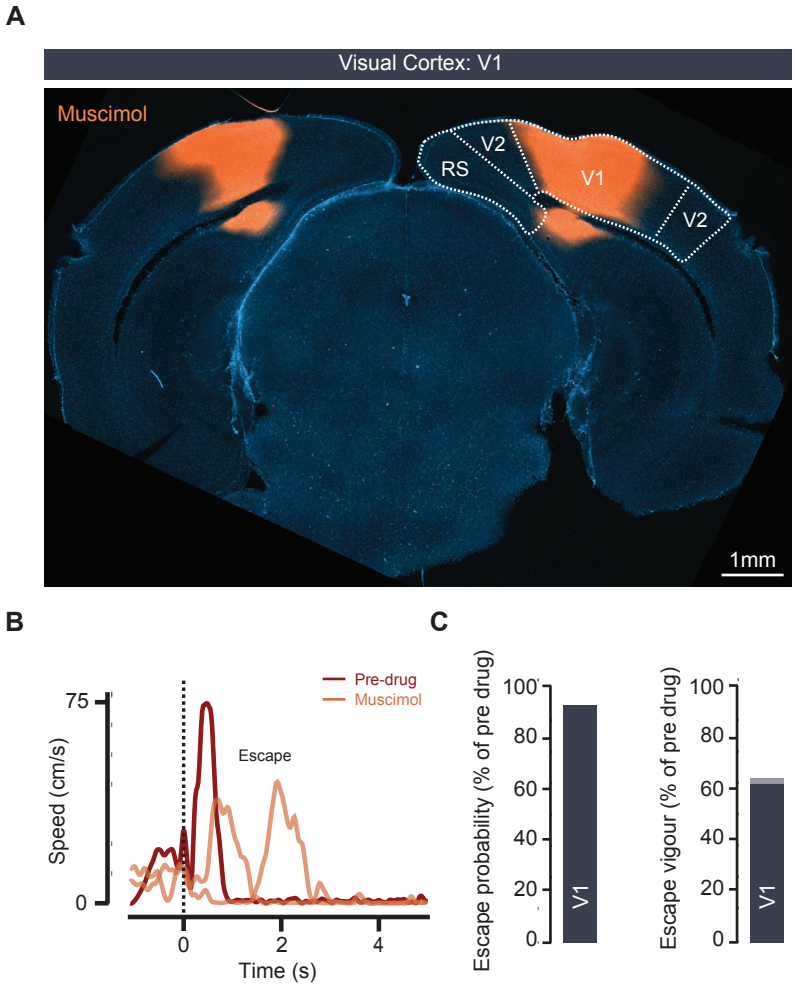

Figure 4.5 V1 is not necessary for visually-evoked escape, but may modulate escape vigour **A:** Image of bilateral muscimol infusion into visual cortex area V1 **B:** Speed traces during threat stimulus presentation show that mice still engage in escape behaviour, but with reduced vigour. **C:** Summary quantification for escape probability (left) and vigour (right) after V1 acute inactivation, showing that escape probability is not significantly affected, and that there is a trend towards decreased vigour. Bar plot shaded area shows s.e.m.

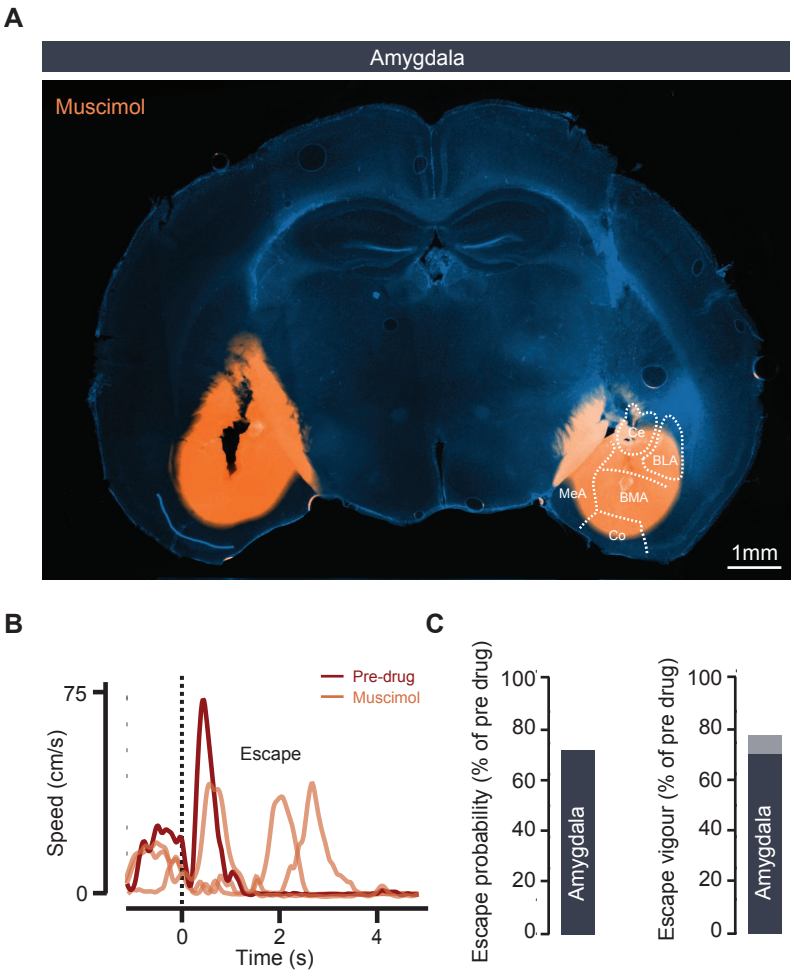

Figure 4.6 Inactivation of the amygdala reduces vigour but does not affect escape probability. **A:** Image of bilateral muscimol infusion into the amygdala **B:** Speed traces during threat stimulus presentation showing reduced vigour during escape. **C:** Summary quantification for escape probability (left) and vigour (right) after acute inactivation of the amygdala, showing that escape probability is not significantly affected, and that vigour is significantly decreased. Bar plot shaded area shows s.e.m.

causes escape behaviour, but did not control for antidromic stimulation or inhibit the PBGN to demonstrate its necessity, it is possible that the observed escape reactions were in fact elicited by SC activation via alternate pathways. We therefore expressed ChR2 in the medial superior colliculus of the same animal, and implanted an optic fibre, in order to investigate whether SC activation can still cause escape behaviour if the PBGN is acutely inactivated. We found that animals displayed intact and robust escape responses to both expanding spot stimuli (N=1/1 animals) and optogenetic activation (N=3/3 animals, P=0.26 for probability, Fisher test; Fig. 4.7). In fact, compared with the pre-muscimol ChR2-evoked escape response, vigour was significantly increased (P=0.045 for vigour, two-tailed t-test; Fig. 4.7C). Importantly, we could trace the axons of mSC VGluT2::ChR2 neurons into the PBGN, strongly suggesting that our preparation activated the reported SC-PBGN pathway, and that the PBGN is not necessary for escape response evoked by visual threats or activation of the medial superior colliculus.

Lastly, we aimed to investigate the role of the ventromedial hypothalamus (VMH). We hypothesised that the VMH would not be necessary to the generation of visually-guided escape behaviour, but may play a modulatory role. Although the dorsomedial VMH has a well-established role in defensive behaviour against predators and receives amygdala input (Gross and Canteras, 2012), it does not appear to receive direct visual input, except for a small number of axons from the population of melanopsin-expressing intrinsically-photosensitive retinal ganglion cells (ipRGCs) which are not thought to transmit spatial information (Hattar et al., 2006; Fernandez et al., 2016)[4]. Furthermore, recent experiments by Kunwar et al. (2015) have shown that a defensive behaviour-driving cell population in the dmVMH, marked by SF-1, is dispensable for escaping from visual threats. Importantly, high speed activity bursts driven by optogenetic activation of these neurons occurs after a considerable latency (>5s), suggesting that they are upstream of escape circuits. We bilaterally targeted the VMH with acute muscimol injections after assessing responses to visual stimuli (N=3 animals), however, all animals showed severely restricted movement post-infusion and appeared in pain, precluding further behavioural tests. Due to the focus of this study on the midbrain, and the outcome of experiments by Kunwar et al. (2015) strongly suggesting that dPAG-projecting VMH neurons are not involved in visually-evoked escape behaviour, we did not pursue this line of investigation.

4.4 Summary

In this Chapter, we manipulated the activity of circuit elements that are thought to play a role in defensive and visually-guided behaviour during an escape behaviour assay. Evidence is

[4] Incidentally, as well as their main projection target of the suprachiasmatic nucleus of the hypothalamus, the major circadian centre of the brain, a subset of ipRGCs also project to the SC and PAG

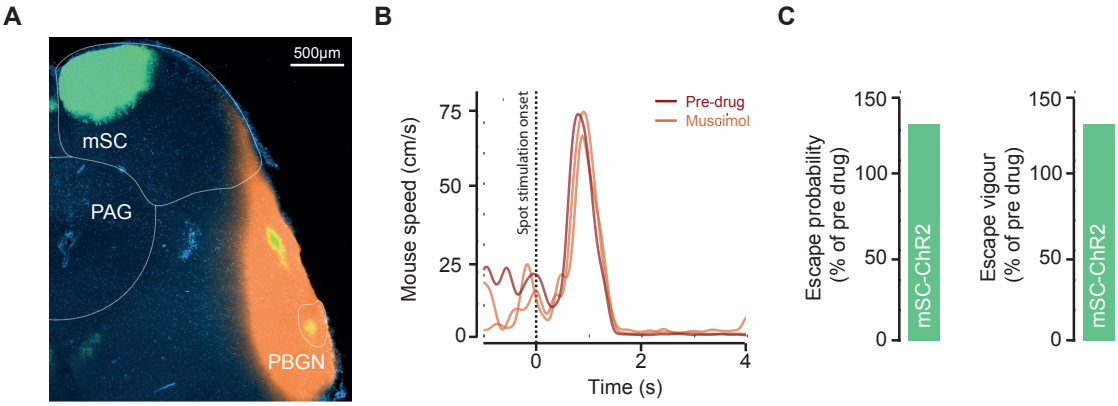

Figure 4.7 Inactivation of the PBGN does not affect escape behaviour **A:** Image showing expression of ChR2-EYFP in excitatory VGluT2^{+} neurons of mSC (green) with projections to the PBGN (yellow) and muscimol infusion (orange). (B) Speed traces for spot-evoked escape response from one mouse before and after acute PBGN inactivation. (C) Summary data for escape probability and vigour during mSC optogenetic stimulation and PBGN acute inactivation, showing no difference.

presented using acute pharmacological inactivation that the mSC and dPAG are necessary for the initiation of escape behaviour in response to sensory stimuli that mimic predatory threats. This necessity was further refined to the glutamatergic population of neurons in the mSC, while genetically-targeted manipulations of the dPAG were unsuccessful in manipulating escape robustly. We next found that broad inactivation of the amygdala and V1 did not reliably alter the probability of escaping to threats, but that amygdala inactivation could reduce the vigour of evoked threats. Inactivation of the PBGN, a projection target of the SC suggested to be important evoking escape, did not reduce the probability or vigour of escape. In conclusion, our results strongly suggest that the mSC and dPAG are critical to initiating instinctive escape reactions.

5 Neural activity during escape behaviour

We sought to make physiological recordings from the two necessary regions identified in Chapter 4 to further investigate their role in the computation of escape. In order to record both during escape and from genetically-defined neurons, we opted to use head-mounted miniature microscopes (Ghosh et al. 2011) in freely-moving animals and combine them with GRIN lenses to reach deep midbrain targets[1]. For the superior colliculus, we targeted our recordings to the deeper layers as they receive multisensory input (Sparks and Hartwich-Young, 1989) and stimulation studies have shown that activation of the deeper layers can cause escape (Sahibzada et al., 1986).

5.1 Computational roles of excitatory neurons in the medial superior colliculus and dorsal periaqueductal gray

We used VGlut2-Cre mice to target the calcium indicator GCaMP6s to excitatory neurons by injecting AAV9-CAG-FLEX-GCaMP6s into the deeper layers of the mSC (dmSC) or dPAG, and implanted GRIN lens cannulae at the target region. We chose to use GCaMP6s variant of the GCaMP6 genetically-encoded calcium indicator family, as it provides the highest sensitivity in single action potential detection of the current generation due to its high signal to noise and is thus well suited for epifluorescent *in vivo* measurements (Chen et al., 2013). After 3 weeks, calcium activity was imaged using head-mounted miniature microscopes while animals explored the arena and were presented with threatening stimuli, often eliciting escape.

We found that neurons in both areas showed clear increases in calcium signals during stimulus-evoked escape (57 dPAG cells from 3 mice, 50 trials; 177 dmSC cells from 8 mice, 70 trials; Fig. 5.1*A-B*), but the temporal profile of their activation was distinct. We observed that dPAG cells were active in the peri-escape initiation period, with a mean onset that was not significantly different from the onset of escape (mean onset= -0.24±0.21s, vs escape onset, t=0; P=0.24, two-tailed t-test; Fig. 5.1*C*). This suggests that activity in dPAG excitatory neurons is time-locked and synchronous to the onset of the escape response.

[1] As an alternative method, we developed a head-fixed behaviour assay and performed preliminary two-photon recordings in the superior colliculus (see *Appendix*).

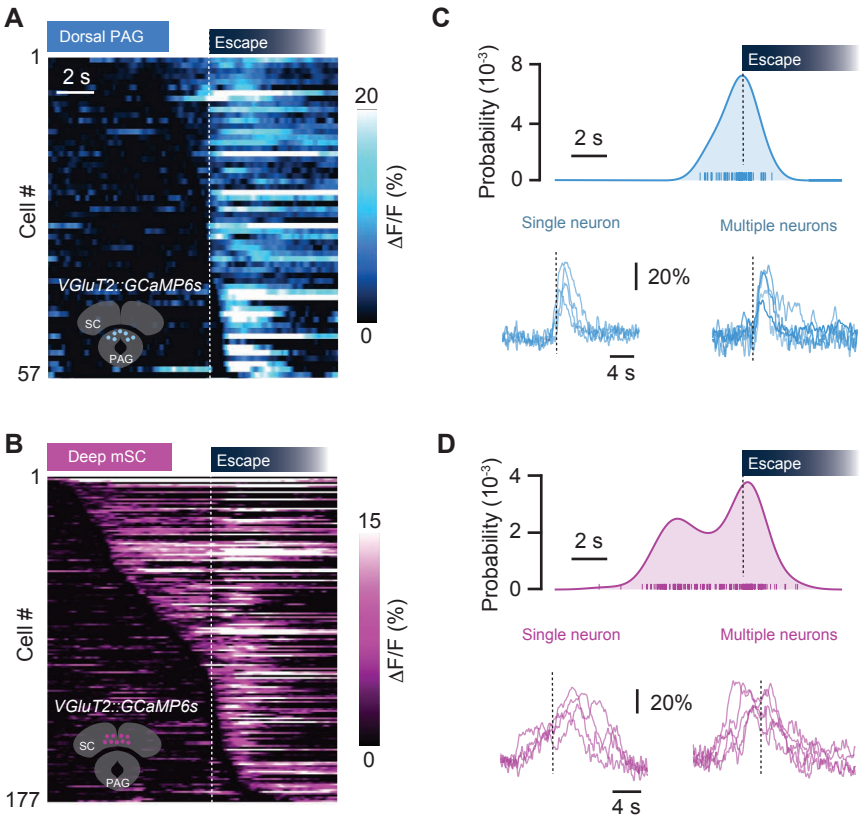

Figure 5.1 Excitatory cells in the dorsal PAG and deep mSC are both active during escape, but with distinct temporal and population profiles. **A:** Raster showing the average calcium response for all recorded dPAG cells, aligned to escape onset and sorted by response onset, with the earliest in time at the top. Colour intensity denotes ΔF/F. **B:** Same as in **A** for dmSC cells. **C:** Top, distribution of calcium response onsets for all dPAG cells, where the curve is the kernel density estimation and markers are the onset of each cell. Bottom, single trial traces for a single neuron (left) and for multiple neurons in the same field of view (right), aligned to escape (dotted line). **D:** Same as in **C** for dmSC neurons.

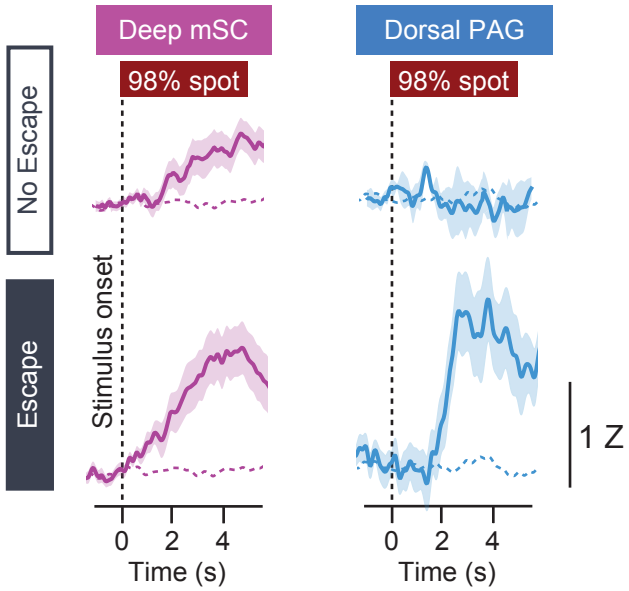

Figure 5.2 Population activity corresponding to outcome of threat presentation trial. The average population activity across all trials in response to 98% contrast spots (z-score) is shown sorted by trial outcome (escape/no escape) for dPAG (blue) and dmSC (pink), while dashed traces show activity with no stimulus presentation. Dashed line shows stimulus onset and shaded areas are s.e.m.

Activity in the majority of dmSC cells, however, preceded escape onset (mean onset= -1.51±0.17s , $P=4.9x10^{-16}$ two-tailed t-test comparison with escape onset; Fig. 5.1*D*). While the distribution of activity onsets in the dPAG was unimodal, we observed a bimodal distribution of activity onsets in the dmSC. Furthermore, analysis of single trials revealed that most mSC cells did not respond exclusively in the pre- or peri-escape period (in 75% of cells the onset varied across trials between pre-escape, and peri-escape). This indicates that the distribution does not reflect two distinct neuronal populations with different roles, but rather a bias on the activity onset of individual cells. On each trial, the onset of the dmSC ensemble activity was -1.77±0.5s relative to the onset of escape (significantly different from escape onset, P= 0.00075, two-tailed t-test), whereas the onset of dPAG ensembles was -0.25±0.48s (P=0.59, two-tailed t-test comparison with escape onset; Fig. 5.1*C-D*), further confirming a temporal difference in the activation of these two networks.

To determine whether dmSC and dPAG activity reflects the stimulus or the escape choice, we separated trials from the same stimulus intensity by trial outcome (Fig. 5.2). This analysis showed that dmSC neurons encode not only the presence of the threat stimulus, but also reflect the choice to escape (z-score=1.93±0.23 for escape, 1.18±0.11 for no escape; P=0.023, two-tailed t-test between escape and no escape; $P=5.8x10^{-10}$ 1-sample t-test between no escape and 0), whereas activity in dPAG neurons increases exclusively during escape trials (z-score=2.28±0.17 for escape, 0.49±0.19 for no escape; P=0.00028, two-tailed t-test between escape and no escape; P=0.11 1-sample t-test

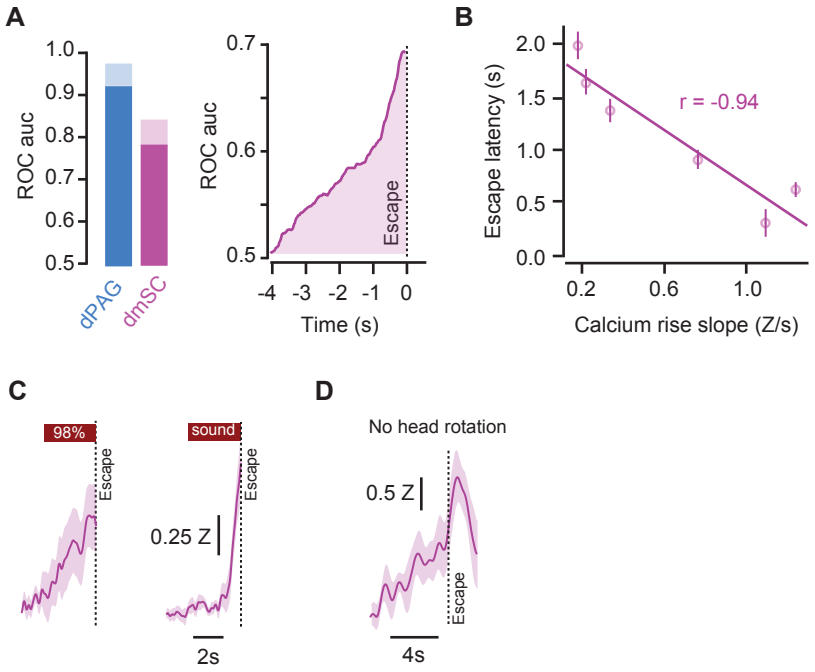

Figure 5.3 ROC analysis of pre-escape activity, and evolution of pre-escape signals in the mSC. **A:** Area under the curve (auc) for ROC analysis of dPAG and dmSC signals (left) and evolution of auc for dmSC signals up to escape onset (right). **B:** Correlation between the rise slope of the population activity and escape latency. **C:** Average population activity in the dmSC for escape trials in response to 98% contrast spots (left) and sound stimuli (right). The slope of the signal rise is steeper for sound-evoked escape. **C:** Average calcium signal for population activity in the dmSC during escape trials where the mouse was already facing the shelter and did not rotate the head (N=5 trials). Error bars in bar plots show s.d., shaded areas of trace averages show s.e.m.

between no escape and 0). This suggests that only dmSC activity reflects the stimulus, while the activity of both the dmSC and, to a greater extent, the dPAG reflects escape choice.

To estimate how well the activity of each of these populations is able to classify the escape choice, we used receiver-operator characteristic (ROC) analysis, and calculated the area under the ROC curve (aucROC), where a value of 1 indicates a perfectly discriminable escape outcome (i.e. escapes and failures to escape are classified correctly with a perfect score) from the neural activity, while a value of 0.5 indicates chance-level classification (thus with no predictive value)[2]. ROC analysis of the ensemble activity reflected this difference and showed that the dPAG is an almost perfect classifier of the trial outcome (auc=0.92), while the dmSC is a noisier, but still very good classifier (auc=0.78; Fig. 5.3*A*). Further evaluation of the ROC evolution from stimulus onset showed that an ideal observer of dmSC activity could correctly predict the decision to escape above chance level 900ms before escape initiation (68% correct at t=–900ms; Fig. 5.3*A*). In addition, the rate of increase of the dmSC ensemble activity was strongly anti-correlated with the

[2] The aucROC is mathematically equivalent to the performance of an ideal observer engaged in a two-alternative forced-choice task based on the measured neural signal, with a value of 0.5 reflecting random chance-level accuracy and values of either 0 or 1 indicating perfect discriminability (but in anti-correlation), and has been used successfully across systems to explore the relationship between neural activity and behaviour (Bizley et al., 2013; Romo et al., 1998; Britten et al., 1992; Niwa et al., 2012; Dayan and Abbott, 2002).

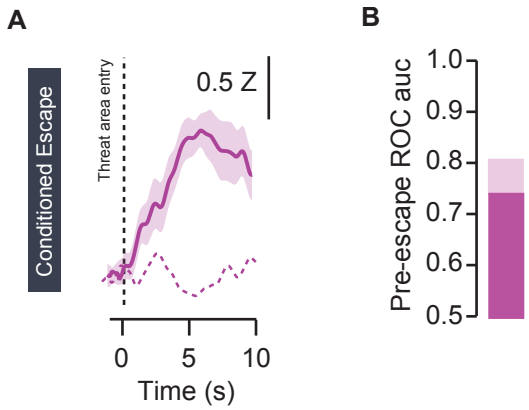

Figure 5.4 dmSC activity during spontaneous escape. **A:** Entering the threat presentation area elicits an increase in dmSC population activity. Dashed line is average activity before conditioning, shaded area is s.e.m. **B:** ROC auc for the dmSC signal before escape onset. Error bar shows s.d.

latency between stimulus presentation and escape (Pearson's r=-0.94, P=0.0048; Fig. 5.3*B*). This suggests that the rate at which network activity in the dmSC increases could be an important determinant of the reaction time, and is in agreement with our model: as the rate at which the accumulation of threat evidence increases, the escape threshold will be reached faster, thus causing faster reaction times to escape. We also observed different rise slopes between escape trials using the sound stimulus and high contrast visual threats, with faster calcium rises during sound stimulus trials (Fig. 5.3*C*), suggesting that increases in network activity in the dmSC can also be affected by the modality of threat.

In this escape assay, stimulation trials begin when an animal enters the threat area with its head direction opposite to the shelter direction, so that threats are delivered when animals are at a consistent location, speed and heading over trials. However, the superior colliculus can generate head movements in addition to eye movements (Sparks and Hartwich-Young, 1989). We therefore initiated a set of trials when the animal was in the threat area but facing the shelter, resulting in escape responses with no observable head-rotation movements, and observed similar population activity to standard trials (Fig. 5.3*D*). These experiments suggest that excitatory dmSC activity is an important determinant of escape initiation, and displays activity components related to both the presence and threatening stimulus and the outcome of the escape decision.

5.2 dmSC neurons are predictive of conditioned escape

Calcium responses in excitatory dmSC cells are temporally correlated with both the threatening stimulus and escape, so we asked whether there would be activity preceding spontaneous escape in the absence of external stimuli. Animals were therefore conditioned to high contrast stimuli to increase the frequency of spontaneous flights from the threat area (as in Fig. 3.6).

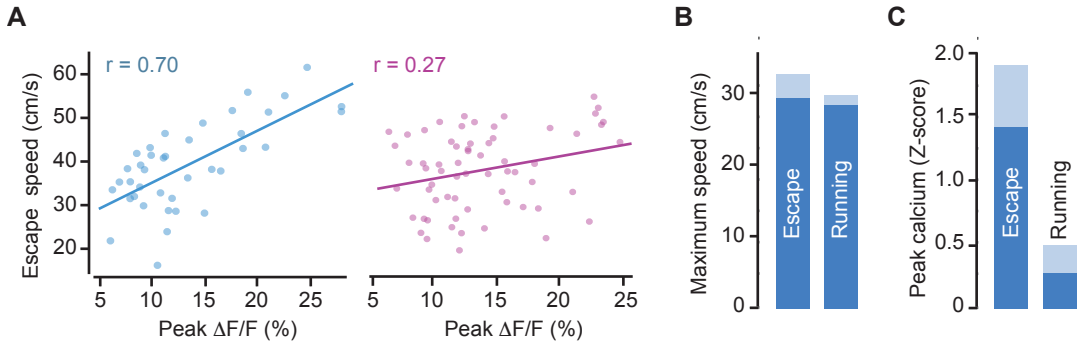

Figure 5.5 Peak of calcium transients encode speed of escape **A:** Correlation between the population activity of dPAG (left) and dmSC (right) and escape speed. Each data point is a single trial. **B:** Threat-evoked slow escapes and fast spontaneous running bouts during foraging are of similar speed (N=6 running bouts and N=6 escape trials, speed not significantly different, P=0.64, two-tailed t-test). **C:** Quantification of peak dPAG population calcium signal during movement trials in **C**, showing that activity increase in the dPAG is specific for escape (P=0.0018, two-tailed t-test).

Analysis of dmSC activity during conditioned flights showed a clear activity increase upon threat area entry and preceding escape, despite no stimulus presentation (mean z-score=1.94±0.17, n=57 trials, N=7 mice, P=0.00013, two-tailed t-test between pre and post-conditioning; Fig. 5.4*A*. Importantly, pre-escape activity in these conditions was still predictive of escape (auc at escape onset = 0.74, significantly above chance 2.1s before escape; Fig. 5.4*B*). Together, these data indicate that dmSC neurons encode a general variable that is correlated with the likelihood of escape.

5.3 Activity in dPAG VGluT+ neurons is strongly correlated with escape vigour

Further analysis of the escape-evoked calcium signals showed a significant correlation between escape speed and peak calcium activity, which was ~3 times stronger in dPAG than in the dmSC (PAG: Pearson's r=0.7, P=6.7x10^{-7}; SC: r=0.25, P=0.04; Fig. 5.5*A*), suggesting that the peak activity in the network could encode the vigour of escape. The speed of movement during escape can be considerably faster than running bouts during foraging. Therefore, to infer whether the observed calcium activity was specific for running during escape, or was related to running behaviour in general locomotion (as reported for the mesencephalic locomotor region; Roseberry et al., 2016), we analysed the trials with the slowest escape and extracted comparable control trials showing the fastest running bouts during exploration (Fig. 5.5*B*. We found that the peak calcium during escape runs was significantly greater than during running bouts of similar speed (5.5*C*), strongly suggesting that the dPAG is not encoding the speed of general locomotion. This is also supported by the finding that muscimol infusion into the dPAG selectively abolishes escape behaviour without affecting running speed during exploration (see Fig.4.4).

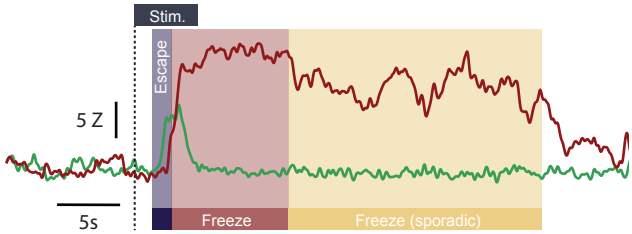

Figure 5.6 Calcium activity in dPAG-VGluT2$^+$ cells during freezing behaviour within the nest. Example traces from single ROIs in the dPAG during a 40% contrast looming spot trial, showing an ROI with escape-correlated activity (green) and freezing-correlated activity (dark red). In the ethogram, 'Freeze' denotes continuous freezing behaviour, after which the animal engaged in periods of freezing with intermittent movement ('sporadic'). This cell was reliably active across trials during long stimulus-evoked freezing bouts.

5.3.1 A subset of dPAG neurons are active during freezing

Once an escape response terminates in the shelter, animals often freeze before resuming foraging. Interestingly, we observed that 4 out of 57 cells (N=3 animals) showed sustained activity throughout this freezing behaviour, and that activity in these cells appears to ramp up during escape (Fig. 5.6). This subset was in the same field-of-view as escape-related dPAG cells but we cannot exclude that they are at the border of the dorsal and ventrolateral PAG, which is known to contain cells that control freezing (Tovote et al., 2016). Notably, we did not observe activity in this subset of cells during bouts of non-threat related immobility, suggesting they are specific for freezing behaviour.

5.4 Summary

We found that VGluT2$^+$ neurons in the dmSC increase their activity during repeated presentation of a threatening stimulus, while VGluT2$^+$ neurons of the dPAG are silent until the initiation of escape, and the magnitude of their peak activity is strongly correlated with the speed of escape. Together with behavioural experiments and decision-making modelling, these results suggest that the SC accumulates evidence of threat-related variable which dPAG neurons then threshold to drive escape behaviour.

6 A neural mechanism for computing escape behaviour

6.1 Optogenetic activation of mSC and dPAG produces escape to a shelter.

In the framework of our model, the calcium activity profiles in Chapter 5 are consistent with dmSC neurons representing a pre-escape variable such as threat intensity and dPAG neurons encoding the result of a thresholding computation. This predicts that direct activation of dmSC neurons should produce psychometric and chronometric curves similar to sensory stimulation, as dmSC activity is still being passed through the threshold mechanism to initiate escape, while stimulation of dPAG neurons above the action potential firing threshold should reliably elicit escape behaviour with short reaction times. We tested this prediction by expressing Channelrhodopsin-2 (ChR2; Boyden et al., 2005) in VGluT2$^+$ neurons (Vong et al., 2011) of mSC or dPAG (Fig. 6.1*A*) and delivering light stimulation *in vivo* (Aravanis et al., 2007).

Stimulation of both the mSC and dPAG with high light intensities caused escape behaviour that was similar to that in response to sensory threats: the flights elicited were fast, shelter-directed (Fig. 6.1*B*), and animals engaged in their usual freezing behaviour upon reaching the nest after the offset of stimulation. Strikingly, the vigour of the flight response increased as a function of stimulation frequency in both brain areas (Fig. 6.1*B*). As a control, we expressed EYFP in dPAG VGluT2$^+$ cells, and found no effect of blue light stimulation, indicating that the escape behaviour was an effect of neural activation and not an experimental artefact from sources such as tissue damage or the animal responding to any ectopic flashing light (Fig. 6.1*C*).

As the escape probability and vigour were high for both dmSC and dPAG activation over a range of frequencies tested (5-40Hz; intensity12.0-13.5 $\mathrm{mW/mm^2}$), we sought to desaturate the behavioural response and increase the dynamic range of the manipulation, by finding a way of systematically controlling the level of VGluT2$^+$ network activation in the two brain regions closer to the threshold for evoking escape behaviour so that we could to test our predictions of how the dmSC and dPAG contribute to escape behaviour. We surmised that this should have the effect of making any differences in the computational roles and behavioural output of VGluT2$^+$ mSC and dPAG activation more discernible. Common parameters for exerting optogenetic control

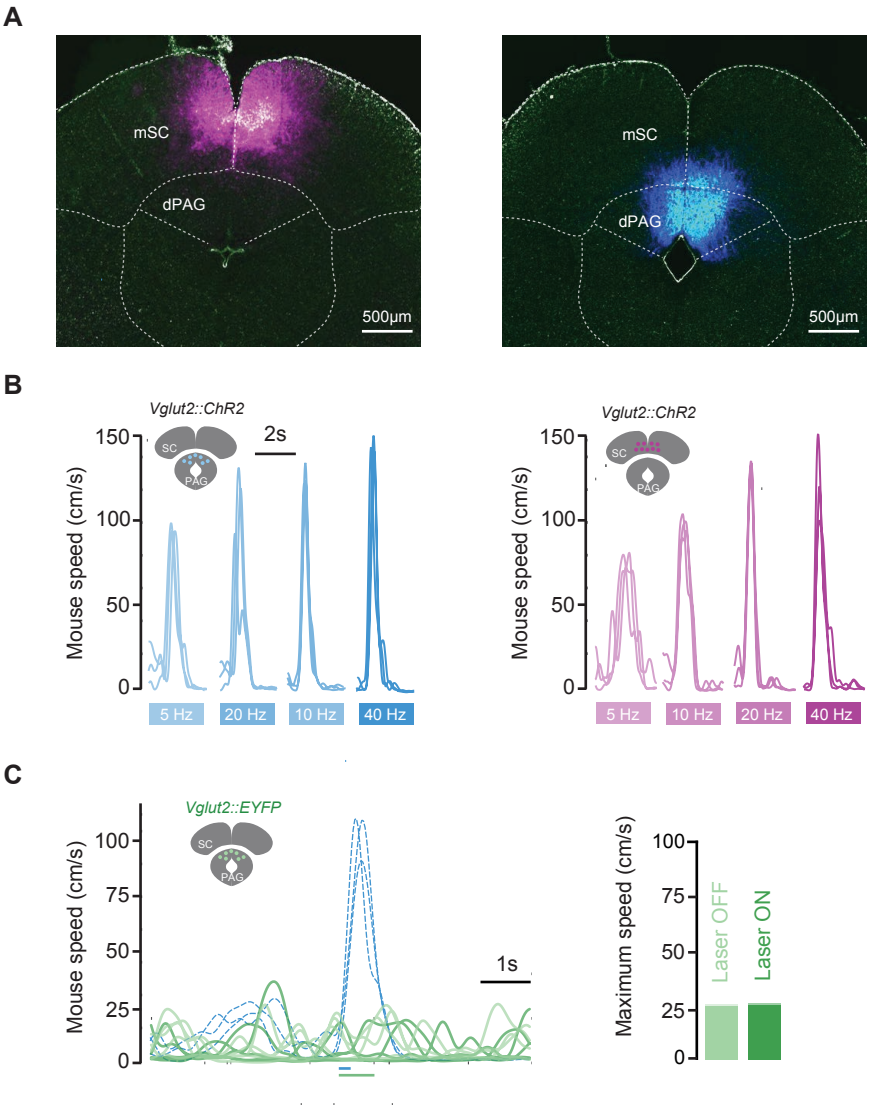

Figure 6.1 VGluT2$^+$ mSC and dPAG neurons drive escape behaviour **A:** Images of ChR2-EYFP expression in VGluT2$^+$ cells of mSC (left) and dPAG (right). **B:** Speed traces show all trials of a stimulation experiment in one dPAG (left) and mSC (right) VGluT2::ChR2 animal at different frequencies (10 pulses at high intensity), showing robust escape behaviour for 5 to 40Hz stimulation. Note the subtle lower speed and higher variability of mSC-evoked escapes at low frequency compared to dPAG. **C:** Stimulation of EYFP expressing cells does not modify behaviour. Left, speed traces for 473nm light stimulation (40Hz, 30 pulses) of one mouse expressing EYFP in the dPAG (dark green), showing no change in running speed. Light green traces show similar speed profiles for the same mouse entering the area without stimulation. Blue dashed traces are from a different animal expressing ChR2 in the dPAG (40Hz, 10 pulses), for comparison. Right, summary data for EYFP control stimulation in dPAG (running speed not significantly different between laser on and off, P=0.48, U-test, N=236 trials from 3 animals). Error bars are s.e.m.

over behaviours are the length and intensity of pulse trains (Lee et al., 2014; Betley et al., 2013; Kunwar et al., 2015). As the time course of the sensory stimuli in our behavioural assay remains invariant whilst the threat level is changed, we decided to keep the time course of the optogenetic stimulus constant by keeping the pulse and train duration the same. Interestingly, cell-attached recordings from ChR2-expressing neurons have shown that the fraction of spiking cells in a network increases as a function of light intensity (Huber et al. 2008). This means that light intensity modulation in optogenetic experiments can be used as a proxy for setting the level of activation in a network by changing the fraction of activated cells. While we found that escape was elicited at all frequencies tested at high light intensity, preliminary experiments showed that the probability of escape behaviour was modulated over a larger dynamic range when varying light intensity at a fixed frequency. We therefore decided to generate stimulus-response curves by modulating intensity over trials, with a fixed stimulus frequency, pulse width and duration.

6.2 Optogenetic investigation of escape behaviour supports different escape roles for the mSC and dPAG

To generate the stimulus-response curves, we tested the behavioural effect of gradually increasing network activation by increasing the light intensity from subthreshold values until flights were initiated, and iteratively increasing the light intensity until the escape probability saturated (Fig. 6.2*A*). For dmSC-VGluT2$^+$ activation, this resulted in a progressive increase in the probability of escape (Fig. 6.2*B, left*), thus accurately recapitulating the behavioural statistics of escape to visual threats.

Likewise we found that increasing activity in the dPAG network increased the probability of escape, but we found that it produced a steeper, all-or-none curve, with stereotyped responses for each intensity (SC: N=4 animals, 278 trials; PAG: N= 6 animals, 451 trials; Fig. 6.2*A-B, right*). Logistic regression confirmed that the slope of the dPAG psychometric curve was significantly steeper than for the dmSC (slope of logistic fit = 15.2, 95% CI [10.3, 20.1] for dPAG and 4.0, 95% CI [2.75, 5.25] for dmSC), in agreement with our model hypothesis that dPAG activation would constitute a direct activation of the escape initiator.

In addition, we measured the latency to elicit escape responses upon stimulation. We found that escape was elicited with shorter latencies in the dPAG than the mSC at low intensities, suggesting that the dPAG is downstream of the mSC in the pathway to initiate escape. Importantly, the long escape latencies of dmSC activation decreased with stronger activation, while escape latencies for dPAG activation were short across the full stimulation intensity range (slope of linear fit for SC=-0.21, 95% CI [0.27,-0.15]; PAG=-0.07, 95% CI [-0.11,-0.03]; Fig. 6.2*C*).

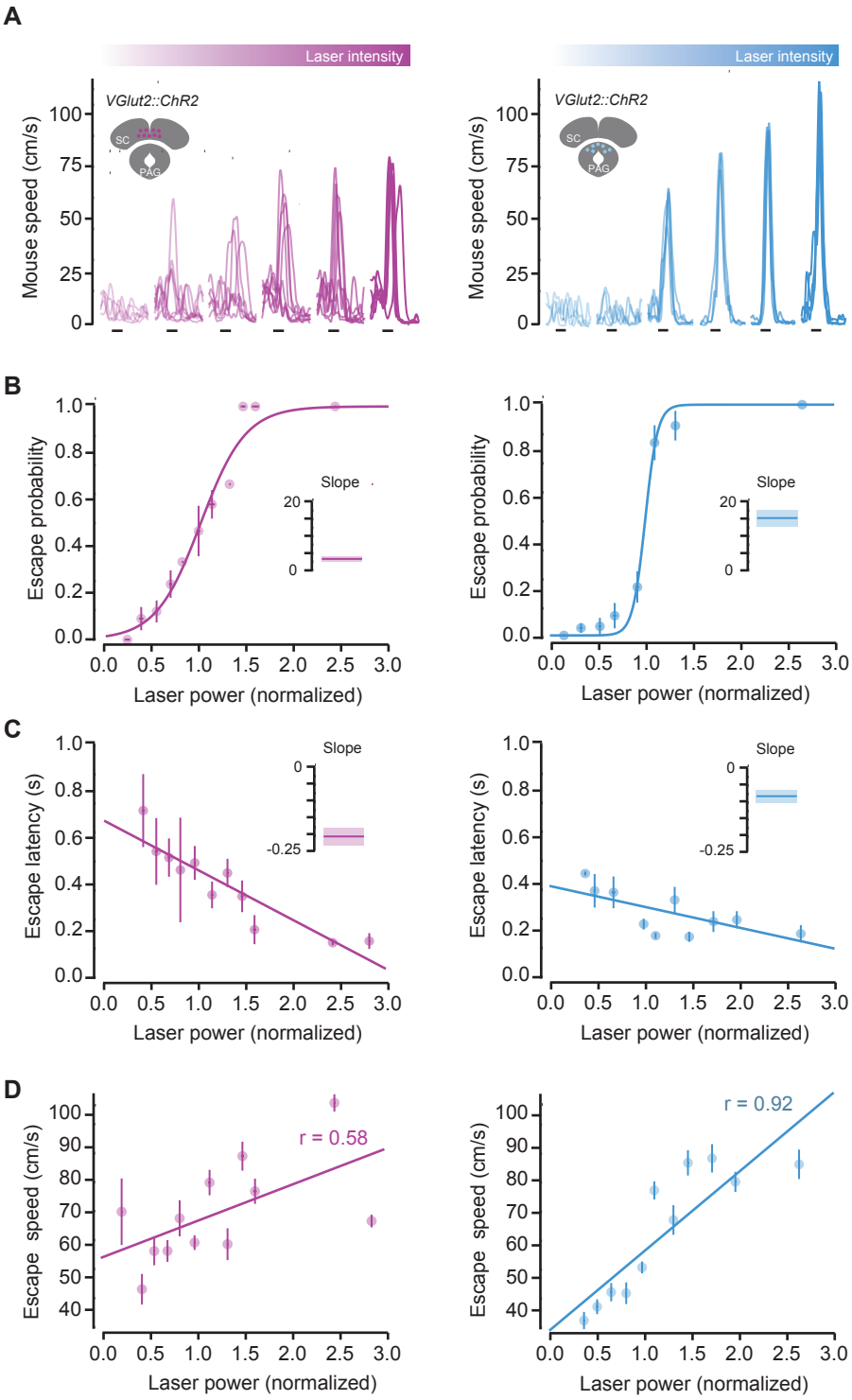

Figure 6.2 Optogenetic stimulation shows different roles for mSC and dPAG in escape behaviour. **A:** Example speed traces for stimulation with increasing blue light intensity at 10Hz (1s pulse train) for one mouse (dPAG right, dSC left). Each trace is from a single trial, black lines show stimulation timing. **B:** Psychometric curve for light intensity versus escape probability showing a gradual increase for dSC stimulation (left) and an all-or-none profile for the dPAG (right). Lines are logistic fits to the data (pooled across all animals and binned light intensities), and insets show the slope of the fit (shaded area is s.d.) **C:** Increasing the stimulation light intensity causes a large reduction in escape latency for mSC (left), while the change in latency is much smaller for dPAG stimulation (right). Lines are linear fits to the data, with inset showing the slope of the linear fit. **D:** Correlation between light intensity and escape speed is much stronger for dPAG stimulation (right) than for mSC (left). Error bars in all panels are s.e.m.

This demonstrates that activity levels in the dmSC determine the onset of escape, as suggested by the calcium imaging data and predicted by the model. Increasing the stimulation strength of both networks was also correlated with an increase in escape speed, but the correlation was much stronger for dPAG stimulation (Pearson's r=0.92, P=1.69x10^{-5}) than for dmSC (Pearson's r=0.58, P=0.04; Fig.6.2*D*), which further supports a model where activity of dPAG neurons represents a post-threshold variable from which escape vigour is computed, and is consistent with the stronger correlation we observed between peak calcium activity and escape speed in dPAG neurons.

6.3 Identification and characterisation of an excitatory SC-PAG circuit

6.3.1 An excitatory convergence of deep SC neurons onto dPAG neurons

Despite decades of functional and anatomical research into the role of the superior colliculus and periaqueductal gray in defensive behaviour (Olds and Olds, 1962; Sahibzada et al., 1986), it is not known whether they are monosynaptically connected. Studies using axonal transport tracers suggest that they are, showing weak labelling in the PAG anterograde from the SC (Redgrave et al., 1987), and retrogradely in the SC (Beitz, 1982), but confirmation using transynaptic techniques along with cellular and physiological knowledge of the purported connection is lacking.

To determine whether excitatory dPAG neurons receive information directly from the dmSC, we first targeted dPAG VGluT2$^+$ neurons using monosynaptic rabies tracing (Wall et al., 2010; Wickersham et al., 2007; Franklin et al., 2017). A helper virus was injected unilaterally into the dPAG of VGluT2-Cre animals, making these cells capable of Cre-dependent retrograde spread by expression of the EnvA-receptor protein, TVA, and rabies glycoprotein, G, while marking them with GFP expression. We then injected a G-depleted, EnvA-pseudotyped rabies virus (EnvA-dG-RV-mCherry), allowing infection and monosynaptic retrograde spread from dPAG VGluT2$^+$ neurons, and labelled by the reporter mCherry. As a precaution against false positive results, we used a lateral angle of 20° to prevent the generation of starter cells in the overlying superior colliculus.

Monosynaptic tracing resulted in extensive labelling of cells in the SC (Fig. 6.3*A*), which we quantified by both layer, mediolateral position (Fig. 6.3*B*-*C*). This analysis revealed a 11.1:1 SC to dPAG convergence ratio across all layers (N=3 animals), with the majority of cells distributed amongst the deep (5.7:1 ratio, ±1.5)) and intermediate SC (4.3:1 ratio, ±0.9) layers. In stark contrast, cells in the superficial layer were only sparsely connected with dPAG VGluT2$^+$ neurons (0.6:1

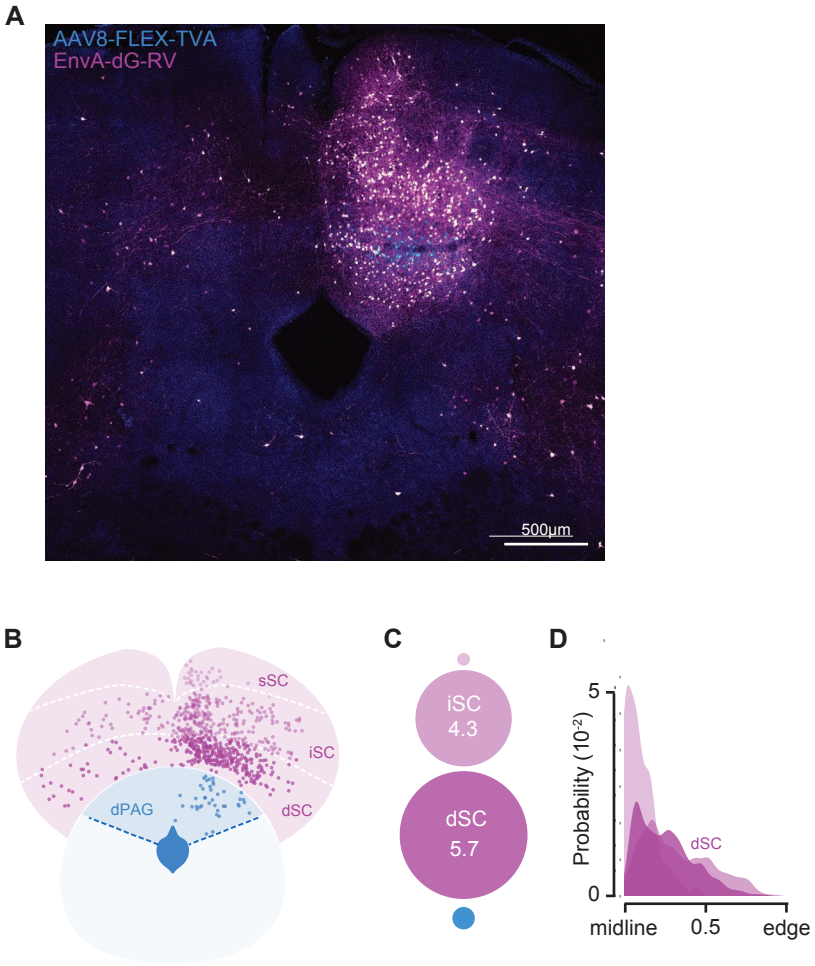

Figure 6.3 Monosynaptic connections exist between the SC and excitatory dPAG neurons, and with a specific spatial pattern. **A:** Image showing starter VGluT2^{+} dPAG cells expressing both TVA-GFP and RV-mCherry, and presynaptic cells expressing RV-mCherry only. **B:** Schematic illustrating the position of starter dPAG (blue) and presynaptic SC cells (pink) across deep, intermediate and superficial SC layers (dSC, iSC, sSC respectively), for the experiment shown in **A**. **C:** Quantification of the mean ratio of presynaptic SC cells for each PAG cell, depicted by circle areas (blue circle represents one PAG cell, numbers show SC:PAG cell ratios). **D:** Kernel density estimation curves for the axial position of presynaptic SC cells for each layer in all experiments.

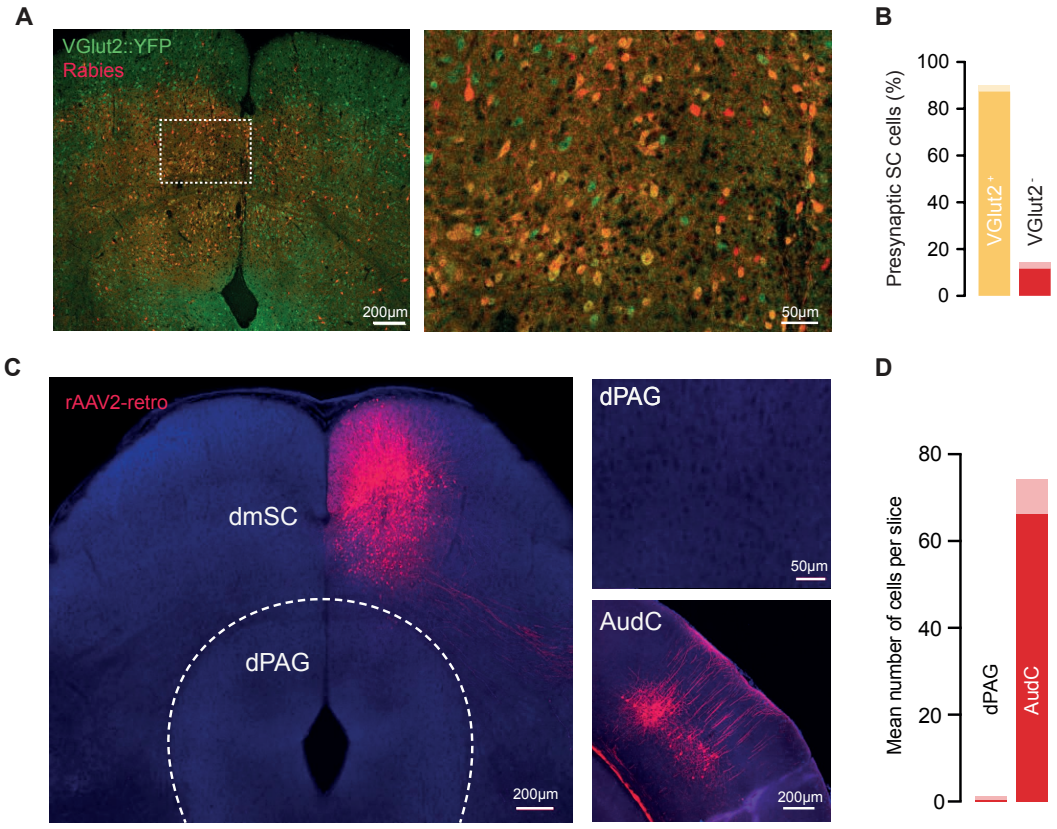

Figure 6.4 dPAG neurons receive input from mostly excitatory cells in the SC and do not project back to the SC. **A:** Image showing presynaptic cells in the mSC infected with rabies virus (red) from starter neurons in the dPAG of a VGluT2::YFP mouse (left). Box indicates area of dmSC magnified and shown on the right. Yellow cells are excitatory mSC presynaptic neurons. **B:** Summary quantification of the fraction of presynaptic cells in the mSC that express VGluT2. **C:** Image showing injection of rAAV2-retro in the mSC (left) and no retrogradely labelled cells in the dPAG (right, top). Retrograde labelling in the auditory cortex is shown for comparison (right, bottom). **D:** Summary quantification for retrogradely labelled cells after mSC rAAV2-retro infection in the dPAG and auditory cortex.

ratio, ±0.3), suggesting that the dPAG predominantly receives visual information indirectly via the deeper layers, and that it chiefly integrates input from the multisensory deeper SC.

We found that dPAG neurons are connected to both ipsilateral and contralateral SC neurons, but unequally, with 3.0±0.75 times more cells labelled on the ipsilateral side. Moreover, we observed a strong bias for presynaptic SC cells being located in the medial part of the SC (82.9±2.6% of 1770 cells within medial bisection of ipsilateral SC, N=3 animals; Fig. 6.3*D*), which suggests that information concerning the upper visual field (Dräger and Hubel, 1976), such as aerial threats, is preferentially integrated by the dPAG. Interestingly, we observed that presynaptic SC neurons that synapse onto dPAG VGluT2$^+$ neurons also send collaterals to other targets such as the PBGN (data not shown). This suggests that there is not a dedicated population of SC neurons that specifically projects to the dPAG.

In order to ascertain the genetic identity of the presynaptic SC cells, we repeated the rabies tracing the experiment in VGluT2::YFP animals (Fig. 6.4*A*). This showed that the majority of presynaptic cells were also positive for YFP (87.9±1.0%, N=4 animals, Fig.6.4*B*), indicating they are VGluT2$^+$ excitatory neurons. The superior colliculus is known to engage in reciprocal connections with other midbrain nuclei, such as the cuneiform nucleus (Appell and Behan, 1990) and the parabigeminal nucleus (Usunoff et al., 2007; Jiang et al., 1996). We therefore asked whether dPAG neurons directly feedback to the SC by performing retrograde tracing from dmSC neurons using an rAAV variant with enhanced retrograde transport (rAAV2-retro-mCherry; Tervo et al., 2016), and confirmed the infection site by co-injection of AAV2-CamkII-GFP. We found that dPAG neurons did not project back to the SC (N=3, Fig. 6.4*C-D*), while known projection targets, such as the auditory cortex, were strongly labelled in the same experiment. Together, these data indicate a feed-forward, columnar organisation of excitatory connectivity between the SC and dPAG, which is strongest in the medial deeper layers of the SC.

6.3.2 Biophysics and synaptic properties of dPAG neurons

Our data suggests that dPAG neurons receive synaptic input from the SC and cause escape behaviour, so by what mechanism might this occur on a cellular level? The physiological properties of single PAG cells are not well characterised, with only several intracellular recording studies published (Sánchez et al., 1988; Lovick and Stezhka, 1999). We therefore sought to characterise the intrinsic properties of VGluT2$^+$ dPAG neurons to understand how individual neurons might integrate synaptic input.

We performed whole-cell patch-clamp recordings from VGluT2$^+$ dPAG neurons in acute coronal slices of VGLUT2::YFP mouse brains (Fig. 6.5*A*). Immediately after entering the whole-cell configuration, the resting membrane potential was measured (RMP=-61.4±2.2mV), and current steps were subsequently applied (Fig. 6.5*B-C*). This revealed that these cells have a time constant of τ=28.2±3ms), a high input resistance (545±47MΩ), and can fire action potentials at high frequency. In some recordings, the fluorescent dye Alexa-594 was included in the internal solution. Two-photon imaging of filled cells revealed that VGluT2$^+$ cells generally have 3-4 long dendrites, with few arborisations, which could be followed hundreds of microns within the slice. These electrophysiological and morphological characteristics are in agreement with those reported for non-genetically identified dPAG cells in the rat (Lovick and Stezhka, 1999).

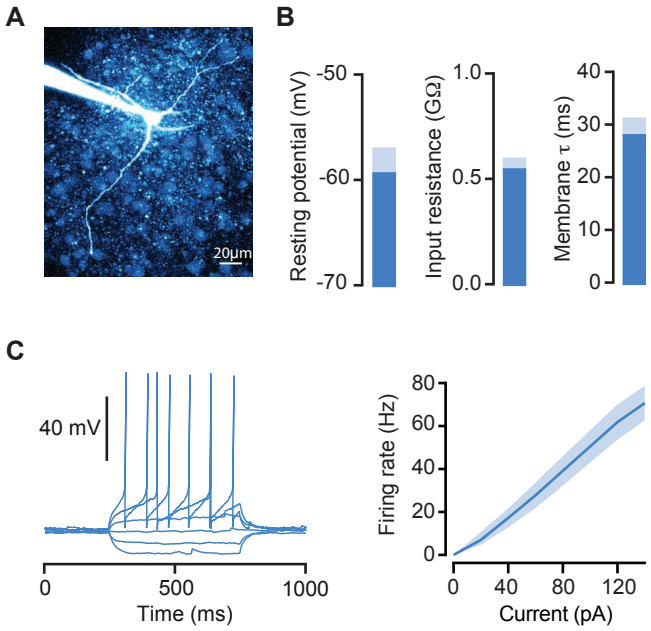

Figure 6.5 Biophysical properties of dPAG neurons. **A:** Two-photon image of a dPAG neuron filled with Alexa-594 during a whole-cell recording, showing long dendrites with minimal branching. **B:** Summary quantification of resting membrane potential, input resistance and membrane time constant for VGluT2$^+$ dPAG neurons. **C:** Example trace of current step injections in a VGluT2$^+$ dPAG neuron, eliciting action potentials (left) and summary current-frequency relationship (right). In all plots shaded area is s.e.m.

6.3.3 Investigation of the SC-PAG connection reveals weak, unreliable transmission

Next, to investigate the properties of the dmSC-dPAG connection identified by monosynaptic tracing, we used ChR2-assisted-circuit mapping in acute slices (Petreanu et al., 2007). We injected the dmSC of VGluT2::YFP mice with AAVs expressing ChR2 in a Cre dependent manner, and performed whole-cell patch-clamp recordings in VGluT2$^+$ dPAG cells. We observed light-evoked excitatory postsynaptic currents (eEPSCs) in 64% of VGluT2$^+$ dPAG neurons upon full-field light stimulation (n=44 cells, N=14 mice; Fig. 6.6*A*), but the strength of the recorded connections were notably weak (mean peak eEPSC amplitude=-37.9±11.9pA. Furthermore, they were unreliable, with a failure rate of 20.3±8% even at maximum light stimulation (Fig. 6.6*B*). The observed high failure rate suggests a low mean quantal content, as a significant fraction of stimuli are failing to release any vesicles and evoke a post-synaptic response.

In order to further understand the statistics of neurotransmitter release onto dPAG neurons, we first aimed to calculate the mean quantal content by the direct method (Isaacson and Walmsley, 1995). We first investigated the relationship between spontaneous EPSCs (sEPSCs) and miniature EPSCs (mEPSCs) recorded in the presence of tetrodotoxin (TTX), which showed that the peak and distribution of the amplitudes are similar (Fig. 6.7*A-C*). We therefore used the sEPSCs for

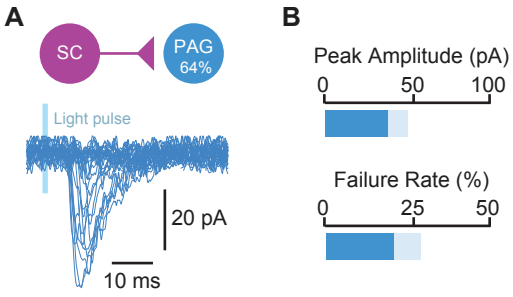

Figure 6.6 mSC neurons synapse onto dPAG neurons with a high rate but weak connection. **A:** Schematic illustrating connectivity rate (top) and single traces for ChR2-evoked EPSCs from mSC to dPAG neurons (bottom). **B:** Properties of mSC-dPAG excitatory connections. In all plots shaded area is s.e.m.

calculating the mean quantal content of evoked EPSCs using the direct method (see *Methods*; Isaacson and Walmsley, 1995), and found that the SC-PAG connection indeed has a low mean quantal content (2.3±0.6; Fig. 6.7*D*). Next we used the method of failures (Del Castillo and Katz, 1954) to calculate an independent value of the mean quantal content, which assumes Poisson statistics, and compared this to the direct method. Importantly, this showed that quantal content calculated directly is not significantly different from that using a Poisson model (slope of linear fit to direct quantal content versus ln(failure rate)$^{-1}$ = 0.92, 95% CI [0.74,1.1]; Fig. 6.7*E*). As the binomial distribution of synaptic release only simplifies to a Poisson distribution as the probability of release approaches 0, this indicates a very low synaptic release probability (Del Castillo and Katz, 1954; Isaacson and Walmsley, 1995).

An important consequence of such an unreliable connection is that the basal probability of eliciting action potentials in dPAG neurons from brief dmSC stimulation is extremely low (0±0 for single light pulses from resting membrane potential, n=13 cells; Fig. 6.8*A, left*), despite VGluT2^{+} dPAG neurons having a high input resistance (see Fig. 6.5*B*). This may act as a synaptic threshold which dmSC input must surpass to activate the dPAG network. Interestingly, repeated light stimulation at 20Hz elicited trains of action potentials (0.1±0.05spikes/pulse; Fig. 6.8*A, right*), more than would be expected from temporal summation given that the inter-stimulus interval is ~2 times longer than the membrane time constant (τ=28.3±3ms, significantly different from the inter-stimulus interval of 50ms, P=5.8x10^{-6}, 1-sample t-test against 50ms).

By what means could dmSC input be overriding the synaptic threshold? To examine this, we investigated the short-term plasticity dynamics of the connection by measuring the paired-pulse ratio (PPR), a measure of changes in presynaptic function (Zucker and Regehr, 2002). This showed the connection to be facilitating on average (PPR=1.13±0.11), which is consistent with its low release probability (Zucker and Regehr, 2002; Branco and Staras, 2009) and provides input amplification at the synaptic level during repeated dmSC activation (Fig. 6.8*B*). Furthermore, we observed that dmSC stimulation triggered a large and long lasting increase in sEPSC frequency

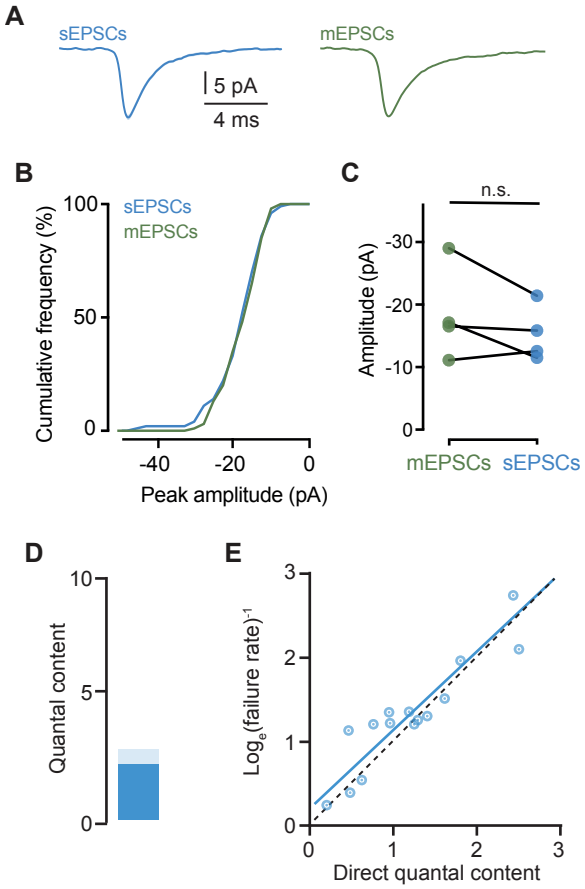

Figure 6.7 Quantal content indicates a Poisson model and thus low release probability. **A:** Average waveforms for sEPSCs, and mESPCs recorded in TTX for one cell, and its respective cumulative histogram for peak amplitudes **B**. **C:** Peak amplitude of sEPSCs and mEPSCs is not significantly different (n=4 cells, P=0.18, 0.79, 0.9 and 0.36 respectively, Kolmogorov-Smirnov test for 100 events in each condition per cell). **D:** Mean quantal content for ChR2-evoked EPSCs, calculated by the direct method. **E:** Plot of quantal content calculated using the direct method, versus quantal content estimation from the method of failures, which assumes Poisson statistics. Blue line is linear fit to the data, unity line is shown by dashes.

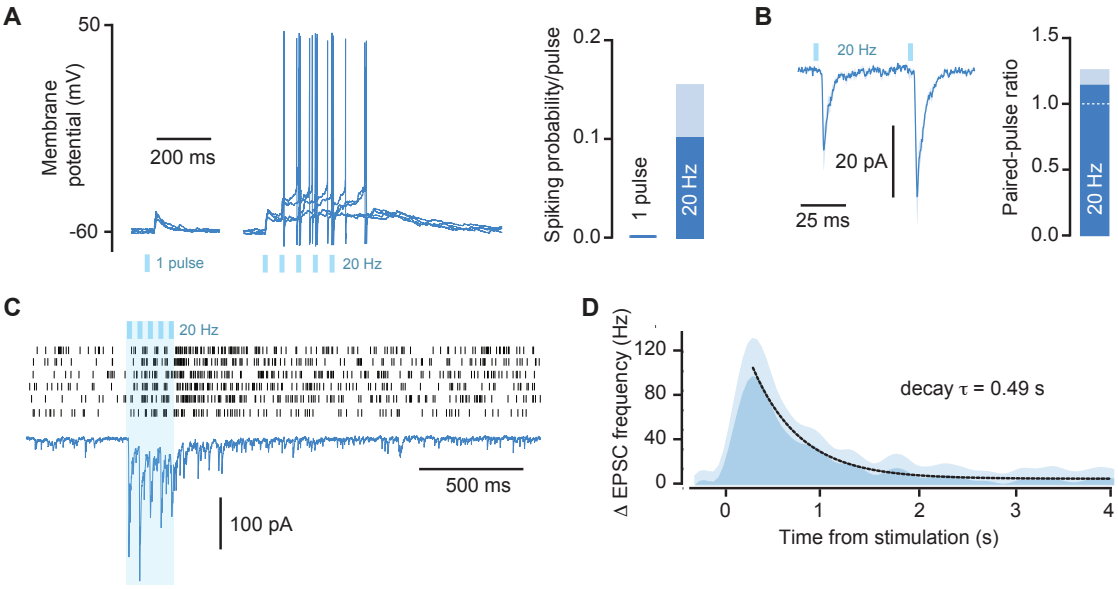

Figure 6.8 Synaptic mechanisms to drive dPAG firing via the weak connection from dmSC. **A:** Membrane potential changes in response to single and 20Hz light stimulation (left, traces are individual trials), and respective summary quantification of spiking probability (right). **B:** Average trace for one cell showing paired-pulse facilitation at 20Hz stimulation (left) and quantification for all cells (right). **C:** Example voltage-clamp trace for a dPAG cell single trial of 20Hz mSC stimulation (bottom) and raster of sEPSCs for 5 trials in the same cell (top). **D:** Summary histogram of the increase is sEPSCs in dPAG cells with 20Hz mSC stimulation. Dashed line is single exponential fit. For bar plots and histograms, shaded areas show s.e.m.

(peak frequency change= 98±42Hz), that decayed to baseline with a 0.49s time constant (Fig. 6.8*C-D*). These appear to be two main reasons why dmSC input is able to overcome the weak SC-PAG connection and drive dPAG spiking.

6.3.4 Recurrent dmSC connectivity helps overcome the synaptic threshold

To determine the origin of this polysynaptic excitatory input, we investigated the intra-region connectivity of VGluT2$^+$ dPAG to dPAG neurons, and dmSC to dmSC neurons. VGluT2::YFP cells in the dmSC or dPAG were virally targeted with ChR2 fused to the fluorescent tag mCherry, and

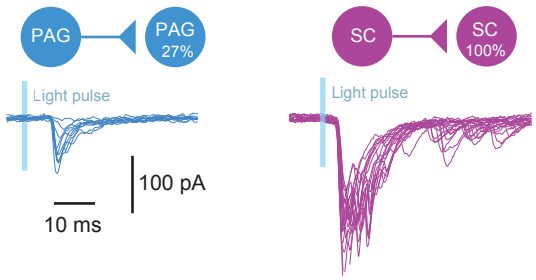

Figure 6.9 Recurrent excitatory connections in the dmSC are the source of polysynaptic input to weakly connected PAG neurons. Schematics illustrating the connectivity rate between dPAG (top, left) and dSC neurons (top, right), and example traces from single cells (bottom).

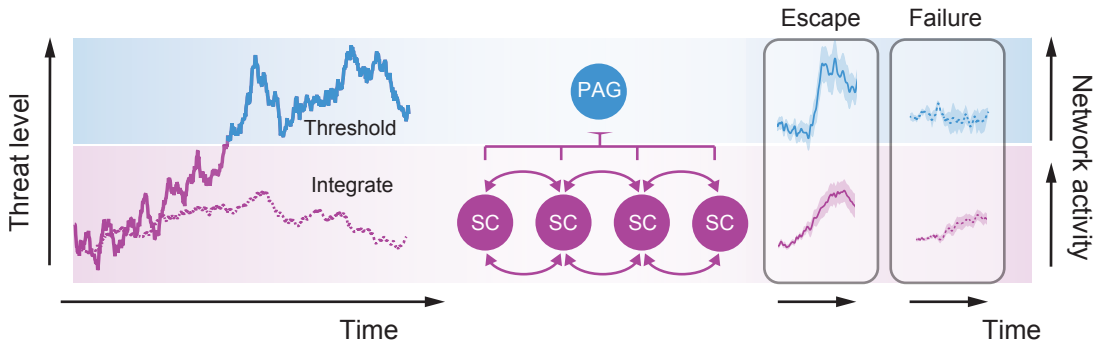

Figure 6.10 A network and synaptic model for computing escape decisions. Schematic of a circuit-level realisation of the behavioural decision making model from Chapter 3. Threat evidence, such as the threat level in the behavioural model (left), is integrated by a recurrent excitatory network of mSC neurons (middle, bottom), and the mSC-dPAG connection sets the threshold for initiating escape (middle, top). When activity in the mSC network is high enough, it drives firing of dPAG neurons, which represents the result of the thresholding computation and determines escape initiation and vigour (solid lines, 'Escape'). If mSC network activity does not reach threshold, dPAG neurons are not activated and escape is not initiated (dotted lines, 'Failure').

$YFP^+/mCherry^-$ cells were identified in the target infection area and recorded from during light stimulation. We found relatively sparse connectivity and weak synaptic input between dPAG cells (connectivity rate=27%, mean peak eEPSC amplitude=-54±8.3pA; n=11 cells, N=2 mice; Fig. 6.9 *left*). Cells in the dmSC however received strong, polysynaptic input from other dmSC cells (connectivity rate=100%, mean peak eEPSC amplitude=-146.7±41.5pA; n=22 cells, N=10 mice; Fig. 6.9 *right*), which is in agreement with previous work that found evidence for local excitatory circuits in the intermediate SC (Pettit et al. 1999). This suggests the presence of an excitatory recurrent network within the deeper layers of the mSC that provides signal amplification at the network level.

Together, these synaptic and network mechanisms provide a means for sustained activation of the dmSC network to overcome the weak connection to $VGluT2^+$ dPAG neurons and drive firing of the dPAG escape network (Fig. 6.10).

6.4 Summary

In this Chapter, we presented experimental evidence that activation of $VGluT2^+$ neurons in either the mSC and dPAG is sufficient to cause escape to a shelter, and that differences in the statistics of the evoked escape suggests that they play different computational roles in escape behaviour. Our optogenetic activation data suggest that the activity level in the mSC determines the onset of escape, as suggested by calcium activity recordings in the previous chapter, while the dPAG causes escape with shorter latency in an all-or-none manner, indicating that dPAG activation represents the activity of the mSC accumulation process passed through a threshold. Next, we showed that deeper mSC $VGluT2^+$ neurons converge and synapse onto dPAG $VGluT2^+$ neurons using

monosynaptic rabies tracing, and that this occurs in a feedforward manner. Characterisation of this connection using *in vitro* ChR2-assisted circuit mapping revealed it is weak and has a low probability of release and eliciting action potentials in dPAG VGluT2$^+$ neurons, which we suggest could function as a threshold of mSC activity. Further investigation of the connection and intra-region connectivity revealed that the SC-PAG synapse is facilitating and that repeated SC activation can cause long-lasting polysynaptic EPSCs due to recurrent excitatory connectivity in the mSC. We suggest that these mechanisms allow sustained mSC VGluT2$^+$ activation to surpass the synaptic threshold of the weak SC-PAG connection, and cause VGluT2$^+$ neurons to fire and initiate escape.

7 Discussion

The midbrain has been identified as an important integrator and output station for transforming threatening stimuli into defensive behaviours, but how it carries out this function was largely unknown. In this study, we present a physiological description of how an excitatory SC-PAG circuit is organised and contributes to different aspects of escape decisions in the mouse. Our results are compatible with a two-stage model where evidence about threats is integrated in the recurrent dmSC network and passed through a threshold at the dPAG level to initiate defensive escape. We propose that an important component of this threshold is the low release probability connection between VGluT2$^+$ dmSC and dPAG neurons, which threats of high intensity have a higher probability of overcoming, and once surpassed, drive dPAG neurons with a higher level of activity and thus increasing the speed of escape. These properties provide a simple explanation for how threatening stimuli of varying intensity and conveyed by the visual and auditory modalities could be represented in the brain and coupled to escape behaviour, both in initiating an escape event and controlling its vigour.

In the following, I will discuss the findings of our top-down study of the circuits and neural mechanisms underlying escape.

7.1 Behavioural evidence of a decision process in control of escape

Our behavioural assay demonstrates that escape in mice is not an all-or-none stereotyped response. By incrementally changing the contrast of the threatening stimulus, we found that the statistics of escape behavioural measures (namely the probability of escape, reaction time and vigour) can be precisely controlled (Fig. 3.1 and 3.4). These measures appear to correspond to key behavioural measures in decision theory (namely accuracy and decision time), which are united in the decision-making framework of bounded evidence accumulation (Schall, 2001; Fetsch et al., 2014). Specifically, we found that escape occurs probabilistically and increases with stimulus strength in a manner that strongly resembles the key behavioural measure of accuracy (i.e. percent correct choice) in psychophysical tasks, such as in random-dot motion discrimination tasks, where accuracy increases with the level of direction coherency (Gold and Shadlen, 2007). The term 'accuracy' implies that an observer can judge the decision to be correct or incorrect.

A key difference in this innate escape task to learned goal-directed tasks, however, is that the escape decision appears to be more than just a stimulus categorisation task (such as 'Are the dots moving left or right?' or 'Is a predator present, or not?') and has innate values attached to the different actions (e.g. escaping or staying put) which we do not know, unlike in learned tasks where we can know the value of decision actions by assigning rewards (Rangel, 2008). We are therefore not able to assess whether the animal has made a correct or incorrect decision to escape on each trial, and instead we can measure the probability of outcomes instead of accuracy per se.

Consistent with decision time measurements in decision making tasks, we found that the reaction time to escape decreases with stimulus strength (Fig. 3.4*A*), and appears to be largely independent of latency to detect the stimulus which varies little with contrast (Fig. 3.3*B*), thus resembling a decision time variable. We observed that the maximum escape speed is strongly correlated with threat intensity and escape probability, and inversely correlated to the reaction time, suggesting that these variables are linked (Fig. 3.4*A-C*). Confidence judgements (i.e. estimating the level of certainty that a choice is correct; in our case, that a predatory threat is imminent and requires evasive action) are thought to be related to evidence strength (e.g. Kepecs et al., 2008) and/or decision time (e.g. Kiani and Shadlen, 2009; Kiani et al., 2014), with confidence increasing as a function of evidence strength (Kiani et al., 2014; Fetsch et al., 2014). One could hypothesise that the escape vigour could be a readout for the confidence with which the escape decision is made, as animals escape with a faster maximum speed as the stimulus strength increases and reaction time decreases. An alternative interpretation is that stronger stimuli are represented in the brain by an increased level of a threat-related variable, and that this is directly linked to escape speed without involving confidence estimations in the decision outcome. Just as the concept of accuracy is difficult to apply to this innate escape task at present due to our ignorance of the associated values, we cannot yet satisfyingly distinguish between value and confidence in this innate goal-directed assay in the way we would be able to in a learned goal-directed task.

Our experiments demonstrate that animals can habituate or sensitise to threatening stimuli, and accordingly decrease or increase the reaction time and vigour of escapes (Fig. 3.5). This further supports the idea that escape is controlled by a decision process and exhibits flexibility based on the variable inputs which are integrated, instead of being a reflex-like process that produces a rigidly stereotyped escape response with little variability in reaction time, vigour and probability.

In this study, we modulated the contrast of the expanding spot visual stimulus, as we found it to exhibit control over evoked escape behaviours over a large dynamic range. Although the modulation of this parameter is somewhat artificial, it could correspond to real-world scenarios such as aerial attacks during changing cloud cover, cast shadows in forest environments, ambient

light level depending on the time of day, or predator species with different coat colours (Billington et al., 2011), and has been shown to affect the strength of looming stimulus representations in the midbrain of the barn owl (Asadollahi et al., 2010). The approach speed of expanding motion stimuli has also been shown to modulate escape (Yilmaz and Meister, 2013) and we therefore expect that it could produce similar probability curves when systematically varied. Furthermore, as innately aversive auditory stimuli generated a behavioural performance which is congruous with visual stimuli (Fig. 3.4*A-C, right*), this supports the idea that there is a generic relationship between the threat intensity associated with stimuli of different modalities, and probability, reaction time and vigour. Based on this observation that the escape statistics closely resemble psychometric curves in decision making tasks, we surmised that the behavioural paradigm could be considered an innate form of a Go/No Go decision making task, and sought to formalise the behavioural statistics by fitting a bounded evidence accumulation model of decision making. We adapted a drift-diffusion model, modified by Shea-Brown et al. (2008), in which a sensory stimulus is integrated into threat level over time, which thus generalises stimuli into a variable of 'threat level' (Fig. 3.4*D*). Importantly, this abstraction is powerful as it can incorporate evidence of a predatory threat independent of sensory modality and over a particular time course, and could be modified to incorporate other factors that influence the perceived threat level, such as the internal state of the animal or multiple lines of threat evidence (e.g. a low level of threat dictated by olfactory cues early on, followed by a high level of threat conveyed by visual and auditory cues from a predator later on in an encounter)[1]. In our assay, we used five presentations of the expanding spot per stimulus, and so the threat level was modelled by the diameter of the expanding visual spot, scaled by the spot contrast, and changing over time with a noise parameter. Escape is initiated if the threat level goes above the threshold for escape, with the reaction time being the time at which this occurs and the vigour being computed as a function of this peak threat level, similar to how confidence can be modelled as a function of evidence strength. As higher threat levels are less affected by noise than lower ones, this leads, on average, to the threshold being reach sooner and thus faster reaction times, while the vigour will be higher.

This model captured the features of the escape data well (Fig. 3.4*A-C, fitted red lines*), and thus constitutes a useful definition of the escape computation which is critical for trying to understand the underlying mechanism, as discussed in the following section. Previous theoretical models of escape decisions have assumed that animals have perfect knowledge of their environment (or that uncertainty about their surroundings is not important; see Zylberberg and Deweese, 2011 for discussion) and that escape decisions are made on purely economical grounds; e.g. a prey

[1] This also provides a link with graphical models of defensive behaviour such as the concept of defensive distance (Blanchard and Blanchard, 1989b), which is thought of as a cognitive construct of perceived threat intensity which varies with the distance to a predator and controls the type and intensity of defensive behaviour observed, from non-defensive behaviour to freezing to attack as distance decreases (McNaughton and Corr, 2004).

animal is aware of a predator at distance, and only flees when the predator is close enough that the cost of fleeing and not fleeing is equal (Ydenberg and Dill, 1986; Cooper and Frederick, 2007). A strength of our model is that both uncertainty and prey-predator distance could be readily incorporated by modifying the threat level variable, and in fact, it may be that the visual stimulus contrast is a proxy for uncertainty, and thus already captured by the amplitude of the threat level. Furthermore, this model provides a framework for future studies on escape decisions. For example, as we show that escape is modulated by prior experience to threatening cues, we can make predictions using our behavioural model and investigate possible neural correlates according to our physiological realisation of this model (for further discussion see Section 7.6).

It may go against naive intuition that the vigour of escape responses is changeable: we might assume that once enough evidence is accumulated that a predator is present, an escape response should be enacted with the fastest possible speed. However, laboratory and field studies have shown that some animals adjust not only their defensive strategy (e.g. escape vs freezing), but their mode and vigour of escape. Presumably, animals do not always exhibit maximum escape performance in the presence of a predator because fleeing comes at a cost (a function of factors such as energetic expenditure, lost foraging and mating opportunity, increased conspicuousness to the predator; Nelson et al., 2004; Cresswell, 2008). This cost should be minimised if animals are optimal economic decision makers, and this sub-maximal performance has been demonstrated most compellingly in fish, who change their maximal escape speed and acceleration in response to perceived imminence of a predatory attack and predator species, potentially increasing survival rates by 2-3 times (Dill, 1990; Domenici et al., 2004; Ydenberg and Dill, 1986; Seamone et al., 2014; Walker et al., 2005).

7.2 The SC as a decision making centre

Previous work has shown that cells in the rodent SC are sensitive to approaching-motion visual cues, and escape responses to such cues are believed to be mediated by the SC (Dean et al., 1989; Westby et al., 1990; Shang et al., 2015; Wei et al., 2015). Using pharmacological and genetic ablation manipulations during behavioural assays, we confirmed that the medial superior colliculus is indeed a critical region for processing overhead visual threats, as stimulus detection and escape behaviour were comprehensively abolished (Fig. 4.1 and Fig. 4.3*A*). We further identified that the necessity of this mSC region is dependent on the excitatory VGluT2^{+} population of cells (Fig. 4.1), and that innately threatening ultrasonic stimuli are also critically processed in the mSC (Fig. 4.4*A*).

There are relatively few studies that have recorded from deeper layer SC cells in unrestrained animals (Felsen and Mainen, 2008, 2012; Pond et al., 1977; Weldon and Best, 1992; Weldon et al.,

2007, 2008; Wei et al., 2015), and only two have focused on defensive behaviour (Pond et al., 1977; Wei et al., 2015; during shock-evoked fighting and visually-evoked freezing, respectively). In this study, we show that activity in excitatory dmSC cells precedes the onset escape responses to threatening stimuli (Fig. 5.1*B*,*D*), is predictive of escape 900ms before the event (Fig. 5.3*A*), and that further activity occurs synchronously with escape onset (Fig. 5.1*D*). An interpretation of these observations requires us to ask whether the activity could reflect either a sensory, motor or other signal related to the stimulus or the response. Intriguingly, we found that the peak population activity was different depending on whether the animal escaped or not to the same threatening stimulus, with lower, but still present, activity for trials with no escape movement (Fig. 5.2). This suggests that the neural representation is not purely sensory, as in this case we would expect the activity profiles to be the same for escape and non-escape trials, nor is it reflecting solely the motor output of escape, as we would then expect the activity profile to be flat for non-escape trials. Furthermore, dmSC cells did not exclusively respond in the pre-escape or peri-escape periods, with 75% of cells varying their onsets between these two periods across trials, which suggests that there are not distinct populations exclusively encoding one variable related to pre-escape or escape roles. Although it is impossible to rule out that the activity purely reflects movements without comprehensively monitoring muscle activity throughout the body, we believe that this is not the case, as clear increases in population activity were observed both in non-escape trials, and in escape trials where the animal was facing the shelter and did not make head rotation movements.

Together with the observation that pre-escape dmSC activity was predictive of escape even for spontaneous escapes from the threat area after conditioning (Fig. 5.4), it instead appears that the dmSC population activity reflects a general variable that is correlated with the likelihood of escape and could be related to an abstract variable of threat level. Interestingly, the reaction time to escape showed a strong negative correlation with the slope of rising population calcium signal, with shorter reaction times being associated with faster calcium rises (Fig. 5.3*B*), which is a characteristic one would predict of an escape decision variable such as the threat level in our accumulator model.

These results present further evidence that the deeper layers of the SC, which have traditionally been considered to have a motor output role, are also involved in decision making (Horwitz et al., 2004; Song et al., 2011; Kim and Basso, 2008; Ratcliff et al., 2007; Thevarajah et al., 2009). Previously, activity in the dSC of the rat has been shown to predict the future trial outcome and discrimination difficulty in a learned odour discrimination task, despite not receiving olfactory information explicitly (Felsen and Mainen, 2008, 2012). This activity was predictive nearly 1s before movement initiation, in line with our own findings (Fig. 5.3*A*). Similarly, deeper layer recordings of primate SC also show activity modulations that predict choice in a decision task

designed to dissociate perceptual judgements from motor signals related to the execution of saccades (Horwitz et al., 2004). One study has previously demonstrated the involvement of the SC in learned defensive behaviour. In a learned avoidance task in rats, where animals must avoid a footshock by detecting and responding to a conditioned whisker pad stimulus, Cohen and Castro-Alamancos (2010) found that activity before the conditioned stimulus was higher for avoid trials, and ramped up during the stimulus, suggesting that the SC encodes the active avoidance behaviour and that the pre-stimulus activity state was predictive of future avoidance. This is in agreement with our finding that dmSC VGluT2$^+$ population activity ramped up upon conditioned animals entering the threat area before spontaneous escape, suggesting that the SC is also computing conditioned threats (Fig. 5.4). However, in both of these cases, as in all decision-making tasks with a motor output, future work in the field must aim to disentangle the activity related to decision elements from pre-motor signals related to the behavioural choice (Shadlen and Newsome, 2001). This is not trivial, as all motor signals are decision-related in a sense, as they reflect the outcome of a decision process. In their work on decision-making in the parietal cortex, Shadlen and Newsome (2001) partially circumvented this conundrum by factoring in a delay period between the presentation of the stimulus and the 'go' signal executing the saccade outcome. However, in our assay, such instruction would turn an instinctive task into a learned one, and undermine the rationale for studying escape as an instinctive behaviour. It will also be of great interest to find out the input source which drives the SC with conditioned threat information, and inactivation experiments after conditioning will be necessary to determine whether this activity is required for spontaneous escapes. The amygdala is likely to be involved in acquiring this conditioned escape behaviour, but it to does not appear to project directly to the SC (Sparks and Hartwich-Young, 1989; Taylor et al., 1986; Cadusseau and Roger, 1985). The dmVMH is a strong candidate region, as it has been shown to be required for the acquisition and recall of predator fear memory (Silva et al., 2016b), and the VMH projects to both the SC and PAG (Canteras et al., 1994). Importantly, our findings are also in agreement with results from human studies that suggest the SC is part of an innate alarm system that detects and processes subliminal threat evidence (Morris et al., 1999; Vuilleumier et al., 2003; Almeida et al., 2015). As visual, auditory, somatosensory collicular maps, as well as corticotectal projections, are long believed to lie in spatial alignment across the collicular layers (Stein et al., 1975; Dräger and Hubel, 1975, 1976; Stein and Clamann, 1981; King and Hutchings, 1987), the deeper SC layers are in an excellent position to integrate multisensory threat cues over time whilst inherently preserving the spatial dimension of the predator cues, and we find evidence of strong recurrent excitatory connectivity in the dmSC which would amplify such signals and help overcome the escape threshold set by the relatively week SC-PAG connection (Fig. 6.9). Indeed, the SC has a well-described role in multisensory integration (Stein et al., 2014; Schiller et al., 2011), and in our

paradigm, dmSC neurons likely receive sensory input from the sSC for visual stimuli (Doubell et al., 2003; Zhao et al., 2014; Liu et al., 2011; Schiller et al., 2011; Mooney et al., 1992) and from the inferior colliculus and auditory cortex for sound stimuli (Xiong et al., 2015; Edwards et al., 1979). We observed that the calcium rise signals showed different rise slopes between escape trials using the sound stimulus and high contrast visual threats, with faster calcium rises during sound stimulus trials (Fig. 5.3*C*). In Chapter 3, we found that the sound stimulus evokes escape with a higher probability and vigour than the highest contrast visual stimulus, although the reaction time for these escapes is slightly longer (Fig. 3.4). Animals often begin to flee to the visual stimulus during the first expansion of the spot, before the maximum size of the spot is reached, so we can be certain that the visual stimulus is innately threatening during this phase. It may be that the sound stimulus, composed of a frequency sweep, is only perceived as threatening towards the higher frequency range which occurs later in the stimulus timecourse, and thus there is a difference between the two stimuli in latency of threat information conveyed by the stimulus relative to the onset of the sensory stimulus, with the auditory stimulus becoming threatening after a relative delay, but representing a higher intensity of threat when it does. This could explain why the rise of the pre-escape calcium signal in sound evoked trials is steeper than for visual stimulation trials, which in line with our model, leads to escapes of greater vigour. It can be difficult to compare the representation of sensory stimuli of different modalities beyond considering their timecourse, but another interpretation might be that the two modalities are represented differently in the deeper layers, irrespective of a transformation into a threat-related variable, which is also supported by the fact that the deeper layers SC contain auditory-responsive cells and receives ascending and descending auditory information, while visual information in the deeper layers comes from superficial layers where an additional step of collicular processing can occur.

In conclusion, our findings further our understanding of the deeper SC as a decision making centre by demonstrating the existence and necessity of a decision making SC role in innate and conditioned threat behaviour, that this decision making function extends to mice, and that excitatory cells show activity upon threat presentation that is not a simple representation of the sensory stimulus, but encodes a higher order signal that is predictive of escape. We suggest that this escape choice-related signal could be an abstract representation of perceived threat valence, such as the threat level in our behaviour model. A persistent question has been whether the SC is simply a relay of sensory information or whether it has the inherent capability to produce defensive behaviours proper (Redgrave and Dean, 1991; Bittencourt et al., 2005)[2]. Our

[2] This is related to the general problem discussed earlier of disentangling the neural correlates of sensory, motor, perceptual and attention functions in decision-making structures such as the SC (Schall, 1999).

experiments suggest a third option; that the SC integrates multisensory threat information, and the SC-PAG synapse provides a thresholded pathway to drive escape responses.

7.3 The dPAG controls escape

The PAG has long been implicated as an important effector of defensive behaviour, including escape (Fanselow, 1994). Most evidence of how the PAG generates these behaviours, however, comes from functional anatomy, activation and lesion studies, with few studies addressing how the neural activity in the PAG encodes behaviour in the unrestrained, awake animal. We found that VGluT2$^+$ dPAG cells become active at the onset of escape initiation, which occurs reliably for single neurons across trials and multiple neurons within in a trial, and that these cells remain silent if a threatening stimulus does not trigger escape (Fig. 5.1*A*,*C*). These characteristics result in dPAG activity being an almost perfect classifier of whether an animal is escaping or not (Fig. 5.3*A*). What, then, does the activity of the PAG constitute? We observed that the peak population activity is highly correlated with escape speed, being 3 times stronger than that of the SC (Fig. 5.5*A*), and thus PAG activity generates a linearly scaled behavioural output. Together, our data suggests that excitatory dPAG cells resemble command-like neurons for escape initiation and that their level of activity encodes the vigour of the escape movement.

To the best of our knowledge, these results represent the first recordings of identified excitatory dPAG cells during escape behaviour. Our results are strongly in agreement with a study by (Deng et al., 2016), who reported that some dPAG cells firing rates were positively correlated with speed during escape from rats. However, as the action potential waveforms of excitatory and inhibitory PAG cells are homogenous and thus extracellular recordings cannot be used to distinguish cell types without optrodes and ChR2-tagging (Unpublished data from V. Stempel and T. Branco, and see Halladay and Blair, 2015), our VGluT2$^+$-targeted calcium recordings amount to an important addition to our understanding of how the PAG encodes defensive behaviour in the freely moving animal, as it is the activation of excitatory dPAG cells which drives escape.

Accordingly, pharmacological inactivation of the dPAG completely abolished escape, demonstrating the necessity of dPAG to escape initiation, and instead caused freezing responses to the visual stimulus, suggesting that threat signals were still processed and that the dPAG is not required for a general threat processing role (Fig. 4.3*B*). Conversely, the majority of dPAG neurons do not appear to be controlling freezing to innately threatening auditory and visual stimuli, which is supported by the fact that prolonged freezing behaviour was invariably enacted during dPAG inactivation (presumably because escape-driving neurons were rendered unavailable to excitation), and only 7% of imaged dPAG neurons were responsive to post-escape freezing in the shelter (Fig. 5.6). We can speculate that the dPAG escape-encoding population, and the separate

freezing population reported in the vlPAG (Tovote et al., 2016), are either in competition through a mechanism of mutual inhibition, or that there is a threat level-dependent hierarchy of preferential activation of dPAG escape neurons vs vlPAG freezing neurons, enacted by interactions between inhibitory neurons to preferentially drive escape over freezing. This would be in line with the finding that dlPAG VGluT2$^+$ cells have presynaptic compartments apposed to GABAergic vlPAG cells, and these GABAergic cells have been shown to cause freezing through disinhibition of VGluT2$^+$ vlPAG cells (Tovote et al., 2016). When dPAG cells are inactivated by muscimol in our experiments, this would promote disinhibition and could lead threat information to cause freezing rather than escape. Perhaps a similar mechanism could occur physiologically when escape routes or shelter are deemed unavailable by the animal: dPAG neurons could be inhibited via neuromodulatory or inhibitory input, allowing freeze-related neurons to preferentially process threat-related signals and drive freezing. The pathway by which SC information would reach the vlPAG in our dPAG inactivation experiments is not known, but our data suggest that the signals that drive innate freezing may not need to be routed through the dPAG, and this would therefore be an interesting subject for further investigation.

7.4 Optogenetic activation experiments support these distinct roles

In an attempt to use *in vivo* optogenetics carefully, we designed our experiments based on the prediction from *in vivo* recordings, inactivation and the literature of activation experiments. After finding that both mSC and dPAG optogenetic activation, at high intensity and over a range of frequencies, produced escape behaviour resembling that evoked by sensory stimulation, we hypothesised that the stimulation-response curves produced by activation of excitatory mSC neurons might more closely resemble wild-type behavioural psychometric curves, because the SC processes threatening stimuli and is upstream of the PAG, so the activation would have an additional processing step before the command-like PAG escape-driving cells. In comparison, we predicted that dPAG activation should show a sharper threshold for evoking escape, as we found the excitatory neurons to be silent during non-escape trials, and active during escape trials, with activity linearly scaled with the vigour of escape. This prediction is in line with response probability curves for defensive behaviours using electrical stimulation and NMDA microinfusions by (Bittencourt et al., 2005), who found that PAG stimulation had both lower thresholds and steeper curves than SC for producing trotting, galloping and eye-bulging in rats, although they did not explicitly measure escape behaviour in an environment with a shelter. The results of our experiments supported this prediction (Fig.6.2), with the slope of the psychometric curve being significantly steeper for the dPAG and resembling all-or-nothing escape behaviour and with a stronger influence on escape speed in comparison to mSC activation, which had a

greater range for modulating escape probability and latency to escape (i.e. reaction time). In our analysis, we took steps to account for differences in infection rates across and within groups, and across brain regions by normalising the stimulation intensities to midpoint intensity values of the individual stimulus-response curves. We argue that this is essential to fairly compare the two brain regions during artificial activation.

7.5 The role of a direct connection between SC to PAG in escape

While earlier studies have posited the question of whether the PAG acquires information about emergencies such as predatory threats directly from the SC (Redgrave and Dean, 1991; Fanselow, 1994), a functional connection had not been demonstrated, and recent research has instead focused on SC-subcortical pathways (Shang et al., 2015; Wei et al., 2015) or alternate routes to the PAG, such as the via the hypothalamus (Xiong et al., 2015; Silva et al., 2016b). Using spatially-restricted monosynaptic rabies tracing and ChR2-assisted circuit mapping, we show a convergent, feedforward and monosynaptic excitatory connection from the intermediate and deep layers of the SC to excitatory cells in the dPAG (Figures 6.3, 6.4, and 6.6) and believe this is an important connection for computing threat information into escape behaviour.

We found that a high proportion (64%) of dPAG excitatory cells receive monosynaptic inputs from the mSC (Fig. 6.6), but that the connection was relatively weak in terms of synaptic current and synaptic release probability, and possessed a very low probability of causing action potentials without sustained input (Figures 6.7 and 6.8*A*). This low release probability means that the connection acts as a high-pass filter, and would threshold activity in the mSC to only elicit escape when a sufficient level of activity, or threat evidence, has accumulated. Intriguingly, we found that the synaptic connection is facilitating, as measured by the paired-pulse ratio (Fig. 6.8*B*), and that recurrent connectivity in the dmSC imparts it with the ability to trigger a strong and long-lasting increase in sEPSC frequency inputted to dPAG neurons (Figures 6.8*C-D* and 6.9 *left*), showing that there are mechanisms for dmSC activity to overcome this synaptic threshold implemented by the SC-PAG connection. As the SC is involved in a host of functions, including saccades, attention and defence, and is thought to play a role in most – if not all – visually-guided behaviour in mammals (Schenberg et al., 2005), overcoming this SC-PAG connection threshold may act as an 'interrupt' mechanism, where a high level of activity in the dmSC overrides the current behavioural goals of the SC, or the medial part only, to engage in urgent escape behaviour via the mSC-dPAG channel. This mechanism thus helps explain how the SC is able to play a role in such diverse behaviours. We do not yet know, however, whether the SC has a parallel streams of processing for different functions, such as threat decisions, at the level of the deeper layers. However, the high rate of recurrent excitatory connectivity we observe in the mSC, in line with

the existence of lateral excitatory connections within laminae previously reported (Saito and Isa, 2004; Pettit et al., 1999), argues against the idea of highly isolated parallel streams.

While we cannot exclude that alternate, polysynaptic pathways involving intermediate circuit nodes (such as the PBGN and cuneiform nucleus) also play a role in either the computation of escape or other behavioural modules of a full defensive response (such as the termination of escape, or freezing in the shelter), the direct SC-PAG connection that we describe constitutes the fastest way for the PAG to learn about escape-requiring emergencies from the SC. Furthermore, our synaptic physiology experiments demonstrate that it possesses the mechanistic properties to implement the threat-to-escape computation. Therefore, we hypothesise that the SC-PAG is likely to be predominant in certain types of predatory threat, such as imminent threats conveyed by the visual and auditory modalities, which require the urgent defensive response of escape over protracted responses such as risk-assessment.

What then, is the significance of this SC-to-PAG pathway in light of recent experiments demonstrating other SC-mediated pathways which are able to cause defensive behaviour? In support of our interpretation that the SC and PAG represent critical brain structures for the transformation of a threatening visual stimulus to escape behaviour, we found that the inactivation of a set of other brain regions implicated in defensive and visually-guided behaviour did not affect the initiation of escape responses and only had a small effect on the vigour: extensive bilateral amygdala and V1 inactivation did not affect escape probability, while respectively reducing and non-significantly reducing the vigour of escape (Figures 4.5 and 4.6). This modulatory role for the amygdala in visually-evoked escape responses is in consensus with experiments in non-human primates, which showed that escape behaviours and defensive vocalizations elicited by SC stimulation are not altered by basolateral amygdala inactivation (Forcelli et al., 2016). Our results are also in agreement with a study of V1 influence on sSC cell looming sensitivity, which showed that although V1 inactivation reduced the gain of these responses, it did not abolish them (Zhao et al., 2014).

As the VMH is an upstream region of the PAG involved in a number of predator and conspecific defensive behaviours, in a set of experiments, we performed extensive muscimol infusions into the VMH and carried out our escape behaviour assay. However, the post-infusion threat test could not be performed as the infusion caused hunching, lack of movement and orbital tightening indicative of pain. Previously, muscimol microinjections specifically into the dmVMH of rats have instead been shown to raise the threshold for tail shock-induced vocalisations, indicating analgesia (Borszcz, 2006), and reduce conditioned freezing (Maria and Brandão, 2011). This suggests that the qualitatively opposite phenotype observed in our experiments could be due to simultaneous $GABA_A$ receptor activation in all sub-nuclei or the surrounding inhibitory neurons in the VMH 'shell', and that more precise targeting is necessary in future experiments. We

therefore cannot exclude that the VMH is involved in escape from rapid visual threats, but optogenetic and inactivation experiments from other laboratories (Kunwar et al., 2015) strongly suggest that defence-driving neurons of the dmVMH, a key sub-nucleus involved in predator fear responses which projects to the dPAG, are neither required for, nor influence, visually-guided escape.

Importantly, we also found that acute inactivation of the PBGN did not change escape evoked by visual or optogenetic mSC activation (Fig. 4.7). The study which proposed an SC-PBGN pathway to be mediating loom evoked escape did not perform necessity experiments on the SC or PBGN, nor control for the specific activation of this pathway when stimulating axons in the PBGN by controlling for antidromic spiking in the SC (Shang et al., 2015). The consequence of this antidromic SC activation would be that escape could be evoked by another pathway, such as a direct SC-PAG connection, rather than through the SC-PBGN-amygdala-hypothalamus pathway which the authors propose. In our view the function of the PBGN in defensive behaviour therefore remains unclear. As it contains visually responsive cells with some specific tuning characteristic differences to the SC (Graybiel, 1978), and projects back to the SC (Usunoff et al., 2007; Baleydier and Magnin, 1979; Jiang et al., 1996), one function could be that this nucleus processes specific visual cues and feeds this back to the SC. Conversely, in this study we show that the PAG does not project back to the SC in the mouse brain, although it has been reported to in some studies using retrograde tracers in the rat (Cadusseau and Roger, 1985) but not others (Taylor et al., 1986). This lack of PAG-SC feedback in the mouse is important, as synchronous artificial activity in multiple midbrain regions (e.g. SC, PAG, cuneiform nucleus, PBGN) or in projections terminating in the SC (e.g from auditory cortex; Zingg et al., 2016) is sufficient to cause escape, and we show the existence of a large recurrently connected excitatory SC network exists. Therefore, any artificial activation of areas with adequate input to the deep SC could cause escape behaviour, irrespective of whether this occurs physiologically, and thus defensive circuits represent a good example of the potential pitfalls of channelrhodopsin-based circuit dissection, reminding one to be "aware of the fact that optogenetic activation assesses what a neuron can do, but not what a neuron does do" (S. Arber in Adamantidis et al., 2015). Activation experiments alone therefore can be misleading: it was thus important to carry out inactivation experiments for our particular threatening stimuli, as threat information conveyed by different modalities and with different parameters (i.e. expanding spots and ultrasound vs. odours, robotic predators) or which preferentially elicit a different repertoire of behaviours, are likely to utilise slightly or totally different pathways. For example, the medial amygdala is critical for processing innately threatening predator odours (Takahashi, 2014), but does not appear critical for processing innately threatening visual stimuli in our experiments, nor does the basolateral amygdala in non-human primates (Forcelli et al., 2016).

Although we have identified a functional SC-PAG connection which could provide a mechanism for making threat decisions, the next logical and crucial step is to perform *in vivo* activation or inactivation of this synaptic connection specifically to provide a causal link to the initiation of escape behaviour.

7.6 Flexibility of escape behaviour

Prior experience, the internal state of an animal and the environmental context have been shown to influence predator avoidance and escape behaviour across species (Filosa et al., 2016; Ramasamy et al., 2015; Vale et al., 2017). We found that the probability and vigour of escape, as well as the reaction time taken to escape, could be up and down regulated by prior exposure to visual stimuli that appear to convey high and low levels of threat Fig. 3.5. In our experiments, we used low contrast stimuli to cause adaptation. It is important to note that eventually, mice can also desensitise and suppress escape to high contrast stimuli after prolonged stimulation over multiple sessions and days, and correspondingly, the number of trials per animal attainable in our escape task will be lower than in learned tasks with extraneous reward and punishment.

A change in the output of a behavioural stimulus-response relationship such as sensory-evoked escape could be implemented at any or all levels in the responsible circuit, from primary sensory neurons to motor neurons. In this system, we speculate that plasticity in early sensory processing does not play a role in this adaptation phenomenon for two reasons. First, our behavioural measure of stimulus detection latency was not significantly changed, while the reaction time to escape was altered in a highly significant manner. As changes in escape probability and vigour were also highly correlated, this could indicate a change in a decision process. Second, the accepted role of sensory adaptation in the retina is to prevent saturation when encoding constant features of stimuli, thus allowing future increases in stimulus strength to be encoded (Laughlin, 1989; Nikolaev et al., 2013), thereby not accounting for decreased responses to future increases in stimulus strength. A hallmark of habituation in classical conditioning is that a stronger stimulus can usually dishabituate and partially recover the initial response, which we do not observe (Rankin et al., 2010). Instead, it appears that the escape decision process is under modulation. Both the PAG and the SC are under heavy influence of neuromodulatory systems, expressing receptors for dopamine, endocannabinoids, serotonin, opioids and adrenaline (Brandão et al., 1999; Bolton et al., 2015; Fogaça et al., 2012; Muthuraju et al., 2016))[3], and we hypothesise that these systems might provide similar mechanisms for long-term plasticity as in other brain areas (Castillo et al., 2012; Chevaleyre et al., 2006; Hamilton et al., 2010; Jay, 2003; Kwon et al., 2015)

[3] Dopamine D_2 receptors, interestingly, are only found in the deeper SC layers, while D_1 receptors are preferentially in the superificial (Bolton et al., 2015).

which could explain the modulations of behavioural output. There is mounting anatomical, pharmacological and functional evidence that serotonergic input from raphe nuclei, in particular the dorsal raphe (Stezhka and Lovick, 1997; Beitz et al., 1986; Janusonis et al., 1999; Pobbe et al., 2011; Pobbe and Zangrossi, 2005; Huang et al., 2017; but also medullary raphe Schenberg and Lovick, 1995), and dopaminergic input from the zona incerta (Bolton et al., 2015) to the SC and/or PAG is able to modulate defensive responses. In the context of escape behaviour, it would be interesting to investigate possible synaptic and neuromodulatory changes in the SC and PAG to test whether this circuit itself is subject to plasticity mechanisms, or whether the behavioural plasticity is dictated by changes in other, higher-order brain areas such as the prefrontal cortex (PFC), which has been shown to mediate behavioural adaptations to social defeat via weakening functional connectivity between the PFC and PAG (Franklin et al., 2017).

To summarise, there are a plethora of candidate plasticity mechanisms that could underly defensive flexibility, and it will be challenging for future research to dissect how these relate precisely to defensive behaviours, for example, in finding out whether some regulate a general defensive state, such as anxiety or panic, or modulate specific defensive behaviours in specific contexts, and how they interact. We there suggest that our behavioural protocol could be useful in helping to understand the mechanistic basis of escape flexibility in innate defensive circuits in the mouse.

7.7 Methods for inactivating the PAG – a critical note

It has been challenging to perform genetically-defined loss-of-function manipulations in the PAG which affect escape behaviour despite the large body of evidence which implicates it. We found that acute optogenetic inhibition of VGluT2$^+$ dPAG neurons showed a trend towards reducing escape probability, while chronic genetic ablation experiments of the same population did not appear to have an effect. This is in stark contrast to the comprehensive abolishment of escape behaviour we observed with microinfusions of muscimol into the caudal dPAG. There are several lines of reasoning that could explain this. In the case of optogenetic inhibition using Arch, it is likely that an insufficient proportion of escape-driving excitatory neurons in the dPAG, which extends over 2mm rostrocaudally, were transfected by viral injections, or the single medially-implanted optic fibre did not provide enough spatial illumination to hyperpolarize them. Another possibility is that escape can be driven by low spike rates[4] which were not reliably inhibited, or that the continuous light stimulus we used to activate Arch paradoxically increased evoked neurotransmitter release (Mahn et al., 2016) within the dPAG, which we show to be weakly recurrently connected, thus failing to inhibit the network when activated by SC-mediated

[4] We found that dPAG VGluT2$^+$ cells were silent until escape without spontaneous activity

visual threat input. However, Tovote et al. (2016) have used Arch in vlPAG VGluT2$^+$ cells to cause severe disruption of innate freezing behaviour.

In contrast to ablation of excitatory VGluT2$^+$ mSC cells severely impairing escape, escape responses were not significantly reduced when targeting dPAG neurons. Without dPAG or deeper SC-specific driver lines, the extent of the ablation is entirely dependent on injection specificity, and these two areas are adjacent. Great care was taken to target as much of the dPAG as possible without ablating the deep SC, but it was not practically possible to ablate all dPAG cells without rendering the experiment invalid through this off-target effect. As lesions to the dPAG in rat having been shown to disrupt flight (Blanchard et al., 1981), it seems likely that the remaining non-ablated cells of the dPAG were still sufficient to evoke escape, although it is possible that other projection targets of the mSC, such as the PBGN and CuN, may compensate for the dPAG and provide an alternate pathway for escape.

From these manipulations, we cannot rule out that alternatively VGluT2$^-$ neurons are able to generate escape responses while a significant proportion of VGluT2$^+$ are inhibited or ablated. However, recent GABAergic manipulations in our laboratory suggest that this is not the case (V. Stempel, Y. Lefler, unpublished) and the results of VGluT2$^+$ Arch-mediated inhibition and genetic ablation are highly likely to be a false negative. Pharmacogenetic manipulations of both general neuronal as well as VGluT2$^+$ cells in the dPAG have been shown to affect social and defensive behaviour, suggesting that the inhibitory construct hM4D is a more reliable tool for inactivating the PAG sufficiently to investigate its behavioural roles, and is thus a strong candidate tool for future studies (Silva et al., 2013; Franklin et al., 2017).

7.8 Experimental outlook

The results of this research, along with recent studies in the field, have highlighted a number of questions for future studies on midbrain defensive behaviours to answer:

What is the causal relationship between the identified SC-PAG connection and escape?

To causally test our proposed synaptic mechanism for escape, it will be important to perform gain- and loss-of-function experiments specifically on the SC-PAG connection. This could be accomplished using projection-specific synaptic chemogenetic inactivation (Stachniak et al., 2014).

What is the intra-SC organisation that supports threat decisions?

Our experiments show a high level of recurrent excitatory connectivity in the dmSC, which provides a mechanism to overcome the weak SC-PAG synaptic connection and may provide a means to accumulate threat evidence. We also find that both intermediate and deep layer excitatory neurons project to dPAG excitatory neurons in similar proportions. It will therefore be important to discover whether there are differential contributions of these two laminae to threat decisions, and whether there is anything particular about the connectivity or properties of these neurons in comparison to non-dPAG connecting cells. For example, they could preferentially connect to looming-sensitive cells in the sSC or tuned auditory inputs.

How is the escape movement coordinated?

We show that SC-PAG mediated escape behaviour is directed towards a shelter, and observed that activity in these regions does not continue once the escape reaction is terminated. It will be of interest to the field of goal-directed and instinctive behaviours to determine how the dPAG drives escape directed towards a particular goal, whether such information is inherited from the SC, and how information from circuits mediating spatial navigation is incorporated into the escape response. By recording activity during escape at high temporal resolution in more complex, larger environments requiring a variety of escape paths, we may gain further insight into how this midbrain circuit coordinates escape. In addition, functional circuit dissection of downstream dPAG targets may also elucidate different roles in motor coordination.

By what circuits and mechanisms is escape behaviour modulated?

There are a number of candidate mechanisms for influencing escape, both at the level of decision-making in the SC and of escape execution in the dPAG. By monitoring neural activity *in vivo* during modulation of defensive behaviour and exploring how different neuromodulatory systems alter information processing in the midbrain, future studies could causally examine the influence of neuromodulation of escape in the behaving animal. We speculate that the systems utilised will be highly context-dependent and could serve to underly the theoretical economic aspect of threat decision making, for example, by changing the escape threshold based on anxiety or energetic considerations, or the gain of escape speed based on the species of predator previously encountered in an environment.

7.9 Concluding remarks

Although the SC and PAG have been implicated in driving defensive behaviours such as escape in a large body of literature, our physiological knowledge of how their neurons accomplish this is in its infancy. Our results provide a mechanistic entry point for understanding how the brain compute escape, a fundamental survival behaviour, and goal-directed behaviours in general.

Bibliography

Abrahams M (2005) The Physiology of Antipredator Behaviour: What You Do With What You've Got. Fish Physiology 24:79–108.

Adamantidis A, Arber S, Bains JS, Bamberg E, Bonci A, Buzsaki G, Cardin JA, Costa RM, Dan Y, Goda Y, Graybiel AM, Hausser M, Hegemann P, Huguenard JR, Insel TR, Janak PH, Johnston D, Josselyn SA, Koch C, Kreitzer AC, Luscher C, Malenka RC, Miesenbock G, Nagel G, Roska B, Schnitzer MJ, Shenoy KV, Soltesz I, Sternson SM, Tsien RW, Tsien RY, Turrigiano GG, Tye KM, Wilson RI (2015) Optogenetics: 10 years after ChR2 in neurons: views from the community. Nature Neuroscience 18:1202–1212.

Agrawal Aa, Laforsch C, Tollrian R (1999) Transgenerational induction of defences in animals and plants. Nature 401:60–63.

Ahmadlou M, Heimel JA (2015) Preference for concentric orientations in the mouse superior. Nature Communications 6:6773.

Albin RL, Makowiec RL, Hollingsworth Z, Dure LS, Penney JB, Young AB (1990) Excitatory amino acid binding sites in the periaqueductal gray of the rat. Neuroscience Letters 118:112–5.

Almeida I, Soares SC, Castelo-Branco M (2015) The distinct role of the amygdala, superior colliculus and pulvinar in processing of central and peripheral snakes. PLoS ONE 10:1–21.

Amano K, Tanikawa T, Iseki H, Kawabatake H, Notani M, Kawamura H, Kitamura K (1978) Single neuron analysis of the human midbrain tegmentum. Rostral mecencephalic reticulotomy for pain relief. Applied Neurophysiology 41:66–78.

Amano K, Tanikawa T, Kawamura H, Iseki H, Notani M, Kawabatake H, Shiwaku T, Suda T, Demura H, Kitamura K (1982) Endorphins and pain relief. Further observations on electrical stimulation of the lateral part of the periaqueductal gray matter during rostral mesencephalic reticulotomy for pain relief. Applied Neurophysiology 45:123–35.

An X, Bandler R, Öngür D, Price JL (1998) Prefrontal cortical projections to longitudinal columns in the midbrain periaqueductal gray in macaque monkeys. Journal of Comparative Neurology 401:455–479.

Anderson DJ, Perona P (2014) Toward a science of computational ethology. Neuron 84:18–31.

Apfelbach R, Blanchard CD, Blanchard RJ, Hayes RA, McGregor IS (2005) The effects of predator odors in mammalian prey species: A review of field and laboratory studies. Neuroscience and Biobehavioral Reviews 29:1123–1144.

Appell PP, Behan M (1990) Sources of Subcortical GABAergic Projections to the Superior Colliculus in the Cat. Journal of Comparative Neurology 302:143–158.

Apter JT (1945) Projection of the Retina on Superior Colliculus of Cats. Journal of Neurophysiology 8:123–134.

Aravanis AM, Wang LP, Zhang F, Meltzer LA, Mogri MZ, Schneider MB, Deisseroth K (2007) An optical neural interface: in vivo control of rodent motor cortex with integrated fiberoptic and optogenetic technology. Journal of Neural Engineering 4:S143–56.

Asadollahi A, Mysore SP, Knudsen EI (2010) Stimulus-driven competition in a cholinergic midbrain nucleus. Nature Neuroscience 13:889–895.

Assareh N, Sarrami M, Carrive P, McNally GP (2016) The organization of defensive behavior elicited by optogenetic excitation of rat lateral or ventrolateral periaqueductal gray. Behavioral Neuroscience 130:406–414.

Augustsson H, Meyerson BJ (2004) Exploration and risk assessment: a comparative study of male house mice (Mus musculus musculus) and two laboratory strains. Physiology & Behavior 81:685–698.

Baleydier C, Magnin M (1979) Afferent and efferent connections of the parabigeminal nucleus in cat revealed by retrograde axonal transport of horseradish peroxidase. Brain Research 161:187–198.

Barbour MA, Clark RW (2012) Ground squirrel tail-flag displays alter both predatory strike and ambush site selection behaviours of rattlesnakes. Proceedings Biological sciences / The Royal Society 279:3827–33.

Barnard CJ (1983) Anti-Predator Behaviour. In: Animal Behaviour: Ecology and Evolution (Barnard CJ, ed), pp 201–217. Boston, MA: Springer US.

Bateson P (2001) Where does our behaviour come from? Journal of Biosciences 26:561–70.

Behbehani MM (1995) Functional characteristics of the midbrain periaqueductal gray. Progress in Neurobiology 46:575–605.

Beitz AJ (1982) The organisation of afferent projections to the midbrain periaqueductal grey of the rat. Neuroscience 7:133–159.

Beitz AJ (1985) The midbrain periaqueductal gray in the rat. I. Nuclear volume, cell number, density, orientation, and regional subdivisions. The Journal of Comparative Neurology 237:445–59.

Beitz AJ (1989) Possible origin of glutamatergic projections to the midbrain periaqueductal gray and deep layer of the superior colliculus of the rat. Brain Research Bulletin 23:25–35.

Beitz AJ, Clements JR, Mullett MA, Ecklund LJ (1986) Differential origin of brainstem serotoninergic projections to the midbrain periaqueductal gray and superior colliculus of the rat. The Journal of Comparative Neurology 250:498–509.

Bengtson S (2002) Origins and Early Evolution of Predation. Paleontological Society Papers 8:289–318.

Benjamini Y, Fonio E, Galili T, Havkin GZ, Golani I (2011) Quantifying the buildup in extent and complexity of free exploration in mice. Proceedings of the National Academy of Sciences 108:15580–15587.

Betley JN, Cao ZFH, Ritola KD, Sternson SM (2013) Parallel, redundant circuit organization for homeostatic control of feeding behavior. Cell 155:1337–1350.

Billington J, Wilkie RM, Field DT, Wann JP (2011) Neural processing of imminent collision in humans. Proceedings of the Royal Society B: Biological Sciences 278:1476–1481.

Bittencourt AS, Carobrez AP, Zamprogno LP, Tufik S, Schenberg LC (2004) Organization of single components of defensive behaviors within distinct columns of periaqueductal gray matter of the rat: Role of N-methyl-D-aspartic acid glutamate receptors. Neuroscience 125:71–89.

Bittencourt AS, Nakamura-Palacios EM, Mauad H, Tufik S, Schenberg LC (2005) Organization of electrically and chemically evoked defensive behaviors within the deeper collicular layers as compared to the periaqueductal gray matter of the rat. Neuroscience 133:873–892.

Bizley JK, Walker KMM, Nodal FR, King AJ, Schnupp JWH (2013) Auditory cortex represents both pitch judgments and the corresponding acoustic cues. Current Biology 23:620–625.

Blanchard DC, Agullana R, Squirrels G (1993) Twenty-two kHz alarm cries to presentation of a predator, by laboratory rats living in visible burrow systems. Physiology and Behavior 50:967–972.

Blanchard DC, Canteras NS, Markham CM, Pentkowski NS, Blanchard RJ (2005) Lesions of structures showing FOS expression to cat presentation: effects on responsivity to a Cat, Cat odor, and nonpredator threat. Neuroscience and Biobehavioral Reviews 29:1243–53.

Blanchard DC, Griebel G, Blanchard RJ (2003) The Mouse Defense Test Battery: Pharmacological and behavioral assays for anxiety and panic. European Journal of Pharmacology 463:97–116.

Blanchard DC, Williams G, Lee EMC, Blanchard RJ (1981) Taming of wild Rattus norvegicus by lesions of the mesencephalic central gray. Physiological Psychology 9:157–163.

Blanchard RJ, Blanchard DC (1989a) Antipredator defensive behaviors in a visible burrow system. Journal of Comparative Psychology 103:70–82.

Blanchard RJ, Blanchard DC (1989b) Attack and defense in rodents as ethoexperimental models for the study of emotion. Progress in Neuropsychopharmacology and Biological Psychiatry 13.

Blanchard RJ, Flannelly KJ, Blanchard DC (1986) Defensive behaviors of laboratory and wild Rattus norvegicus.

Blumstein DT (2003) Flight-initiation distance in birds is dependent on intruder starting distance.

Blumstein DT (2007) Feeling the heat: ground squirrels heat their tails to discourage rattlesnake attack. Proceedings of the National Academy of Sciences of the United States of America 104:14177–8.

Boakes Ra (2010) Darwin and Animal Behavior. In: Encyclopedia of Animal Behavior (Breed M, Moore J, eds), pp 454–460. New York: Academic Press.

Bolhuis JJ, Giraldeau LA (2005) The Study of Animal Behavior. The Behavior of Animals: Mechanisms, Function And Evolution pp 1–9.

Bolton AD, Murata Y, Kirchner R, Kim SY, Young A, Dang T, Yanagawa Y, Constantine-Paton M (2015) A Diencephalic Dopamine Source Provides Input to the Superior Colliculus, where D1 and D2 Receptors Segregate to Distinct Functional Zones. Cell Reports 13:1003–1015.

Borszcz GS (2006) Contribution of the ventromedial hypothalamus to generation of the affective dimension of pain. Pain 123:155–168.

Boyden ES, Zhang F, Bamberg E, Nagel G, Deisseroth K (2005) Millisecond-timescale, genetically targeted optical control of neural activity. Nature Neuroscience 8:1263–1268.

Branco T, Staras K (2009) The probability of neurotransmitter release: variability and feedback control at single synapses. Nature Reviews Neuroscience 10:373–383.

Brandão ML, Anseloni VZ, Pandóssio JE, De Araújo JE, Castilho VM (1999) Neurochemical mechanisms of the defensive behavior in the dorsal midbrain. Neuroscience and Biobehavioral Reviews 23:863–75.

Britten KH, Shadlen MN, Newsome WT, Movshon Ja (1992) The analysis of visual motion: a comparison of neuronal and psychophysical performance. The Journal of Neuroscience 12:4745–4765.

Brönmark C, Miner JG (1992) Predator-induced phenotypical change in body morphology in crucian carp. Science 258:1348–50.

Brown A, Yates PA, Burrola P, Ortuñ D, Vaidya A, Jessell TM, Pfaff SL, O 'leary DDM, Lemke G (2000) Topographic Mapping from the Retina to the Midbrain Is Controlled by Relative but Not Absolute Levels of EphA Receptor Signaling. Cell 102:77–88.

Brown J, Hunsperger R, Rosvold H (1969) Defense, attack, and flight elicited by electrical stimulation of the hypothalamus of the cat. Experimental Brain Research 8:113–129.

Browne D (2007) Konrad Lorenz on Instinct and Phylogenetic Information. The Rutherford Journal - The New Zealand Journal for the History and Philosophy of Science and Technology Online Jou.

Brunton BW, Botvinick MM, Brody CD (2013) Rats and Humans Can Optimally Accumulate Evidence for Decision-Making. Science 340:95–98.

Buma P, Veening J, Hafmans T, Joosten H, Nieuwenhuys R (1992) Ultrastructure of the periaqueductal grey matter of the rat: An electron microscopical and horseradish peroxidase study. Journal of Comparative Neurology 319:519–535.

Buron G, Hacquemand R, Pourie G, Lucarz A, Jacquot L, Brand G (2007) Comparative behavioral effects between synthetic 2,4,5-trimethylthiazoline (TMT) and the odor of natural fox (Vulpes vulpes) feces in mice. Behavioral Neuroscience 121:1063–1072.

Byun H, Kwon S, Ahn HJ, Liu H, Forrest D, Demb JB, Kim IJ (2016) Molecular features distinguish ten neuronal types in the mouse superficial superior colliculus. Journal of Comparative Neurology 524:2300–2321.

Cadusseau J, Roger M (1985) Afferent projections to the superior colliculus in the rat, with special attention to the deep layers. Journal fur Hirnforschung 26:667–81.

Cameron AA, Khan IA, Westlund KN, Willis WD (1995) The efferent projections of the periaqueductal gray in the rat: A Phaseolus vulgaris leucoagglutinin study. II. Descending projections. Journal of Comparative Neurology 351:585–601.

Canteras NS (2002) The medial hypothalamic defensive system: hodological organization and functional implications. Pharmacology, Biochemistry, and Behavior 71:481–491.

Canteras NS, Chiavegatto S, Ribeiro do Valle LE, Swanson LW (1997) Severe reduction of rat defensive behavior to a predator by discrete hypothalamic chemical lesions. Brain Research Bulletin 44:297–305.

Canteras NS, Goto M (1999) Fos-like immunoreactivity in the periaqueductal gray of rats exposed to a natural predator. Neuroreport 10:413–8.

Canteras NS, Simerly RB, Swanson LW (1994) Organization of projections from the ventromedial nucleus of the hypothalamus: a Phaseolus vulgaris-leucoagglutinin study in the rat. Journal of Comparative Psychology 348:41–79.

Card G, Dickinson MH (2008) Visually Mediated Motor Planning in the Escape Response of Drosophila. Current Biology 18:1300–1307.

Carvalho-Netto EF, Martinez RCR, Baldo MVC, Canteras NS (2010) Evidence for the thalamic targets of the medial hypothalamic defensive system mediating emotional memory to predatory threats. Neurobiology of Learning and Memory 93:479–486.

Cassidy J (1979) Half a Century on the Concepts of Innateness and Instinct: Survey, Synthesis and Philosophical Implications. Zeitschrift für Tierpsychologie 50:364–386.

Castillo PE, Younts TJ, Chávez AE, Hashimotodani Y (2012) Endocannabinoid Signaling and Synaptic Function. Neuron 76:70–81.

Cezario AF, Ribeiro-Barbosa ER, Baldo MVC, Canteras NS (2008) Hypothalamic sites responding to predator threats–the role of the dorsal premammillary nucleus in unconditioned and conditioned antipredatory defensive behavior. The European Journal of Neuroscience 28:1003–15.

Chen TW, Wardill TJ, Sun Y, Pulver SR, Renninger SL, Baohan A, Schreiter ER, Kerr Ra, Orger MB, Jayaraman V, Looger LL, Svoboda K, Kim DS (2013) Ultrasensitive fluorescent proteins for imaging neuronal activity. Nature 499:295–300.

Chevaleyre V, Takahashi KA, Castillo PE (2006) Endocannabinoid-Mediated Synaptic Plasticity in the Cns. Annual Review of Neuroscience 29:37–76.

Chiou LC, Chou HH (2000) Characterization of synaptic transmission in the ventrolateral periaqueductal gray of rat brain slices. NSC 100:829–834.

Cohen JD, Castro-Alamancos MA (2010) Neural correlates of active avoidance behavior in superior colliculus. The Journal of Neuroscience 30:8502–8511.

Comoli E (2012) Segregated anatomical input to sub-regions of the rodent superior colliculus associated with approach and defense. Frontiers in Neuroanatomy pp 1–19.

Comoli E, Ribeiro-Barbosa ER, Canteras NS (2000) Afferent connections of the dorsal premammillary nucleus. The Journal of Comparative Neurology 423:83–98.

Comoli E, Ribeiro-Barbosa ER, Canteras NS (2003) Predatory hunting and exposure to a live predator induce opposite patterns of Fos immunoreactivity in the PAG. Behavioural Brain Research 138:17–28.

Cools AR, Coolen JM, Smit JC, Ellenbroek BA (1984) The striato-nigro-collicular pathway and explosive running behaviour: functional interaction between neostriatal dopamine and collicular GABA. European Journal of Pharmacology 100:71–7.

Cools AR, Ellenbroek BA, van den Heuvel CM (1983) Picrotoxin microinjections into the brain: a model of abrupt withdrawal 'jumping' behaviour in rats not exposed to any opiate? European Journal of Pharmacology 90:237–43.

Cooper W (2015) Theory: models of escape and refuge use. In: Escaping from Predators: An Integrative View of Escape Decisions (Cooper W, Blumstein D, eds), 1st edition, pp 17–61. Cambridge University Press.

Cooper WE, Frederick WG (2007) Optimal flight initiation distance. Journal of Theoretical Biology 244:59–67.

Cresswell W (2008) Non-lethal effects of predation in birds. Ibis 150:3–17.

Cresswell W, Butler SJ, Whittingham MJ, Quinn JL (2009) Very short delays prior to escape from potential predators may function efficiently as adaptive risk-assessment periods. Behaviour 146:795–813.

Cziko G (2000) The Things We Do: Using the Lessons of Bernard and Darwin to Understand the What, How, and why of Our Behavior. Cambridge, Mass.: MIT Press.

Darwin C (1859) On the Origin of Species. London: John Murray.

Dawkins R, Krebs JR (1979) Arms Races between and within Species. Proceedings of the Royal Society of London Series B Biological Sciences 205:489 LP – 511.

Day HEW, Masini CV, Campeau S (2004) The pattern of brain c-fos mRNA induced by a component of fox odor, 2,5-dihydro-2,4,5-Trimethylthiazoline (TMT), in rats, suggests both systemic and processive stress characteristics. Brain Research 1025:139–151.

Dayan P, Abbott L (2002) Theoretical Neuroscience: Computational and Mathematical Modeling of Neural Systems (Computational Neuroscience). Journal of Cognitive Neuroscience p 480.

De Molina F, Hunsperger RW (1962) Organization of the subcortical system governing defence and flight reactions in the cat. Journal of Physiology 160:200–13.

De Oca BM, DeCola JP, Maren S, Fanselow MS (1998) Distinct regions of the periaqueductal gray are involved in the acquisition and expression of defensive responses. The Journal of Neuroscience 18:3426–32.

De Vries SEJ, Clandinin TR (2012) Loom-sensitive neurons link computation to action in the Drosophila visual system. Current Biology 22:353–362.

Dean P, Mitchell I, Redgrave P (1988) Responses resembling defensive behaviour produced by microinjection of glutamate into superior colliculus of rats. Neuroscience 24:501–510.

Dean P, Redgrave P, Westby GWM (1989) Event or emergency? Two response systems in the mammalian superior colliculus. Trends in Neurosciences 12:137–147.

Del Castillo J, Katz B (1954) Quantal components of the end-plate potential. Journal of Physiology 124:560–573.

Deng H, Xiao X, Wang Z (2016) Periaqueductal Gray Neuronal Activities Underlie Different Aspects of Defensive Behaviors. The Journal of Neuroscience 36:7580–8.

Depaulis A, Bandler R (eds) (1991) The Midbrain Periaqueductal Gray Matter. Boston, MA: Springer US.

Dhillon H, Zigman JM, Ye C, Lee CE, McGovern RA, Tang V, Kenny CD, Christiansen LM, White RD, Edelstein EA, Coppari R, Balthasar N, Cowley MA, Chua S, Elmquist JK, Lowell BB (2006) Leptin directly activates SF1 neurons in the VMH, and this action by leptin is required for normal body-weight homeostasis. Neuron 49:191–203.

Di Scala G, Mana MJ, Jacobs WJ, Phillips AG (1987) Evidence of Pavlovian conditioned fear following electrical stimulation of the periaqueductal grey in the rat. Physiology & Behavior 40:55–63.

Dielenberg RA, Hunt GE, McGregor IS (2001) 'When a rat smells a cat': The distribution of Fos immunoreactivity in rat brain following exposure to a predatory odor. Neuroscience 104:1085–1097.

Dill LM (1990) Distance-to-cover and the escape decisions of an African cichlid fish, Melanochromis chipokae. Environmental Biology of Fishes 27:147–152.

Domenici P, Standen EM, Levine RP (2004) Escape manoeuvres in the spiny dogfish (Squalus acanthias). Journal of Experimental Biology 207:2339–2349.

Doubell TP, Skaliora I, Baron J, King AJ (2003) Functional connectivity between the superficial and deeper layers of the superior colliculus: an anatomical substrate for sensorimotor integration. The Journal of Neuroscience 23:6596–6607.

Dräger UC, Hubel DH (1975) Responses to visual stimulation and relationship between visual, auditory, and somatosensory inputs in mouse superior colliculus. Journal of Neurophysiology 38:690–713.

Dräger UC, Hubel DH (1976) Topography of visual and somatosensory projections to mouse superior colliculus. Journal of Neurophysiology 39:91–101.

Edwards SB, Ginsburgh CL, Henkel CK, Stein BE (1979) Source of subcortical projections to the superior colliculus in the cat. Journal of Comparative Neurology 184:309–330.

Eisner T, Aneshansley DJ (1999) Spray aiming in the bombardier beetle: photographic evidence. Proceedings of the National Academy of Sciences of the United States of America 96:9705–9.

Ellis EM, Gauvain G, Sivyer B, Murphy GJ (2016) Shared and distinct retinal input to the mouse superior colliculus and dorsal lateral geniculate nucleus. Journal of Neurophysiology 116:602–610.

Ewert JP (2013) Innate Releasing Mechanism. In: Encyclopedia of Sciences and Religions (Runehov ALC, Oviedo L, eds), p 1059. Dordrecht: Springer Netherlands.

Fadok JP, Krabbe S, Markovic M, Courtin J, Xu C, Massi L, Botta P, Bylund K, Müller C, Kovacevic A, Tovote P, Lüthi A (2017) A competitive inhibitory circuit for selection of active and passive fear responses. Nature 542:96–100.

Fanselow MS (1994) Neural organization of the defensive behavior system responsible for fear. Psychonomic Bulletin & Review 1:429–438.

Fanselow MS, DeCola J (1995) Ventral and Dorsolateral Regions of the Midbrain Periaqueductal Gray (PAG) Control Different Stages of Defensive. Aggressive Behaviour 21:63–77.

Favaro PDN, Gouvêa TS, de Oliveira SR, Vautrelle N, Redgrave P, Comoli E (2011) The influence of vibrissal somatosensory processing in rat superior colliculus on prey capture. Neuroscience 176:318–327.

Feinberg EH, Meister M (2015) Orientation columns in the mouse superior colliculus. Nature 519:229–232.

Felsen G, Mainen ZF (2008) Neural Substrates of Sensory-Guided Locomotor Decisions in the Rat Superior Colliculus. Neuron 60:137–148.

Felsen G, Mainen ZF (2012) Midbrain contributions to sensorimotor decision making. Journal of Neurophysiology 108:135–147.

Fendt M (2006) Exposure to Urine of Canids and Felids, but not of Herbivores, Induces Defensive Behavior in Laboratory Rats. Journal of Chemical Ecology 32:2617.

Fernandez DC, Chang YT, Hattar S, Chen SK (2016) Architecture of retinal projections to the central circadian pacemaker. Proceedings of the National Academy of Sciences p 201523629.

Ferrero DM, Lemon JK, Fluegge D, Pashkovski SL, Korzan WJ, Datta SR, Spehr M, Fendt M, Liberles SD (2011) Detection and avoidance of a carnivore odor by prey. Proceedings of the National Academy of Sciences of the United States of America 108:11235–11240.

Fetsch CR, Kiani R, Shadlen MN (2014) Predicting the accuracy of a decision: A neural mechanism of confidence. Cold Spring Harbor Symposia on Quantitative Biology 79:185–197.

Filosa A, Barker AJ, Maschio MD, Baier H, Filosa A, Barker AJ, Maschio MD, Baier H (2016) Feeding State Modulates Behavioral Choice and Processing of Prey Stimuli in the Zebrafish Tectum Feeding State Modulates Behavioral Choice and Processing of Prey Stimuli in the Zebrafish Tectum. Neuron 90:596–608.

Floyd NS, Price JL, Ferry AT, Keay KA, Bandler R (2000) Orbitomedial prefrontal cortical projections to distinct longitudinal columns of the periaqueductal gray in the rat. Journal of Comparative Neurology 422:556–578.

Fogaça MV, Lisboa SF, Aguiar DC, Moreira FA, Gomes FV, Casarotto PC, Guimarães FS (2012) Fine-tuning of defensive behaviors in the dorsal periaqueductal gray by atypical neurotransmitters. Brazilian Journal of Medical and Biological Research 45:357–365.

Forcelli P, DesJardin J, West E, Holmes A, Elorette C, Wellman L, Malkova L (2016) Amygdala selectively modulates defensive responses evoked from the superior colliculus in non-human primates. Social Cognitive and Affective Neuroscience pp 1–11.

Fox AS, Oler JA, Tromp DPM, Fudge JL, Kalin NH (2015) Extending the amygdala in theories of threat processing. Trends in Neurosciences 38:319–329.

Franklin TB, Silva Ba, Perova Z, Marrone L, Masferrer ME, Zhan Y, Kaplan A, Greetham L, Verrechia V, Halman A, Pagella S, Vyssotski AL, Illarianova A, Branco T, Gross CT (2017) Prefrontal cortical control of a brainstem social behavior circuit. Nature Neuroscience 20:1–14.

Gale SD, Murphy GJ (2014) Distinct Representation and Distribution of Visual Information by Specific Cell Types in Mouse Superficial Superior Colliculus. The Journal of Neuroscience 34:13458–13471.

Gandhi NJ, Katnani HA (2011) Motor functions of the superior colliculus. Annual Review of Neuroscience 34:205–231.

Gioia M, Tredici G, Bianchi R (1998) Dendritic arborization and spines of the neurons of the cat and human periaqueductal gray: A light, confocal laser scanning, and electron microscope study. Anatomical Record 251:316–325.

Gold J, Shadlen M (2007) The neural basis of decision making. Annual Review of Neuroscience 30:535–574.

Graybiel AM (1978) A satellite system of the superior colliculus: the parabigeminal nucleus and its projections to the superficial collicular layers. Brain Research 145:365–374.

Griebel G, Blanchard DC, Blanchard RJ (1996) Evidence that the behaviors in the mouse defense test battery relate to different emotional states: A factor analytic study. Physiology and Behavior 60:1255–1260.

Griffiths P (2009) The distinction between innate and aquired characteristics.

Gross CT, Canteras NS (2012) The many paths to fear. Nature Reviews Neuroscience 13:651–658.

Gross HP (1978) Natural selection by predators on the defensive apparatus of the three-spined stickleback, Gasterosteus aculeatus L. Canadian Journal of Zoology 56:398–413.

Guizar-Sicairos M, Thurman ST, Fienup JR (2008) Efficient subpixel image registration algorithms. Optics Letters 33:156–158.

Halladay LR, Blair HT (2015) Distinct ensembles of medial prefrontal cortex neurons are activated by threatening stimuli that elicit excitation versus inhibition of movement. Journal of Neurophysiology p jn.00656.2014.

Halpern M (1968) Effects of midbrain central gray matter lesions on escape-avoidance behavior in rats. Physiology & Behavior 3:171–178.

Hamilton TJ, Wheatley BM, Sinclair DB, Bachmann M, Larkum ME, Colmers WF (2010) Dopamine modulates synaptic plasticity in dendrites of rat and human dentate granule cells. Proceedings of the National Academy of Sciences of the United States of America 107:18185–90.

Han W, Tellez LA, Rangel M, Shammah-Lagnado SJ, Van Den Pol AN, De Araujo IE (2017) Integrated Control of Predatory Hunting by the Central Nucleus of the Amygdala. Cell 168:311–324.e18.

Hanlon R (2007) Cephalopod dynamic camouflage. Current Biology 17:400–404.

Hanlon RT, Conroy LA, Forsythe JW (2008) Mimicry and foraging behaviour of two tropical sand-flat octopus species off North Sulawesi, Indonesia. Biological Journal of the Linnean Society 93:23–38.

Hattar S, Kumar M, Park A, Tong P, Tung J, Yau KW, Berson DM (2006) Central projections of melanopsin-expressing retinal ganglion cells in the mouse. The Journal of Comparative Neurology 497:326–349.

Haubensak W, Kunwar PS, Cai H, Ciocchi S, Wall NR, Ponnusamy R, Biag J, Dong HW, Deisseroth K, Callaway EM, Fanselow MS, Lüthi A, Anderson DJ (2010) Genetic dissection of an amygdala microcircuit that gates conditioned fear. Nature 468:270–276.

Hebb D (1949) The organization of behavior. New York: Wiley.

Helmchen F, Denk W, Kerr JND (2013) Miniaturization of Two-Photon Microscopy for Imaging in Freely Moving Animals. Cold Spring Harbor Protocols 2013:pdb.top078147–pdb.top078147.

Helmchen F, Fee MS, Tank DW, Denk W (2001) A Miniature Head-Mounted Two-Photon Microscope. Neuron 31:903–912.

Hemelt ME, Keller A (2008) Superior colliculus control of vibrissa movements. Journal of Neurophysiology 100:1245–54.

Herberholz J, Marquart GD (2012) Decision making and behavioral choice during predator avoidance. Frontiers in Neuroscience 6:1–15.

Hess W, Brügger M (1943) Das subkortikale Zentrum der affektiven Abwehrraktion. Helvetica Physica Acta 1:33–52.

Hirayama K, Gillette R (2012) A Neuronal Network Switch for Approach / Avoidance Toggled by Appetitive State. Current Biology 22:118–123.

Holmes A, Parmigiani S, Ferrari PF, Palanza P, Rodgers RJ (2000) Behavioral profile of wild mice in the elevated plus-maze test for anxiety. Physiology and Behavior 71:509–516.

Hölscher C, Schnee A, Dahmen H, Setia L, Mallot HA (2005) Rats are able to navigate in virtual environments. The Journal of Experimental Biology 208:561 LP – 569.

Horwitz GD, Batista AP, Newsome WT (2004) Representation of an Abstract Perceptual Decision in Macaque Superior Colliculus. Journal of Neurophysiology 91:2281–2296.

Huang L, Yuan T, Tan M, Xi Y, Hu Y, Tao Q, Zhao Z, Zheng J, Han Y, Xu F, Luo M, Sollars PJ, Pu M, Pickard GE, So KF, Ren C (2017) A retinoraphe projection regulates serotonergic activity and looming-evoked defensive behaviour. Nature Communications 8:14908.

Huberman AD, Niell CM (2011) What can mice tell us about how vision works? Trends in Neurosciences 34:464–473.

Hunsperger RW (1956) Role of substantia grisea centralis mesencephali in electrically-induced rage reactions. Progress in Neurobiology pp 289–94.

Inayat S, Barchini J, Chen H, Feng L, Liu X, Cang J (2015) Neurons in the Most Superficial Lamina of the Mouse Superior Colliculus Are Highly Selective for Stimulus Direction. The Journal of Neuroscience 35:7992–8003.

Isa T, Hall WC (2009) Exploring the superior colliculus in vitro. Journal of Neurophysiology 102:2581–2593.

Isaacson JS, Walmsley B (1995) Counting quanta: direct measurements of transmitter release at a central synapse. Neuron 15:875–84.

Isogai Y, Si S, Pont-Lezica L, Tan T, Kapoor V, Murthy VN, Dulac C (2011) Molecular organization of vomeronasal chemoreception. Nature 478:241–245.

Isosaka T, Matsuo T, Yamaguchi T, Funabiki K, Nakanishi S, Kobayakawa R, Kobayakawa K (2015) Htr2a-Expressing Cells in the Central Amygdala Control the Hierarchy between Innate and Learned Fear. Cell 163:1153–1164.

Janusonis S, Fite KV, Foote W (1999) Topographic Organization of Serotonergic Dorsal Raphe Ne urons Projecting to the Superior Colliculus in the Mongolian Gerbil (Meriones unguiculatus). The Journal of Comparative Neurology 355:342–355.

Jay TM (2003) Dopamine: A potential substrate for synaptic plasticity and memory mechanisms. Progress in Neurobiology 69:375–390.

Jiang ZD, King AJ, Moore DR (1996) Topographic organization of projection from the parabigeminal nucleus to the superior colliculus in the ferret revealed with fluorescent latex microspheres. Brain Research 743:217–232.

Johansen JP, Cain CK, Ostroff LE, LeDoux JE (2011) Molecular mechanisms of fear learning and memory. Cell 147:509–524.

Johansen JP, Tarpley JW, LeDoux JE, Blair HT (2010) Neural substrates for expectation-modulated fear learning in the amygdala and periaqueductal gray. Nature Neuroscience 13:979–986.

Jones M, Mandelik Y, Dayan T (2001) Coexistence of Temporally Partitioned Spiny Mice: Roles of Habitat Structure and Foraging Behavior. Ecology 82:2164–2176.

Kaifosh P, Zaremba JD, Danielson NB, Losonczy A (2014) SIMA : Python software for analysis of dynamic fluorescence imaging data. Frontiers in Neuroinformatics 8:1–10.

Keay KA, Bandler R (2004) Periaqueductal Gray. In: The Rat Nervous System: 3rd Edition, pp 1–5. San Diego: Elsevier.

Kepecs A, Uchida N, Zariwala Ha, Mainen ZF (2008) Neural correlates, computation and behavioural impact of decision confidence. Nature 455:227–231.

Kiani R, Corthell L, Shadlen MN (2014) Choice certainty is informed by both evidence and decision time. Neuron 84:1329–1342.

Kiani R, Shadlen MN (2009) Representation of confidence associated with a decision by neurons in the parietal cortex. Science 324:759–764.

Kim B, Basso Ma (2008) Saccade target selection in the superior colliculus: a signal detection theory approach. The Journal of Neuroscience 28:2991–3007.

Kim EJ, Horovitz O, Pellman BA, Tan LM, Li Q, Richter-Levin G, Kim JJ (2013) Dorsal periaqueductal gray-amygdala pathway conveys both innate and learned fear responses in rats. Proceedings of the National Academy of Sciences of the United States of America 110:14795–800.

Kincheski GC, Mota-Ortiz SR, Pavesi E, Canteras NS, Carobrez AP (2012) The Dorsolateral Periaqueductal Gray and Its Role in Mediating Fear Learning to Life Threatening Events. PLoS ONE 7:e50361.

King AJ (1993) The Wellcome Prize Lecture. A map of auditory space in the mammalian brain: neural computation and development. Experimental Physiology 78:559–590.

King AJ, Hutchings ME (1987) Spatial response properties of acoustically responsive neurons in the superior colliculus of the ferret: a map of auditory space. Journal of Neurophysiology 57:596–624.

Knudsen EI (1991) Dynamic space codes in the superior colliculus. Current Opinion in Neurobiology 1:628–632.

Kobayakawa K, Kobayakawa R, Matsumoto H, Oka Y, Imai T, Ikawa M, Okabe M, Ikeda T, Itohara S, Kikusui T, Mori K, Sakano H (2007) Supplementary: Innate versus learned odour processing in the mouse olfactory bulb. Nature 450:503–508.

Kollack-Walker S, Don C, Watson SJ, Akil H (1999) Differential expression of c-fos mRNA within neurocircuits of male hamsters exposed to acute or chronic defeat. Journal of Neuroendocrinology 11:547–559.

Kotler B, Blaustein L, Brown J (1992) Predator facilitation: the combined effect of snakes and owls on the foraging behavior of gerbils. Annales Zoologici Fennici 47:465–468.

Koutsikou S, Apps R, Lumb BM (2017) Top down control of spinal sensorimotor circuits essential for survival. Journal of Physiology 595:4151–4158.

Koutsikou S, Crook JJ, Earl EV, Leith JL, Watson TC, Lumb BM, Apps R (2014) Neural substrates underlying fear-evoked freezing: the periaqueductal grey-cerebellar link. Journal of Physiology 592:2197–2213.

Krakauer JW, Ghazanfar AA, Gomez-Marin A, Maciver MA, Poeppel D (2017) Neuron Perspective Neuroscience Needs Behavior: Correcting a Reductionist Bias. Neuron 93:480–490.

Krasne FB, Wine J (1975) Extrinsic modulation of crayfish escape behaviour. Journal Of Experimental Biology 63:433–450.

Kunwar PS, Zelikowsky M, Remedios R, Cai H, Yilmaz M, Meister M, Anderson DJ (2015) Ventromedial hypothalamic neurons control a defensive emotion state. eLife 4.

Kwon OB, Lee JH, Kim HJ, Lee S, Lee S, Jeong MJ, Kim SJ, Jo HJ, Ko B, Chang S, Park SK, Choi YB, Bailey CH, Kandel ER, Kim JH (2015) Dopamine Regulation of Amygdala Inhibitory Circuits for Expression of Learned Fear. Neuron 88:378–389.

Laughlin BYSB (1989) The role of sensory adaptation in the retina. Journal Of Experimental Biology 62:39–62.

LeDoux J (2003) The emotional brain, fear, and the amygdala. Cellular and Molecular Neurobiology 23:727–38.

LeDoux JE (2000) Emotion circuits in the brain. Annual Review of Neuroscience 23:155–184.

LeDoux JE (2014) Coming to terms with fear. Proceedings of the National Academy of Sciences of the United States of America 111:2871–8.

Lee H, Kim DW, Remedios R, Anthony TE, Chang A, Madisen L, Zeng H, Anderson DJ (2014) Scalable control of mounting and attack by Esr1+ neurons in the ventromedial hypothalamus. Nature 509:627–32.

Lehrman DS (1953) A Critique of Konrad Lorenz's Theory of Instinctive Behavior. The Quarterly Review of Biology 28:337–363.

Li C, Maglinao T, Takahashi LK (2004) Medial amygdala modulation of predator odor induced unconditioned fear in the rat. Behavioral Neuroscience 118:324–332.

Liang F, Xiong XR, Zingg B, ying Ji X, Zhang LI, Tao HW (2015) Sensory Cortical Control of a Visually Induced Arrest Behavior via Corticotectal Projections. Neuron 86:755–767.

Lima S, Dill L (1990) Behavioral decisions made under the risk of predation: a review and prospectus. Canadian Journal of Zoology 68:619–640.

Lin D, Boyle MP, Dollar P, Lee H, Lein ES, Perona P, Anderson DJ (2011) Functional identification of an aggression locus in the mouse hypothalamus. Nature 470:221–6.

Linnman C, Moulton EA, Barmettler G, Becerra L, Borsook D (2012) Neuroimaging of the periaqueductal gray: State of the field. NeuroImage 60:505–522.

Lipp HP, Hunsperger RW (1978) Threat, attack and flight elicited by electrical stimulation of the ventromedial hypothalamus of the marmoset monkey Callithrix jacchus. Brain, Behavior and Evolution 15:260–93.

Liu YJ, Wang Q, Li B (2011) Neuronal Responses to Looming Objects in the Superior Colliculus of the Cat. Brain, Behavior and Evolution 77:193–205.

Lorenz K (1937) The Companion in the Bird's World. The Auk 54:245–273.

Lorenz K (1941) Vergleichende Bewegungsstudien an Anatinen. Journal of Ornithology 29:194–294.

Lovick TA, Stezhka VV (1999) Neurones in the dorsolateral periaqueductal grey matter in coronal slices of rat midbrain: electrophysiological and morphological characteristics. Experimental Brain Research 124:53–58.

Mahn M, Prigge M, Ron S, Levy R, Yizhar O (2016) Biophysical constraints of optogenetic inhibition at presynaptic terminals. Nature Neuroscience 19:554–556.

Mameli M, Bateson P (2011) An evaluation of the concept of innateness. Philosophical Transactions of the Royal Society B: Biological Sciences 366:436–443.

Mantyh PW (1982) Forebrain projections to the periaqueductal gray in the monkey, with observations in the cat and rat. The Journal of Comparative Neurology 206:146–58.

Maria J, Brandão ML (2011) GABAergic mechanisms of anterior and ventromedial hypothalamic nuclei in the expression of freezing in response to a light-conditioned stimulus. Psychology & Neuroscience 4:211–217.

Marler P (2004) Innateness and the instinct to learn. Anais da Academia Brasileira de Ciencias 76:189–200.

Marr D (1982) Vision: A computational investigation into the human representation and processing of visual information. San Francisco: W. H. Freeman and Company.

Martin J, Lopez P (1999) When to come out from a refuge: risk-sensitive and state-dependent decisions in an alpine lizard. Behavioral Ecology 10:487–492.

Martinez RC, Carvalho-Netto EF, Ribeiro-Barbosa ÉR, Baldo MVC, Canteras NS (2011) Amygdalar roles during exposure to a live predator and to a predator-associated context. Neuroscience 172:314–328.

May PJ (2006) The mammalian superior colliculus: Laminar structure and connections. Progress in Brain Research 151:321–378.

Mcdonald AJ (1998) Cortical pathways to the mammalian amygdala. Progress in Neurobiology 55:257–332.

McDonald J (2014) Handbook of Biological Statistics (3rd ed.). Baltimore: Sparky House Publishing.

Mcgaugh JL (2004) The Amygdala Modulates the Consolidation of Memories of Emotionally Arousing Experiences. Annual Review of Neuroscience 27:1–28.

McGregor IS, Schrama L, Ambermoon P, Dielenberg RA (2002) Not all 'predator odours' are equal: Cat odour but not 2, 4, 5 trimethylthiazoline (TMT; fox odour) elicits specific defensive behaviours in rats. Behavioural Brain Research 129:1–16.

McNaughton N, Corr PJ (2004) A two-dimensional neuropsychology of defense: Fear/anxiety and defensive distance. Neuroscience and Biobehavioral Reviews 28:285–305.

Mitchell IJ, Redgrave P, Dean P (1988) Plasticity of behavioural response to repeated injection of glutamate in cuneiform area of rat. Brain Research 460:394–397.

Mongeau R, Miller GA, Chiang E, Anderson DJ (2003) Neural correlates of competing fear behaviors evoked by an innately aversive stimulus. The Journal of Neuroscience 23:3855–3868.

Mooney RD, Huang X, Rhoades RW (1992) Functional influence of interlaminar connections in the hamster's superior colliculus. The Journal of Neuroscience 12:2417–32.

Morris JS, Ohman A, Dolan RJ (1999) A subcortical pathway to the right amygdala mediating "unseen" fear. Proceedings of the National Academy of Sciences 96:1680–1685.

Motta SC, Carobrez AP, Canteras NS (2017) The periaqueductal gray and primal emotional processing critical to influence complex defensive responses, fear learning and reward seeking. Neuroscience and Biobehavioral Reviews 76:39–47.

Motta SC, Goto M, Gouveia FV, Baldo MVC, Canteras NS, Swanson LW (2009) Dissecting the brain's fear system reveals the hypothalamus is critical for responding in subordinate conspecific intruders. Proceedings of the National Academy of Sciences of the United States of America 106:4870–5.

Mrsic-Flogel TD, Hofer SB, Creutzfeldt C, Cloëz-Tayarani I, Changeux JP, Bonhoeffer T, Hübener M (2005) Altered map of visual space in the superior colliculus of mice lacking early retinal waves. The Journal of Neuroscience 25:6921–8.

Mukamel E, Nimmerjahn A, Schnitzer M (2009) Automated analysis of cellular signals from large-scale calcium imaging data. Neuron 63:747–760.

Münch TA, da Silveira RA, Siegert S, Viney TJ, Awatramani GB, Roska B (2009) Approach sensitivity in the retina processed by a multifunctional neural circuit. Nature Neuroscience 12:1308–1316.

Muthuraju S, Talbot T, Brand??o ML (2016) Dopamine D2 receptors regulate unconditioned fear in deep layers of the superior colliculus and dorsal periaqueductal gray. Behavioural Brain Research 297:116–123.

Nashold BS, Wilson WP, Slaughter DG (1969) Sensations evoked by stimulation in the midbrain of man. Journal of Neurosurgery 30:14–24.

Nekaris KAI, Pimley ER, Ablard KM (2007) Predator Defense by Slender Lorises and Pottos. In: Primate Anti-Predator Strategies (Gursky SL, Nekaris KAI, eds), pp 222–240. Boston, MA: Springer US.

Nelson EH, Matthews CE, Rosenheim JA (2004) Predators reduce prey population growth by inducing changes in prey behavior. Ecology 85:1853–1858.

Nikolaev A, Leung KM, Odermatt B, Lagnado L (2013) Synaptic mechanisms of adaptation and sensitization in the retina. Nature Neuroscience 16:934–41.

Niwa M, Johnson JS, O'Connor KN, Sutter ML (2012) Activity Related to Perceptual Judgment and Action in Primary Auditory Cortex. The Journal of Neuroscience 32:3193–3210.

Nonacs P, Blumstein DT (2010) Predation risk and behavioural life history. In: Evolutionary Behavioral Ecology (Westneat MW, Fox C, eds), 1st edition, chapter 13, pp 207–221. Oxford University Press.

Olds M, Olds J (1962) Approach-escape interactions in rat brain. American Journal of Physiology 203:803–810.

Olsson I, Suryanarayana SM, Robertson B, Grillner S (2017) Griseum centrale, a homologue of the periaqueductal gray in the lamprey. IBRO Reports 2:24–30.

Owings DHD, Coss RRG (2008) Hunting California Ground Squirrels: Constraints and Opportunities for Northern Pacific Rattlesnakes. In: The Biology of Rattlesnakes, January 2008, pp 155–168. Loma Linda University Press.

Ozawa T, Ycu EA, Kumar A, Yeh LF, Ahmed T, Koivumaa J, Johansen JP (2017) A feedback neural circuit for calibrating aversive memory strength. Nature Neuroscience 20:90–97.

Paley W (1802) Natural Theology or Evidences of the Existence and Attributes of the Deity. London: R. Faulder.

Papes F, Logan DW, Stowers L (2010) The Vomeronasal Organ Mediates Interspecies Defensive Behaviors through Detection of Protein Pheromone Homologs. Cell 141:692–703.

Peek MY, Card GM (2016) Comparative approaches to escape. Current Opinion in Neurobiology 41:167–173.

Petreanu L, Huber D, Sobczyk A, Svoboda K (2007) Channelrhodopsin-2–assisted circuit mapping of long-range callosal projections. Nature Neuroscience 10:663–668.

Pettersson LB, Nilsson PA, Bronmark C (2000) Predator recognition and defence strategies in crucian carp, Carassius carassius. Oikos 88:200–212.

Pettit DL, Helms MC, Lee P, Augustine GJ, Hall WC (1999) Local Excitatory Circuits in the Intermediate Gray Layer of the Superior Colliculus. Journal of Neurophysiology 81.

Pobbe RLH, Zangrossi H (2005) 5-HT1A and 5-HT2A receptors in the rat dorsal periaqueductal gray mediate the antipanic-like effect induced by the stimulation of serotonergic neurons in the dorsal raphe nucleus. Psychopharmacology 183:314–321.

Pobbe RLH, Zangrossi H, Blanchard DC, Blanchard RJ (2011) Involvement of dorsal raphe nucleus and dorsal periaqueductal gray 5-HT receptors in the modulation of mouse defensive behaviors. European Neuropsychopharmacology 21:306–315.

Pond FJ, Sinnamon HM, Adams DB (1977) Single unit recording in the midbrain of rats during shock-elicited fighting behavior. Brain Research 120:469–484.

Poran NS, Coss RG (1990) Development of Antisnake Defenses in California Ground Squirrels (Spermophilus beecheyi): I. Behavioral and Immunological Relationships. Behaviour 112:222–245.

Ramasamy RA, Allan BJM, Mccormick MI (2015) Plasticity of Escape Responses : Prior Predator Experience Enhances Escape Performance in a Coral Reef Fish. PLoS ONE pp 1–9.

Ramón y Cajal S (1909) Histologie du Systeme Nerveux de l'Homme et des Vertebres. Maloine, Paris: 1911. chap. II. Demography v.1:3–43.

Rangel A (2008) The Computation and Comparison of Value in Goal-directed Choice. In: Neuroeconomics: Decision Making and the Brain (Glimcher PW, Fehr E, eds), 1st edition. Elsevier.

Rangel MJ, Baldo MVC, Canteras NS (2018) Influence of the anteromedial thalamus on social defeat-associated contextual fear memory. Behavioural Brain Research 339:269–277.

Rankin CH, Abrams T, Barry RJ, Bhatnagar S, Clayton D, Colombo J, Coppola G, Geyer MA, Glanzman DL, Marsland S, Mcsweeney F, Wilson DA, Wu Cf, Thompson RF (2010) Habituation Revisited: An Updated and Revised Description of the Behavioral Characteristics of Habituation. Neurobiology of Learning and Memory 92:135–138.

Ratcliff R, Hasegawa YT, Hasegawa RP, Smith PL, Segraves MA (2007) Dual diffusion model for single-cell recording data from the superior colliculus in a brightness-discrimination task. Journal of Neurophysiology 97:1756–1774.

Ratcliff R, Rouder JN (1998) Modeling response times for two-choice decisions. Psychological Science 9:347–356.

Redgrave P, Dean P (1991) Does the PAG Learn about Emergencies from the Superior Colliculus? In: The Midbrain Periaqueductal Gray Matter, pp 199–209. Boston, MA: Springer US.

Redgrave P, Dean P, Mitchell IJ, Odekunle A, Clark A (1988) The projection from superior colliculus to cuneiform area in the rat - I. Anatomical studies. Experimental Brain Research 72:611–625.

Redgrave P, Mitchell IJ, Dean P (1987) Descending projections from the superior colliculus in rat: a study using orthograde transport of wheatgerm-agglutinin conjugated horseradish peroxidase P. Experimental Brain Research 68.

Rees A (1996) Sensory maps: Aligning maps of visual and auditory space. Current Biology 6:955–958.

Resulaj A, Kiani R, Wolpert DM, Shadlen MN (2009) Changes of mind in decision-making. Nature 461:263–266.

Rigato E, Minelli A (2013) The great chain of being is still here. Evolution: Education and Outreach 6:1–6.

Romanes GJ, Darwin C (1883) Mental evolution in animals. With a posthumous essay on instinct by Charles Darwin. London: Kegan Paul Trench & Co.

Romo R, Hernández A, Zainos A, Salinas E (1998) Somatosensory discrimination based on cortical microstimulation. Nature 392:387–390.

Root CM, Denny CA, Hen R, Axel R (2014) The participation of cortical amygdala in innate, odour-driven behaviour. Nature 515:269–273.

Roseberry TK, Lee AM, Lalive AL, Wilbrecht L, Bonci A, Kreitzer AC, Roseberry TK, Lee AM, Lalive AL, Wilbrecht L, Bonci A (2016) Cell-Type-Specific Control of Brainstem Locomotor Circuits by Basal Ganglia Article Cell-Type-Specific Control of Brainstem Locomotor Circuits by Basal Ganglia. Cell 164:526–537.

Rosen JB, Asok A, Chakraborty T (2015) The smell of fear: Innate threat of 2,5-dihydro-2,4,5-trimethylthiazoline, a single molecule component of a predator odor. Frontiers in Neuroscience 9:1–12.

Rundus AS, Owings DH, Joshi SS, Chinn E, Giannini N (2007) Ground squirrels use an infrared signal to deter rattlesnake predation. Proceedings of the National Academy of Sciences of the United States of America 104:14372–6.

Sahibzada N, Dean P, Redgrave P (1986) Movements Resembling Orientation or Avoidance Elicited by Electrical Stimulation of the Superior Colliculus in Rats. The Journal of Neuroscience 6:723–733.

Saito Y, Isa T (2004) Laminar specific distribution of lateral excitatory connections in the rat superior colliculus. Journal of Neurophysiology 92:3500–10.

Sánchez D, Ganfornina MD, Ribas J (1988) Periaqueductal gray neurons' activity in a mesencephalic slice preparation. Brain Research 455:166–169.

Schall JD (1999) Weighing the evidence: how the brain makes a decision. Nature Neuroscience 2:108–109.

Schall JD (2001) Neural basis of deciding, choosing and acting. Nature Reviews Neuroscience 2:33–42.

Schall JD (2004) On building a bridge between brain and behavior. Annual Reviews of Psychology 55:23–50.

Schenberg LC, Lovick TA (1995) Attenuation of the midbrain-evoked defense reaction by selective stimulation of medullary raphe neurons in rats. American Journal of Physiology 269:R1378–89.

Schenberg LC, Póvoa RMF, Costa ALP, Caldellas AV, Tufik S, Bittencourt AS (2005) Functional specializations within the tectum defense systems of the rat. Neuroscience and Biobehavioral Reviews 29:1279–1298.

Schiller PH (1984) The Superior Colliculus and Visual Function.

Schiller PH, Schiller, H P (2011) The Superior Colliculus and Visual Function. In: Comprehensive Physiology. Hoboken, NJ, USA: John Wiley & Sons, Inc.

Schmidt-Hieber C, Hausser M (2013) Cellular mechanisms of spatial navigation in the medial entorhinal cortex. Nature Neuroscience .

Seamone S, Blaine T, Higham TE (2014) Sharks modulate their escape behavior in response to predator size, speed and approach orientation. Zoology 117:377–382.

Shadlen NN, Newsome WT (2001) Neural basis of a perceptual decision in the parietal cortex (area lip) of the rhesus monkey. Journal of Neurophysiology 86:1916–1936.

Shang C, Liu Z, Chen Z, Shi Y, Wang Q, Liu S, Li D, Cao P (2015) A parvalbumin-positive excitatory visual pathway to trigger fear responses in mice. Science 348:1472–1477.

Shea-Brown E, Gilzenrat MS, Cohen JD (2008) Optimization of Decision Making in Multilayer Networks: The Role of Locus Coeruleus. Neural Computation 20:2863–94.

Sherk H (1979) A comparison of visual-response properties in cat's parabigeminal nucleus and superior colliculus. Journal of Neurophysiology 42:1640–55.

Shi X, Barchini J, Ledesma HA, Koren D, Jin Y, Liu X, Wei W, Cang J (2017) Retinal origin of direction selectivity in the superior colliculus. Nature Neuroscience 20:550–558.

Sih A (1992) Prey Uncertainty and the Balancing of Antipredator and Feeding Needs. The American Naturalist 139:1052–1069.

Sih A, Ziemba R, Harding KC (2000) New insights on how temporal variation in predation risk shapes prey behavior. Trends in Ecology & Evolution 15:3–4.

Silva BA, Gross CT, Gräff J (2016a) The neural circuits of innate fear: detection, integration, action, and memorization. Learning and Memory 23:544–55.

Silva BA, Mattucci C, Krzywkowski P, Cuozzo R, Carbonari L, Gross CT (2016b) The ventromedial hypothalamus mediates predator fear memory. European Journal of Neuroscience 43:1431–1439.

Silva Ba, Mattucci C, Krzywkowski P, Murana E, Illarionova A, Grinevich V, Canteras NS, Ragozzino D, Gross CT (2013) Independent hypothalamic circuits for social and predator fear. Nature Neuroscience 16:1731–3.

Song JH, Rafal RD, McPeek RM (2011) Deficits in reach target selection during inactivation of the midbrain superior colliculus. Proceedings of the National Academy of Sciences of the United States of America 108:E1433–40.

Sparks DL (1988) Neural cartography: sensory and motor maps in the superior colliculus. Brain, Behavior and Evolution 31:49–56.

Sparks DL, Hartwich-Young R (1989) The deep layers of the superior colliculus.

Sperry RW (1963) Chemoaffinity in the orderly growth of nerve fiber patterns and connections. Proceedings of the National Academy of Sciences of the United States of America 50:703.

Stachniak TJ, Ghosh A, Sternson SM (2014) Chemogenetic Synaptic Silencing of Neural Circuits Localizes a Hypothalamus→Midbrain Pathway for Feeding Behavior. Neuron 82:797–808.

Stein B, Magalhaes-Castro B, Kruger L (1975) Superior colliculus: visuotopic-somatotopic overlap. Science 189:224–226.

Stein BE, Clamann HP (1981) Control of pinna movements and sensorimotor register in cat superior colliculus. Brain, Behavior and Evolution 19:180–92.

Stein BE, Stanford TR, Rowland BA (2014) Development of multisensory integration from the perspective of the individual neuron. Nature Reviews Neuroscience 15:520–35.

Stein L (1965) Facilitation of avoidance beahviour by positive brain stimulation. Journal of Comparative and Physiological Psychology 60:9–19.

Sternson SM (2013) Hypothalamic survival circuits: Blueprints for purposive behaviors. Neuron 77:810–824.

Stezhka VV, Lovick TA (1997) Projections from dorsal raphe nucleus to the periaqueductal grey matter: Studies in slices of rat midbrain maintained in vitro. Neuroscience Letters 230:57–60.

Stowers L, Kuo TH (2015) Mammalian pheromones: Emerging properties and mechanisms of detection. Current Opinion in Neurobiology 34:103–109.

Sukikara MH, Mota-Ortiz SR, Baldo MV, Felicio LF, Canteras NS (2010) The periaqueductal gray and its potential role in maternal behavior inhibition in response to predatory threats. Behavioural Brain Research 209:226–233.

Swanson LW, Petrovich GD (1998) What is the amygdala? Trends in neurosciences 21:323–331.

Takahashi LK (2014) Olfactory systems and neural circuits that modulate predator odor fear. Frontiers in Behavioral Neuroscience 8:72.

Taraborelli P, Corbalán V, Giannoni S (2003) Locomotion and escape modes in rodents of the Monte Desert (Argentina). Ethology 109:475–485.

Taylor AM, Jeffery G, Lieberman AR (1986) Subcortical afferent and efferent connections of the superior colliculus in the rat and comparisons between albino and pigmented strains. Experimental Brain Research 62:131–42.

Tervo DGR, Hwang BY, Viswanathan S, Gaj T, Lavzin M, Ritola KD, Lindo S, Michael S, Kuleshova E, Ojala D, Huang CC, Gerfen CR, Schiller J, Dudman JT, Hantman AW, Looger LL, Schaffer DV, Karpova AY (2016) A Designer AAV Variant Permits Efficient Retrograde Access to Projection Neurons. Neuron 92:372–382.

Thevarajah D, Mikulic A, Dorris MC (2009) Role of the Superior Colliculus in Choosing Mixed-Strategy Saccades. The Journal of Neuroscience 29:1998–2008.

Thompson DW (1910) Historia animalium. 1st edition. Oxford: Clarendon Press.

Tinbergen N (1951) The sudy of instinct. Oxford: Clarendon Press.

Tinbergen N (1963) On aims and methods of Ethology. Zeitschrift für Tierpsychologie 20:410–433.

Tovote P, Esposito MS, Botta P, Chaudun F, Fadok JP, Markovic M, Wolff SBE, Ramakrishnan C, Fenno L, Deisseroth K, Herry C, Arber S, Luthi A (2016) Midbrain circuits for defensive behaviour. Nature 534:206–212.

Tovote P, Fadok JP, Lüthi A (2015) Neuronal circuits for fear and anxiety. Nature Reviews Neuroscience 16:317–331.

Uexküll JV (1957) A stroll through the worlds of animals and men: A picture book of invisible worlds. Translated by C. H. Schiller. New York: International Universities Press.

Usunoff KG, Schmitt O, Itzev DE, Rolfs A, Wree A (2007) Efferent connections of the parabigeminal nucleus to the amygdala and the superior colliculus in the rat: A double-labeling fluorescent retrograde tracing study. Brain Research 1133:87–91.

Vale R, Evans DA, Branco T (2017) Rapid Spatial Learning Controls Instinctive Defensive Behavior in Mice. Current Biology 27:1342–1349.

Vargas LC, De Azevedo Marques T, Schenberg LC (2000) Micturition and defensive behaviors are controlled by distinct neural networks within the dorsal periaqueductal gray and deep gray layer of the superior colliculus of the rat. Neuroscience Letters 280:45–48.

Vélez-Fort M, Rousseau CV, Niedworok CJ, Wickersham IR, Rancz EA, Brown APY, Strom M, Margrie TW (2014) The stimulus selectivity and connectivity of layer six principal cells reveals cortical microcircuits underlying visual processing. Neuron 83:1431–1443.

Vianna DML, Brandão ML (2003) Anatomical connections of the periaqueductal gray: Specific neural substrates for different kinds of fear. Brazilian Journal of Medical and Biological Research 36:557–566.

Vianna DML, Landeira-Fernandez J, Brandão ML (2001) Dorsolateral and ventral regions of the periaqueductal gray matter are involved in distinct types of fear. Neuroscience and Biobehavioral Reviews 25:711–719.

Vong L, Ye C, Yang Z, Choi B, Chua S, Lowell B (2011) Leptin Action on GABAergic Neurons Prevents Obesity and Reduces Inhibitory Tone to POMC Neurons. Neuron 71:142–154.

Vuilleumier P, Armony JL, Driver J, Dolan RJ (2003) Distinct spatial frequency sensitivities for processing faces and emotional expressions. Nature Neuroscience 6:624–631.

Walker JA, Ghalambor CK, Griset OL, McKenney D, Reznick DN (2005) Do faster starts increase the probability of evading predators? Functional Ecology 19:808–815.

Wang L, Chen IZ, Lin D (2015) Collateral Pathways from the Ventromedial Hypothalamus Mediate Defensive Behaviors. Neuron 85:1344–1358.

Wang L, Sarnaik R, Rangarajan K, Liu X, Cang J (2010) Visual receptive field properties of neurons in the superficial superior colliculus of the mouse. The Journal of Neuroscience 30:16573–84.

Watson TC, Cerminara NL, Lumb BM, Apps XR (2016) Neural Correlates of Fear in the Periaqueductal Gray. The Journal of Neuroscience 36:12707–12719.

Wei P, Liu N, Zhang Z, Liu X, Tang Y, He X, Wu B, Zhou Z, Liu Y, Li J, Zhang Y, Zhou X, Xu L, Chen L, Bi G, Hu X, Xu F, Wang L (2015) Processing of visually evoked innate fear by a non-canonical thalamic pathway. Nature Communications 6:6756.

Weldon DA, Best PJ (1992) Changes in sensory responsivity in deep layer neurons of the superior colliculus of behaving rats. Behavioural Brain Research 47:97–101.

Weldon DA, DiNieri JA, Silver MR, Thomas AA, Wright RE (2007) Reward-related neuronal activity in the rat superior colliculus. Behavioural Brain Research 177:160–164.

Weldon DA, Patterson CA, Colligan EA, Nemeth CL, Rizio AA (2008) Single unit activity in the rat superior colliculus during reward magnitude task performance. Behavioral Neuroscience 122:183–90.

Westby GW, Keay Ka, Redgrave P, Dean P, Bannister M (1990) Output pathways from the rat superior colliculus mediating approach and avoidance have different sensory properties. Experimental Brain Research 81:626–38.

White BJ, Berg DJ, Kan JY, Marino RA, Itti L, Munoz DP (2017) Superior colliculus neurons encode a visual saliency map during free viewing of natural dynamic video. Nature Communications 8:14263.

Wilent WB, Oh MY, Buetefisch CM, Bailes JE, Cantella D, Angle C, Whiting DM (2010) Induction of panic attack by stimulation of the ventromedial hypothalamus. Journal of Neurosurgery 112:1295–8.

Wootton RJ (1989) Ecology of Teleost Fishes. Dordrecht: Springer Netherlands.

Xiong XR, Liang F, Zingg B, Ji Xy, Ibrahim LA, Tao HW, Zhang LI (2015) Auditory cortex controls sound-driven innate defense behaviour through corticofugal projections to inferior colliculus. Nature Communications 6:7224.

Yang CF, Chiang MC, Gray DC, Prabhakaran M, Alvarado M, Juntti SA, Unger EK, Wells JA, Shah NM (2013) Sexually Dimorphic Neurons in the Ventromedial Hypothalamus Govern Mating in Both Sexes and Aggression in Males. Cell 153:896–909.

Ydenberg RC, Dill LM (1986) The Economics of Fleeing from Predators. Advances in the Study of Behavior 16:229–249.

Yilmaz M, Meister M (2013) Rapid innate defensive responses of mice to looming visual stimuli. Current Biology 23:2011–2015.

Young J (1962) The Life of Vertebrates. 2nd edition. New York and Oxford: Oxford University Press.

Zhang Y, Kim IJ, Sanes JR, Meister M (2012) The most numerous ganglion cell type of the mouse retina is a selective feature detector. Proceedings of the National Academy of Sciences 109:E2391–8.

Zhao X, Liu M, Cang J (2014) Visual cortex modulates the magnitude but not the selectivity of looming-evoked responses in the superior colliculus of awake mice. Neuron 84:202–213.

Zingg B, Chou Xl, Zhang Zg, Mesik L, Liang F, Tao HW, Zhang LI (2016) AAV-Mediated Anterograde Transsynaptic Tagging: Mapping Corticocollicular Input-Defined Neural Pathways for Defense Behaviors. Neuron pp 1–15.

Zong W, Wu R, Li M, Hu Y, Li Y, Li J, Rong H, Wu H, Xu Y, Lu Y, Jia H, Fan M, Zhou Z, Zhang Y, Wang A, Chen L, Cheng H (2017) Fast high-resolution miniature two-photon microscopy for brain imaging in freely behaving mice. Nature Methods 14:713–719.

Zucker RS, Regehr WG (2002) Short-Term Synaptic Plasticity. Annual Review of Physiology 64:355–405.

Zylberberg J, Deweese MR (2011) How should prey animals respond to uncertain threats? Frontiers in Computational Neuroscience 5:20.

8 Appendix

8.1 A head-fixed assay for monitoring neural activity during defensive behaviours

In studying the neural basis of behaviour, a compromise is often necessary to strike a balance between obtaining an accurate behavioural readout and a suitable type of physiological information (e.g. from electroencephalogram (EEG) to vesicular release signals) when answering a particular biological question.

An fundamental challenge to address is that the animal must behave (i.e. move) while recording, yet the brain needs to be kept still in relation to the recording system. For functional imaging, for example, this has been solved by either by head-fixing the animal under the microscope where it can interact with a virtual or artificial environment (Hölscher et al., 2005) or by mounting a compact, cellular-resolution imaging system on the head of a freely moving animal (Helmchen et al., 2013). A crucial requirement of our study is that the environment for the animal is as conducive to natural behaviour as possible, as the internal state of the animal has been shown to influence innate survival behaviours across species (Hirayama and Gillette, 2012; Filosa et al., 2016; Martin and Lopez, 1999).

In parallel with developing our behavioural assay and incorporating physiological recording techniques for freely-moving animals, we aimed to develop a head-fixed behaviour assay for understanding defensive responses to innately threatening stimuli. The advantages of a head-fixed assay include the ability to probe neural activity with two-photon microscopy[1], and the relative ease with which intra-cellular and large-scale extra-cellular electrophysiology, such as silicon probe recordings, can be accomplished, and it is also easier to achieve precise spatiotemporal control over sensory stimuli than in freely moving assays. Two-photon imaging allows real-time non-invasive monitoring of the activity of networks and cellular components like synapses and dendrites at depths up to ~900 µm.

[1] Two-photon imaging has a number of advantages over epifluorescent imaging, such as achieving sub-cellular resolution *in vivo* by lowering the volume of excitation and reducing out-of-focus background signals, imaging at depth in part due to longer excitation wavelengths and collecting more emission light, and acquiring multiple colour channels with ease. While head-mounted miniaturised two-photon microscopes were developed over 15 years ago (Helmchen et al., 2001), their performance has recently been improved to make them viable alternatives to epifluorescent imaging (Zong et al., 2017).

We therefore built a virtual-reality environment (VRE) to be used in conjunction with a moveable-objective two-photon microscope or electrophysiological recording techniques. This environment contained a shelter and an area for exploration, while we tested various systems to allow the animal to move within the environment while simulating predators and measuring the behavioural output, with the aim of evoking escape and freezing defensive behaviours.

The VRE was based on the design of Schmidt-Hieber and Häusser (2013), and uses a spherical projection system, where a spherical mirror reflects a warped image onto a screen inside a dome that covers 240°, which is almost the entire horizontal field of view of the mouse, and head-restrained mouse is positioned at the centre of the dome (Fig. 8.1*A*). For the movement system, we first tried floating a polystyrene sphere on air, allowing 2-D movement in the environment. However, the sphere is inherently unstable for the mouse, which required multiple training sessions to keep its balance. As mice can escape directly forwards when unrestrained, we posited that 2D movement might not be critical to evoking defensive behaviours, and the advantage of a virtual environment is that endless linear environments can be made. We therefore used a polystyrene disc (25cm diameter, 10cm width) that rotates on ball-bearings, which allowed a more natural running gait at the expense of changing heading. With this system, animals required no training to move forwards and backwards, and showed few signs of initial distress and were able to reach the end of the corridor environment several times in the first session. We used expanding spot stimuli displayed in the sky of the virtual environment to drive defensive behaviour (Fig. 8.1*C*). The most common behaviour was freezing, but if the animal was close to the shelter, stimuli also caused frantic, short, sharp movements backwards or forwards, resembling escape. We also performed preliminary proof-of-principle experiments carrying out two-photon imaging in the mSC during anaesthesia (Fig. 8.1*D*).

We did not continue with this method for the following reasons. Firstly, the virtual environment only worked well as a learned foraging paradigm with frequent rewards to encourage exploration of the environment. This would introduce a number of confounding factors to studying innate defensive reactions to threatening stimuli, such as the satiety state of the animal, which would change throughout a session, and would involve a training period and could introduce conflicting goals to modify instinctive defensive decisions. Although the virtual shelter was perceived as a safe place by the animals without training, it did not seem to be valued as highly as a real-world shelter in an arena, which may have biased the animal against escaping to it unless very close. We concluded that recordings during freely-moving behaviour would allow us better understand the relation of neural activity to the instinctive escape decision, and would allow us to use exactly the same behavioural assay for all experiments in this project. Other questions, such as the lines of investigation suggested in Chapter 7 (Experimental Outlook), will be better suited to a head-fixed assay.

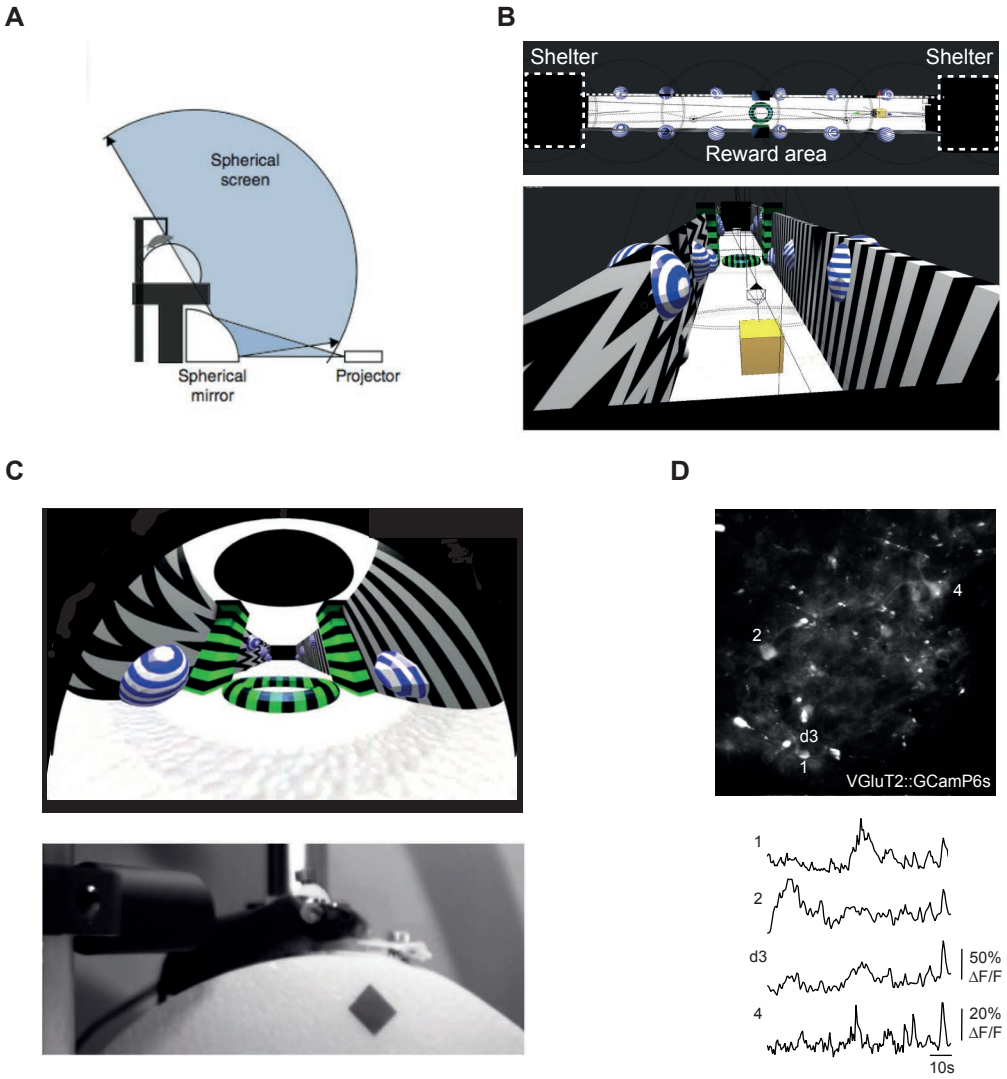

Figure 8.1 A head-fixed behavioural assay for simulating threats during foraging. **A:** Schematic of virtual reality setup (Schmidt-Hieber and Hausser, 2013). **B:** Design of the virtual looping linear track environment in the Blender game engine, showing a shelter at each end which loops to create a series of corridors interspersed with shelters, with a reward-triggering area in the centre. Animals must stop for 4s in this area to receive a milkshake reward (bottom). For the animal to control its position in the environment, an optical computer mouse tracks the movement of the disc at a poll rate of 1kHz and converts this to movement of the camera in a virtual-reality scene of a corridor with distance cues and an open sky. **C:** Point-of-view of the animal, showing warping for spherical projection correction. An expanding spot stimulus is triggered while the animal approaches the reward zone (top). Side-view of head-fixed animal on the disk, with reward delivery tube positioned in front (bottom). In this example, the animal is freezing in response to the stimulus. **D:** Two-photon imaging of the calcium indicator GCaMP6s expressed in VGluT2^{+} neurons in the mSC during anaesthesia. Mean intensity z-projection of a field-of-view in the mSC (top) and activity traces from three cell bodies and one dendrite identified in the field-of-view (bottom).